RADC-TDR-64-397 ,

INVESTIGATION OF MEASUREMENT ERRORS OF THE RAT SCAT CROSS SECTION FACILITY

TECHNICAL DOCUMENTARY REPORT NO. RADC-TDR-64-397
July 1964

Space Surveillance and Instrumentation Branch
Rome Air Development Center
Research and Technology Division
Air Force Systems Command
Griffiss Air Force Base, New York

Project No. 6503

(Prepared by General Dynamics/Fort Worth,
A Division of General Dynamics Corporation,
Under Contract No. AF30(602)-2831)

NOTICES

Copies available at Office of Technical Services.

Qualified requesters may obtain copies from Defense Documentation Center.

When US Government drawings, specifications, or other data are used for any purpose other than a definitely related government procurement operation, the government thereby incurs no responsibility nor any obligation whatsoever, and the fact that the government may have formulated, furnished, or in any way supplied the said drawings, specifications, or other data is not to be regarded by implication or otherwise, as in any manner licensing the holder or any other person or corporation, or conveying any rights or permission to manufacture, use, or sell any patented invention that may in any way be related thereto.

Do not return this copy. Retain or destroy.

UNCLASSIFIED
Security Classification

DOCUMENT CONTROL DATA - R&D
(Security classification of title, body of abstract and indexing annotation must be entered when the overall report is classified)

1. ORIGINATING ACTIVITY (Corporate author) GENERAL DYNAMICS/FORT WORTH P. O. Box 748 Fort Worth, Texas 76101	2a. REPORT SECURITY CLASSIFICATION UNCLASSIFIED 2b. GROUP N.A.

3. REPORT TITLE

INVESTIGATION OF MEASUREMENT ERRORS OF THE RAT SCAT CROSS SECTION FACILITY

4. DESCRIPTIVE NOTES *(Type of report and inclusive dates)*

FINAL

5. AUTHOR(S) *(Last name, first name, initial)*

Freeny, C.C., Leeth, T.R., Jones, J.W., and Brust, M.F.

6. REPORT DATE	7a. TOTAL NO. OF PAGES	7b. NO. OF REFS
July 1964	115	5

8a. CONTRACT OR GRANT NO.	9a. ORIGINATOR'S REPORT NUMBER(S)
AF30(602)-2831 b. PROJECT NO. 6503 c. d.	RADC-TDR-64-397 9b. OTHER REPORT NO(S) *(Any other numbers that may be assigned this report)* GD/FW Report No. FZE-222-7

10. AVAILABILITY/LIMITATION NOTICES

1. Qualified requesters may obtain copies from DDC.
2. DDC release to OTS is authorized.

11. SUPPLEMENTARY NOTES	12. SPONSORING MILITARY ACTIVITY
NONE	Rome Air Development Center Griffiss AFB New York 13442

13 ABSTRACT The contents of this report relate the test programs and results therefrom of the RAT SCAT research and development program instigated to investigate the measuring fields as a function of range geometry, and measurement accuracies, of the RAT SCAT cross section measurement facility. Investigations under the program being reported were limited to monostatic cross section measurements using the principle polarizations, horizontal and vertical, and frequencies in the range 1 to 10 gigacycles. A model for the field over the target region involving antenna height, antenna size, target height, frequency and distance to the target is presented along with appropriate measured data. These models are in most cases standard first order approximations used in estimating fields on a ground plane range. Major potential errors are classified into four categories for which investigations were conducted. In most cases theoretical error models were developed in terms of parameters which could be obtained from experiments conducted at the RAT SCAT Site. The test programs and results therefrom are presented for each of the four types of errors investigated as well as the ground plane model. Based on results obtained using measured data, conclusions and recommendations arising from the various areas of investigation are given. This is report No. 7 of the RAT SCAT research and development program.

DD FORM 1 JAN 64 1473

UNCLASSIFIED
Security Classification

1-a

KEY WORDS	LINK A		LINK B		LINK C	
	ROLE	WT	ROLE	WT	ROLE	WT
Electromagnetic Fields						
Antenna Radiation Patterns						
Ranges (Establishments)						
Radar						
Measurement						

INSTRUCTIONS

1. ORIGINATING ACTIVITY: Enter the name and address of the contractor, subcontractor, grantee, Department of Defense activity or other organization *(corporate author)* issuing the report.

2*a*. REPORT SECURITY CLASSIFICATION: Enter the overall security classification of the report. Indicate whether "Restricted Data" is included. Marking is to be in accordance with appropriate security regulations.

2*b*. GROUP: Automatic downgrading is specified in DoD Directive 5200.10 and Armed Forces Industrial Manual. Enter the group number. Also, when applicable, show that optional markings have been used for Group 3 and Group 4 as authorized.

3. REPORT TITLE: Enter the complete report title in all capital letters. Titles in all cases should be unclassified. If a meaningful title cannot be selected without classification, show title classification in all capitals in parenthesis immediately following the title.

4. DESCRIPTIVE NOTES: If appropriate, enter the type of report, e.g., interim, progress, summary, annual, or final. Give the inclusive dates when a specific reporting period is covered.

5. AUTHOR(S): Enter the name(s) of author(s) as shown on or in the report. Enter last name, first name, middle initial. If military, show rank and branch of service. The name of the principal author is an absolute minimum requirement.

6. REPORT DATE: Enter the date of the report as day, month, year, or month, year. If more than one date appears on the report, use date of publication.

7*a*. TOTAL NUMBER OF PAGES: The total page count should follow normal pagination procedures, i.e., enter the number of pages containing information.

7*b*. NUMBER OF REFERENCES: Enter the total number of references cited in the report.

8*a*. CONTRACT OR GRANT NUMBER: If appropriate, enter the applicable number of the contract or grant under which the report was written.

8*b*, 8*c*, & 8*d*. PROJECT NUMBER: Enter the appropriate military department identification, such as project number, subproject number, system numbers, task number, etc.

9*a*. ORIGINATOR'S REPORT NUMBER(S): Enter the official report number by which the document will be identified and controlled by the originating activity. This number must be unique to this report.

9*b*. OTHER REPORT NUMBER(S): If the report has been assigned any other report numbers *(either by the originator or by the sponsor)*, also enter this number(s).

10. AVAILABILITY/LIMITATION NOTICES: Enter any limitations on further dissemination of the report, other than those imposed by security classification, using standard statements such as:

(1) "Qualified requesters may obtain copies of this report from DDC."

(2) "Foreign announcement and dissemination of this report by DDC is not authorized."

(3) "U. S. Government agencies may obtain copies of this report directly from DDC. Other qualified DDC users shall request through _____."

(4) "U. S. military agencies may obtain copies of this report directly from DDC. Other qualified users shall request through _____."

(5) "All distribution of this report is controlled. Qualified DDC users shall request through _____."

If the report has been furnished to the Office of Technical Services, Department of Commerce, for sale to the public, indicate this fact and enter the price, if known.

11. SUPPLEMENTARY NOTES: Use for additional explanatory notes.

12. SPONSORING MILITARY ACTIVITY: Enter the name of the departmental project office or laboratory sponsoring *(paying for)* the research and development. Include address.

13. ABSTRACT: Enter an abstract giving a brief and factual summary of the document indicative of the report, even though it may also appear elsewhere in the body of the technical report. If additional space is required, a continuation sheet shall be attached.

It is highly desirable that the abstract of classified reports be unclassified. Each paragraph of the abstract shall end with an indication of the military security classification of the information in the paragraph, represented as *(TS)*, *(S)*, *(C)*, or *(U)*

There is no limitation on the length of the abstract. However, the suggested length is from 150 to 225 words.

14. KEY WORDS: Key words are technically meaningful terms or short phrases that characterize a report and may be used as index entries for cataloging the report. Key words must be selected so that no security classification is required. Identifiers, such as equipment model designation, trade name, military project code name, geographic location, may be used as key words but will be followed by an indication of technical context. The assignment of links, rules, and weights is optional.

FOREWORD

In order to meet the need for a National Radar Reflectivity Range, Rome Air Development Center (RADC) awarded a development contract on 29 June 1962 to General Dynamics/Fort Worth (GD/FW) to design, fabricate, and develop the Radar Target Scatter Site (Project RAT SCAT) on the Alkali Flats, Holloman AFB, New Mexico, (Contract AF30(602)-2831). The operational RAT SCAT Site was delivered to the Air Force on 30 June 1964.

The RAT SCAT facility was developed for full-scale radar cross section measurements. In the pursuit of this development, an R&D Program was undertaken to provide for the specific needs of Project RAT SCAT as requirements appeared in the implementation of the function of the Site. A significant portion of this work was subcontracted. Emphasis was placed on those areas thought to be most promising in achieving measurement objectives. The presentation of the results of the R&D Program is covered in eight reports which were prepared as RADC Technical Documentary Reports.

This report (General Dynamics/Fort Worth Report No. FZE-222-7) is No. 7 in the series. It contains a discussion of the theoretical investigations and test programs which were designed for the purpose of studying the measuring fields as a function of range geometry and measurement accuracies at the RAT SCAT cross section measurement facility. The material in this report was prepared by C. C. Freeny, T. R. Leeth, J. W. Jones, and M. F. Brust of General Dynamics/Fort Worth.

The contents of this report and the abstract are unclassified.

RADC-TDR-64-397
July 1964

ABSTRACT

The contents of this report relate the test programs and results therefrom of the RAT SCAT research and development program instigated to investigate the measuring fields as a function of range geometry, and measurement accuracies, of the RAT SCAT cross section measurement facility. Investigations under the program being reported were limited to monostatic cross section measurements using the principle polarizations, horizontal and vertical, and frequencies in the range 1 to 10 gigacycles.

A model for the field over the target region involving antenna height, antenna size, target height, frequency and distance to the target is presented along with appropriate measured data. These models are in most cases standard first order approximations used in estimating fields on a ground plane range.

Major potential errors are classified into four categories for which investigations were conducted. In most cases theoretical error models were developed in terms of parameters which could be obtained from experiments conducted at the RAT SCAT Site. The test programs and results therefrom are presented for each of the four types of errors investigated as well as the ground plane model.

Based on results obtained using measured data, conclusions and recommendations arising from the various areas of investigations are given.

This is report No. 7 of the RAT SCAT research and development program.

PUBLICATION REVIEW

This report has been reviewed and is approved. For further technical information on this project, contact EMASP (D. M. Montana).

Approved:

DONALD M. MONTANA
Program Director's Office
Space Surveillance and
Instrumentation Branch

Approved:

JOSEPH FALLER
Chief, Space Surveillance and
Instrumentation Branch
Surveillance and Control Division

Preceding page blank

TABLE OF CONTENTS

LIST OF FIGURES

SECTION 1

INTRODUCTION

The RAT SCAT cross section measurements facility utilizes the ground plane in producing RF fields for purposes of measuring target radar cross section. The investigations behind the work reported in this document were instigated to evaluate the nature of the fields in the target region and investigate errors to be expected by use of these fields. In addition, measurement errors from other sources such as target supports, calibration, and extraneous illumination were studied in the program being reported. Because the fields produced over the target region are closely related to a potential measurement error (referred to as near field error in this document), the measuring fields to be expected at the RAT SCAT Site are reported in the section devoted to near field error.

The primary objectives of the measurement error program are summarized in the following statements:

1. Determine the significant sources of error that are present when cross section measurements are made at the RAT SCAT Site

2. Obtain theoretical models and/or experimental data with which to ascertain the relative importance of these error sources and estimate the magnitude of said errors.

The program was limited to investigations in the frequency range of 1 to 10 gigacycles and was concerned with errors involved in monostatic cross sections using the principle polarizations (horizontal and vertical). Results of investigations concerning circular polarization and bistatic measurements are reported in separate reports.

Objective 1 was approached with the aid of theoretical considerations. Objective 2 was approached with the aid of theoretical models and information concerning ground plane ranges available from the literature and background information gathered through the operation of the GD/FW cross section facility; a ground plane range. Experiments were devised and conducted at the RAT SCAT Site to ascertain the validity of the models. Individual experiments were designed with the ruling criteria that they tend to isolate the effect of a single error source such that its importance could be determined from measurements.

Preliminary investigations indicated that the significant sources of error inherent in the radar cross section measurement system can be grouped into the following categories:

1. Near field errors - All those errors produced because of the finite length of the radar range. In general these errors can be attributed to the nonuniformity of the field that illuminates the target. Both phase and amplitude nonuniformities have been considered in the investigation of this error source.

2. Background errors - All those errors produced by the presence of background return at the receiver antenna. Here background return denotes the energy that is backscattered by things other than the target. This return has been treated as a random quantity having an amplitude and a phase. For the investigation of this error source statistical techniques were employed.

3. Extraneous illumination errors - All those errors produced by the presence of extraneous target return at the receiver antenna. Here extraneous target return denotes the energy that is backscattered by the target; but, ideally, should not have been. This phenomenon can be the result of target reillumination by energy that was originally scattered into the pit or onto the rotator table or it can be the result of energy that is reflected directly to the receiving antenna but ideally should have been lost. Under normal operating conditions target reillumination is the major contributor to the error source. Hence, this aspect of the problem received the major portion of the effort spent on extraneous illumination.

4. Calibration and instrumentation errors - Calibration errors can be defined as all those errors due to discrepancies in the absolute reference level for any specific measurement and all those errors due to discrepancies in the relative reference level for any particular series of measurements. This error source tends to be due largely to systematic errors or those that can be eliminated if enough precision in the measurement technique is employed. There is a certain amount of inherent error involved, of course, and this has been treated by the use of statistical techniques. Instrumentation errors can be defined as all those errors due to receiver or incoherent noise, to system nonlinearity, and to drift in equipment parameters. Instrumentation errors

tend to be inherent; however, at the RAT SCAT Site they do not appear to be particularly important sources of error. Effort expended in the investigation of these error sources has been directed primarily toward the determination of the upper bounds of these errors.

In the detailed consideration of each of the above mentioned error sources, a general discussion and description of the model or theoretical description of the source is first presented. The experiment(s) designed to isolate the source and to determine the validity of the model are next outlined. Results of the experiments are then presented and discussed. When appropriate, recommendations are made and conclusions are drawn on the basis of the results obtained.

SECTION 2

NEAR FIELD ERROR INVESTIGATION

General

The radar cross section or backscattering cross section of a target is conventionally defined as the area intercepting that amount of power which, when scattered isotropically, produces an echo equal to that observed from the target. Symbolically this definition can be written as in Equation 1.

$$\sigma = \lim_{R \longrightarrow \infty} 4\pi R^2 \frac{\overline{S^s}}{\overline{S^i}} , \qquad (1)$$

where

R = range from transmitter to target

$\overline{S^i}$ = incident Poynting vector

$\overline{S^s}$ = back-scattered Poynting vector.

Hence, the radar cross section of a target is an abstraction; a quantity that cannot be exactly measured because of the physical restriction of a finite measurement range. It is the effect of this restriction in which interest lies. In particular the effect of the finite length ground plane range utilized at the RAT SCAT Site is the subject of the near field error investigation.

A theoretical description of the near field error is presented along with a description of the experiments devised and carried out to verify the theoretical models. On the basis of these efforts a prediction of errors attributed to finite R appears feasible for a large class of targets.

Theoretical Models

Ground Plane Model

Geometry tends to play an important role in any theoretical description of the errors produced by a finite ground plane range, as illustrated in Figure 1, where the vertical plane is of

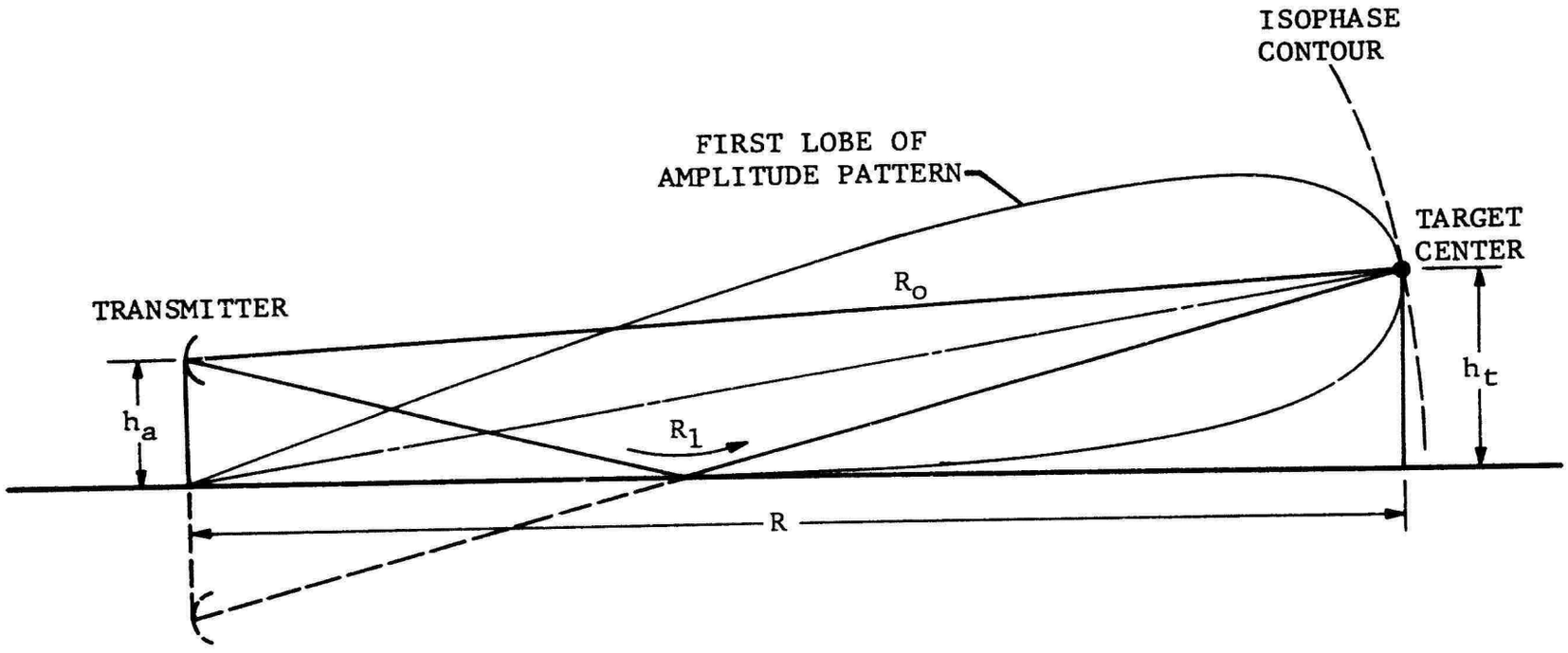

Fig. 1 GROUND PLANE RANGE GEOMETRY FOR THE VERTICAL PLANE

interest. The electric field intensity in the region of the target can be considered to be the result of a direct and a reflected wave if any ground wave is ignored. Neglection of the ground wave contribution is justifiable because of the frequency range, finite conductivity, and range lengths involved in this report. The electric field is described mathematically by Equation 2.

$$E = E_r + E_d = E_o \left[1 + \rho \epsilon^{-i(\phi + k \Delta R)} \right] \epsilon^{-ikR_o} , \quad (2)$$

where

ρ = magnitude of ground plane reflection coefficient

ϕ = argument of ground plane reflection coefficient

$k\Delta R$ = phase of reflected field with respect to direct field.

Here the assumption has been made that the transmit antenna can be considered a point source (i.e., the antenna acts as an isotropic radiator over the region of interest; hence, the antenna pattern functions that normally appear in Equation 2 have been replaced by unity. If the additional assumption is made that the complex reflection coefficient is -1, then by writing R_1 and R_o in terms of R, h_a and h_t, it can be shown that the amplitude and argument of the complex field pattern are closely approximated by the expressions in Equations 3 and 4, respectively (Reference 1).

$$\left| E/E_o \right| \cong \left| 2 \sin \left(\frac{khaht}{R} \right) \right| , \quad (3)$$

$$\Phi \cong k \left[R + (h_a^2 + h_t^2)(1/2R) \right] - \frac{\pi}{2} , \quad (4)$$

where

R = horizontal distance between target and antenna

h_a = antenna height, h_t = target height

$k = 2\pi/\lambda$

λ = wavelength .

For the grazing angles and frequencies considered, and surface conditions of the RAT SCAT ground plane, the assumption of a -1 reflection coefficient appears appropriate (Reference 1).

Vertical Plane Near Field Error

The amplitude field patterns given by Equation 3, along with the assumptions that (1) the transmit antenna and the receive antenna occupy the same spatial positions and their radiation patterns are identical and (2) the cross section of the target is proportional to the square of its vertical dimension, are used to derive an expression for near field error due to vertical field nonuniformity. The error expression so derived is given in Equation 5. To arrive at Equation 5 the target center is assumed to be located at the peak of the first lobe of the amplitude pattern as in Figure 1, and the amplitude pattern is used to weight the return from each vertical segment of the target. This weighting process is carried out over half the target and the result doubled, because the weighting function is even. In order to correspond to the measurements from a calibrated system, it is necessary to normalize the weighting function to the illumination level at target center.

$$E'_{n_{f_v}} = \frac{\sigma_m}{\sigma_t} = \frac{1}{(D_v)^2} \left| 2 \int_0^{D_v/2} \left|E/E_o\right|^2 \, dy \right|^2 , \qquad (5)$$

where

$$\left| \frac{E}{E_o} \right|^2 = \cos^2\left(\frac{2\pi}{\lambda R} h_a y\right), \text{ (Normalized to field at center of first lobe)}$$

σ_m = measured cross section

σ_t = target cross section (for uniform illumination)

D_v = target dimension in vertical direction.

When the operations indicated in Equation 5 are carried out, and error $E'_{n_{f_v}}$ is expressed in db, Equation 6 follows.

$$E_{n_{f_v}} = 20 \log_{10} \left[\frac{1}{2}\left(1 + \frac{\sin 2\pi/K_v}{2\pi/K_v}\right)\right], \qquad (6)$$

where

$$K_v = R \lambda / h_a D_v.$$

This then is a theoretical expression for the near field error for a target whose single characteristic dimension is oriented vertically. The expression for E_{nfv} is plotted versus the generalized parameter K_v in Figure 2. It is based upon the fundamental assumption that the error is due primarily to the nonuniformity of the illumination amplitude and consequently that the error due to illumination phase nonuniformity can be ignored. Justification for this assumption is based on field probe data and a good agreement between Equation 6 and experimental data.

Horizontal Plane Near Field Error

The geometric relationship used to derive a theoretical error function for the horizontal plane is illustrated in Figure 3. For this case the assumption of a point source implies that the phase front is spherical; hence, the situation is reduced to the conventional near field degradation for a free space environment (Reference 2). That is, the major contributor to the near field error is the nonuniformity of the phase of the illumination rather than the nonuniformity of the amplitude of the illumination. For a target whose characteristic dimension is oriented in the horizontal plane (see Figure 3) a near field error expression can be derived in the following manner.

Relative to target center the two-way phase distribution across the target can be approximated by an examination of Figure 3. This relationship is given in Equation 7,

$$2 \phi (X) = 2k \Delta R (X) = kX^2/R, \qquad (7)$$

where X denotes horizontal displacement relative to target center. On the basis of Equation 7, and the assumption that phase curvature is the primary error source, Equation 7, similar to Equation 5, can be written for the horizontal plane near field error.

$$E'_{nf_h} = \left| \frac{2}{D_H} \int_0^{D_H/2} \exp(-i\, kX^2/R)\, dX \right|^2, \qquad (8)$$

where

D_H = horizontal target dimension.

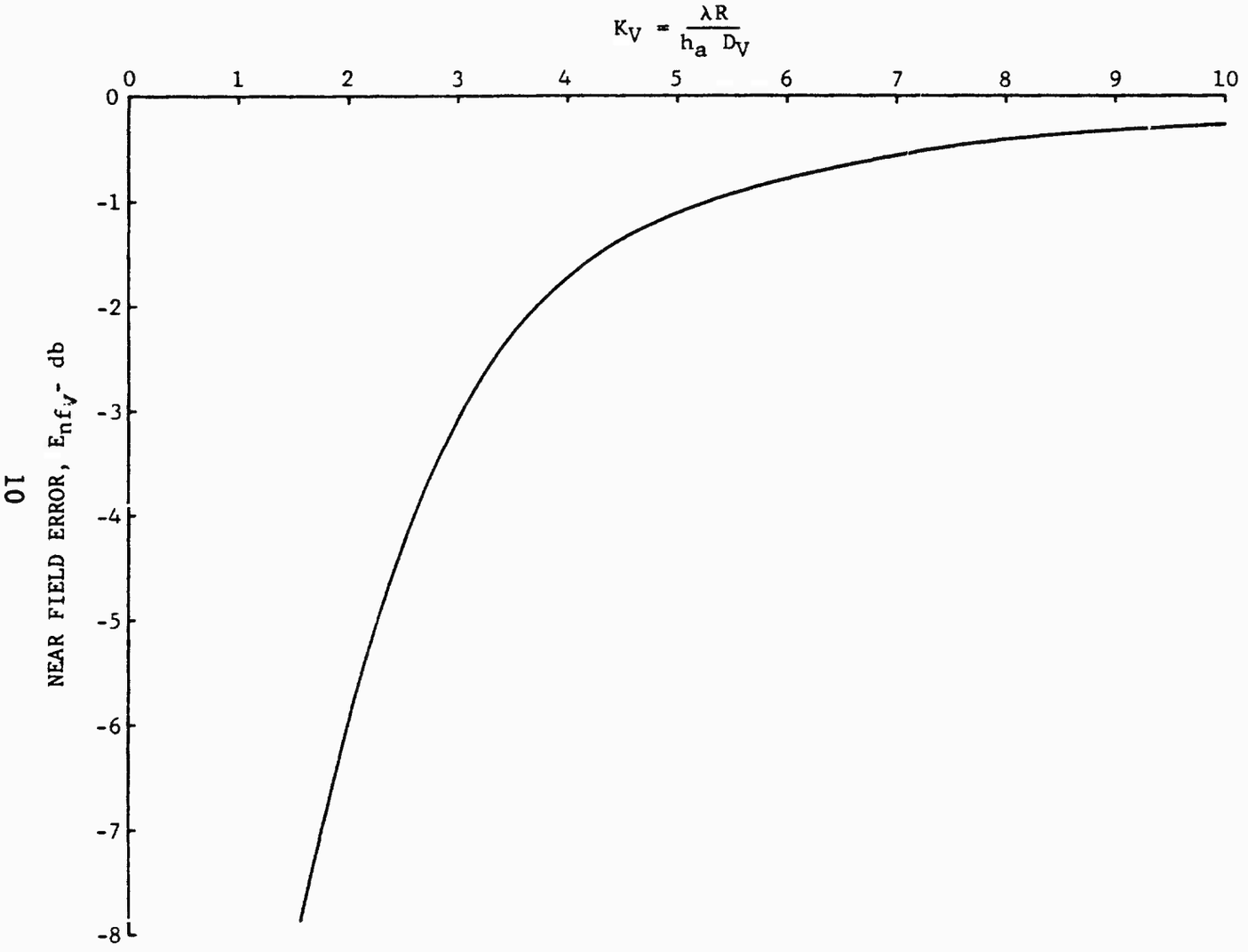

Fig. 2 PREDICTED VERTICAL PLANE NEAR FIELD ERROR

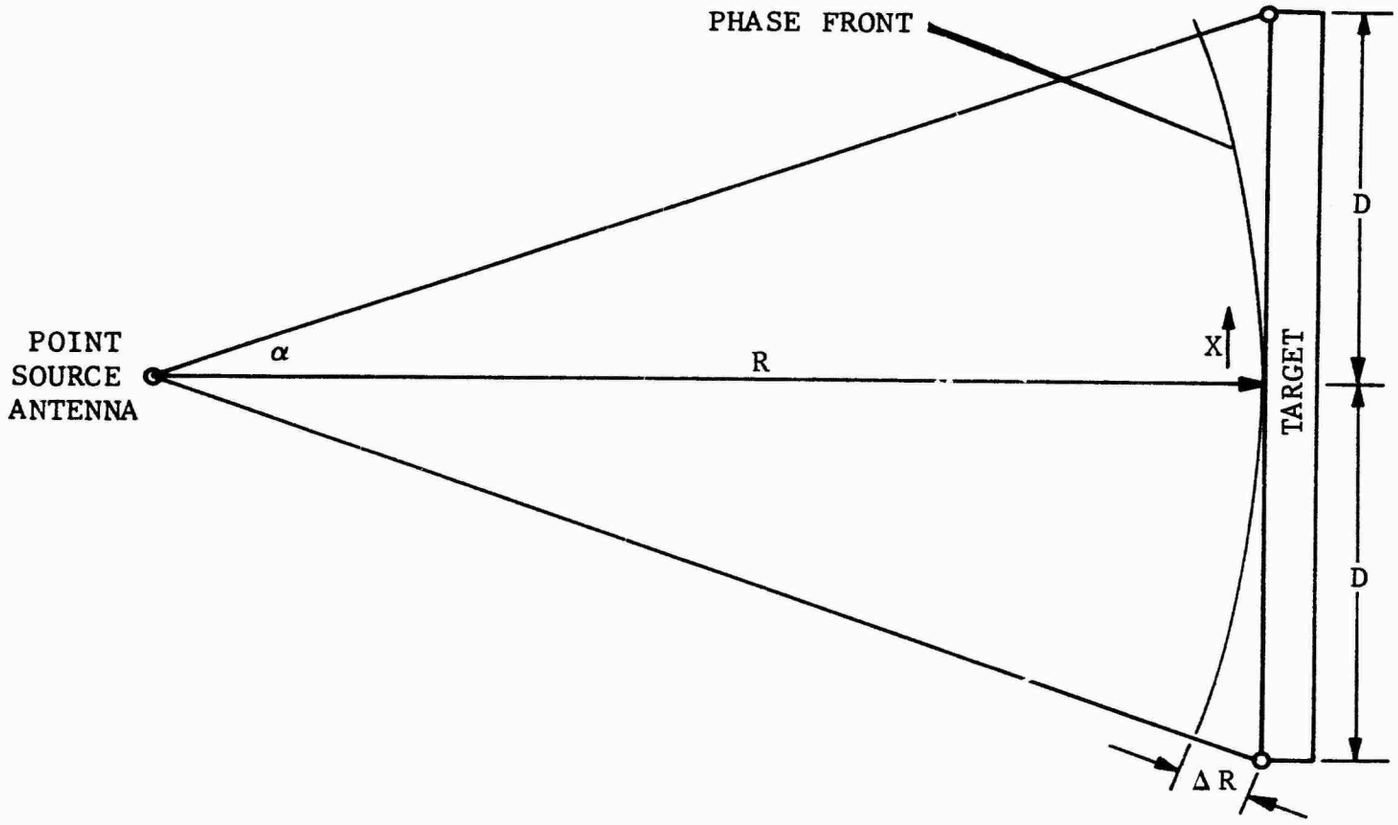

Fig. 3 GROUND PLANE RANGE GEOMETRY FOR THE HORIZONTAL PLANE

The assumptions concerning reciprocity and the nature of the target are necessary in this case just as they were in the vertical plane case. The relationship in Equation 8 can be reduced to the form given in Equation 9 where the error is expressed in db.

$$E_{n_{fh}} = 10 \log_{10} \left\{ \frac{1}{k_H} \left[C^2 \left(1/\sqrt{K_H}\right) + S^2 \left(1/\sqrt{K_H}\right) \right] \right\}, \quad (9)$$

where

$K_H = \lambda R / D_H^2$

$C(1/\sqrt{K_H})$ = real part of the Fresnel integral

$S(1/\sqrt{K_H})$ = imaginary part of the Fresnel integral.

Shown in Figure 4 is a plot of $E_{n_{fh}}$ in db as given by Equation 9 versus the generalized parameter K_H. This then is a theoretical model for the near field error for a one-dimensional "target" that has been oriented horizontally. It is based upon the fundamental assumption that this error is due primarily to the nonuniformity of phase.

Two Dimensional Near Field Error

The one-dimensional models discussed above avoid the general case where the error is due to the nonuniformity of both the amplitude and the phase of the target illumination. This general case would be accounted for by the two-dimensional model represented by Equation 10.

$$E'_{n_f} = \left| \int_0^1 \int_0^1 A^2(D'_H, D'_V) \, \epsilon^{-i2\phi(D'_H, D'_V)} \, dD'_H \, dD'_V \right|^2, \quad (10)$$

where

$A(D'_H, D'_V)$ = amplitude distribution

$\phi(D'_H, D'_V)$ = phase distribution

$D'_H = 2x/D_H$ = normalized horizontal target dimension

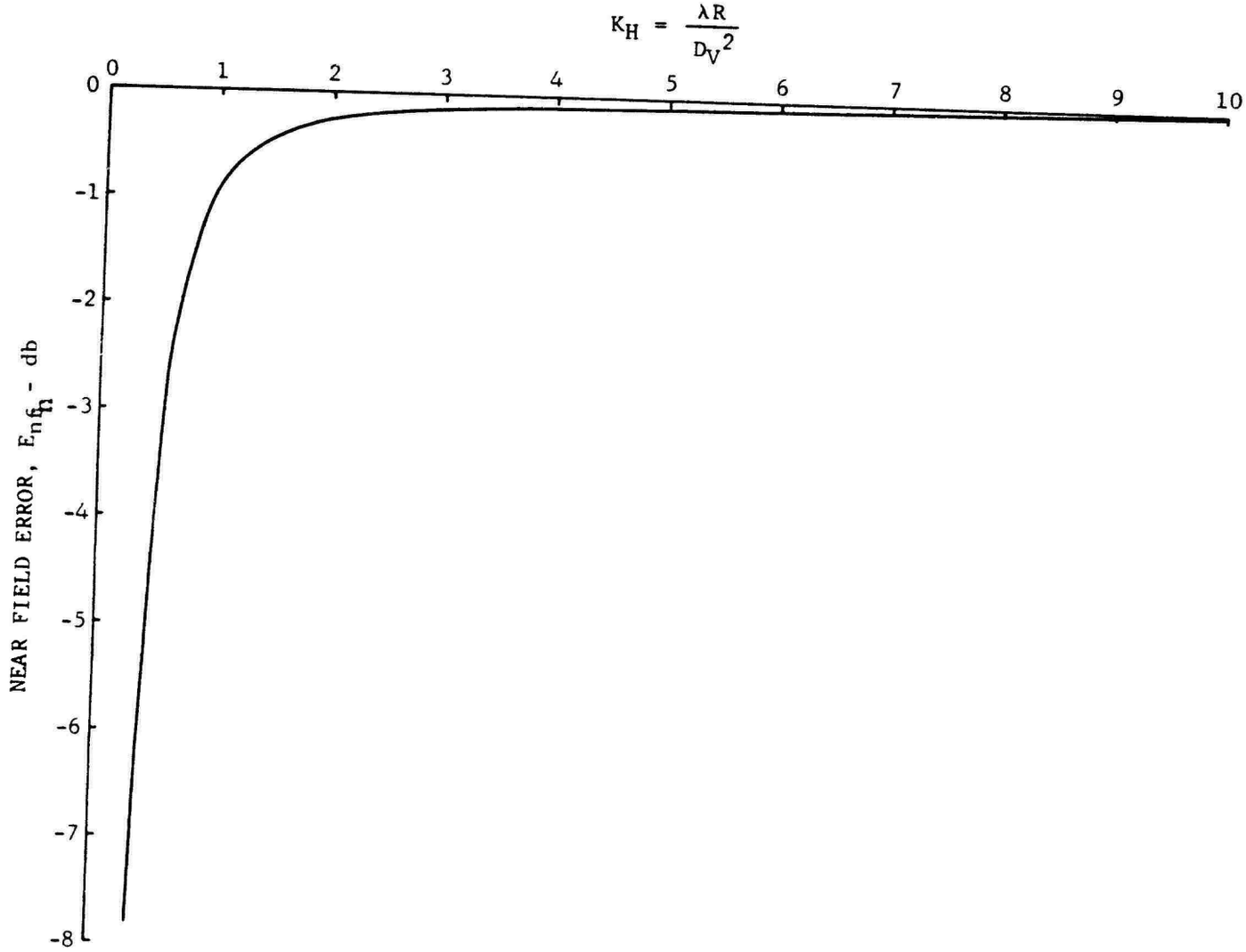

Fig 4 PREDICTED HORIZONTAL PLANE NEAR FIELD ERROR

$D_V' = 2y/D_V$ = normalized vertical target dimension

x = horizontal displacement about target center

y = vertical displacement about target center.

Here, as in the one dimensional models, the target center is assumed to be located at the peak of a symmetrical amplitude pattern. Also, the cross section of the target for uniform illumination is assumed to be proportional to the square of the target area.

In the most general case the above distributions would take into account any lack of complete reciprocity as well as the geometrical configuration of the target. Unfortunately Equation 10 is in general not integrable even if the expression for the distributions can be written. It will, however, be shown later with the aid of results from several experiments that the one dimensional models are appropriate. They provide, in fact, reasonable approximations of the near field errors actually encountered for the type of targets used in constructing the models. Under these conditions Equation 10 can be separated into a product of two independent error terms and hence, be used to estimate near field error for targets with two characteristic dimensions.

Test Program

Amplitude Probes

Because of the numerous assumptions involved in arriving at the various theoretical models, experimental evidence was necessary to provide adequate support for the theory. Most of the assumptions used in the model formulations directly influenced and/or used properties of the fields at the target. The theoretical amplitude patterns can be easily checked by probing the field in the vicinity of the proposed target location with an appropriate transducer or by probing the two-way field in the region of interest with a sphere. For such measurements the only strong requirement is that the probing device not seriously perturb the field. Determination of the one-way vertical plane patterns of either the transmit or the receive antenna amplitude require the use of a transducer. Because the horizontal plane amplitude patterns are known to closely approximate free space patterns, a two-way sphere probe was employed in the horizontal plane. For such probes a sphere of sufficiently large cross section to eliminate noise problems was used.

Phase Probes

Phase probes were obtained by measuring the return from arrays of spheres for which the geometrical relationships between the spheres and the radar antennas were known.

Vertical Phase Probe

The relationship given by Equation 4 provides a starting point for an experiment to measure the vertical plane phase front. This is the equation of an isophase contour and it can be shown that the expression describes an ellipse. For purposes of comparing experiment with theory it is convenient to fix the parameters range (R) and reference target height (h_o) in Equation 4. It is then possible to derive the theoretical phase variation along a line that passes through the reference point and is perpendicular to the ground plane. If h_o represents the fixed position of one sphere and h_s is the vertical displacement of a second sphere with respect to the first, then Equation 4, neglecting the approximate sign, can be rewritten as in Equation 11.

$$\Phi(h_o + h_s) = \Phi(h_o) + \Phi(h_s) \quad , \tag{11}$$

where

$$\Phi(n_o) = k\left(R + \frac{h_a^2 + h_o^2}{2R}\right) - \pi/2 \quad .$$

Thus the desired phase variation is given by Equation 12.

$$\Phi(h_s) = k/R \left(h_o h_s + {h_s^2}/{2}\right) \quad . \tag{12}$$

This is the predicted phase variation along a line that passes through (h_o, R) and is perpendicular to the ground plane. Figure 5 provides a description of the geometry involved in this analysis. From Figure 5 it can be seen that if the phase front of the incident energy formed a plane perpendicular to the earth, there would be no variation in the measured cross section of the two-member array if one sphere was displaced with respect to the other along their common center line. However, due to the elliptical curvature of the incident phase front, there will be a variation in the measured cross section as one sphere is displaced. If this cross section variation is measured, the curvature of the phase front may then be computed. Equation 13 is an expression for the phase in terms of the measured cross section values.

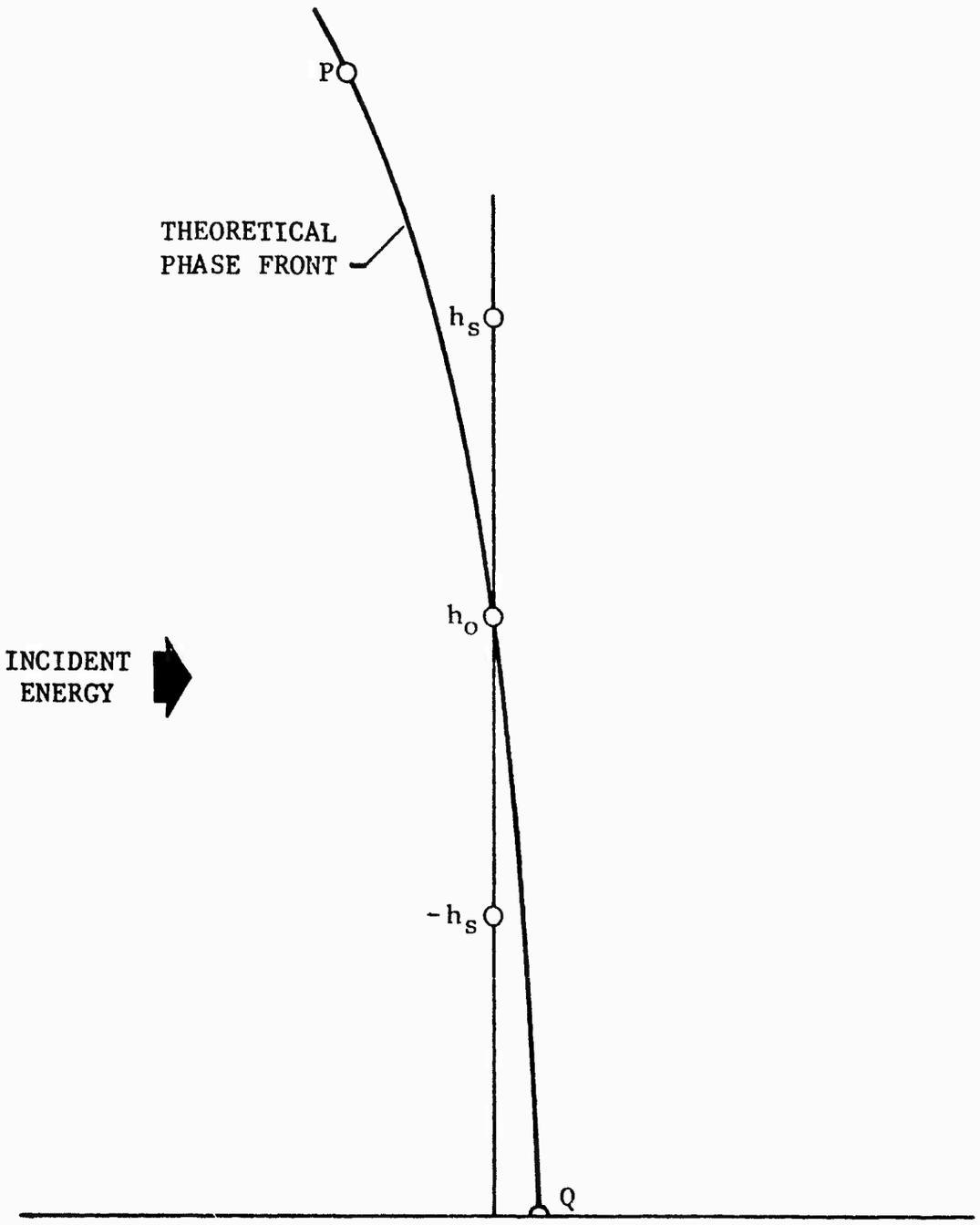

Fig. 5 PHASE PROBE GEOMETRY, VERTICAL PLANE

$$\Phi(h_s) = 1/2 \cos^{-1} \frac{\sigma_{ts} - (\sigma_{ds} + \sigma_{rs})}{2\sqrt{\sigma_{ds}\ \sigma_{rs}}}, \qquad (13)$$

where

σ_{ts} = measured cross section of the array

σ_{ds} = measured cross section of displaced sphere

σ_{rs} = measured cross section of reference sphere.

For this experiment the selection of sphere sizes depends on a trade-off between the degree of coupling allowed and the effect of the background error source. Coupling between spheres can conveniently be reduced by the choice of small spheres but the effect of background can only be eliminated by the choice of spheres that exhibit large cross sections. Two spheres with diameters of 3.5 inches and 4.5 inches were used for the phase probe. The error due to field amplitude variation is eliminated by measuring the cross section of the displaced sphere with respect to the reference sphere at each of its positions.

Horizontal Phase Probe

A horizontal plane phase probe can be accomplished in a manner somewhat similar to the experiment outlined above. In this case a reference sphere was mounted on a support column at the center of the rotator table. Another sphere was mounted at the same altitude but displaced horizontally with respect to the first sphere. If the radar cross section of the array is recorded as it is rotated through 3o0 degrees of azimuth for several values of horizontal displacement, a measure of the horizontal plane phase front can be obtained. Such data should be directly comparable to the phase distribution predicted by the relationship given in Equation 7. In order to extract the desired phase information from the cross section measurements of the sphere array, the geometry of the experiment, as shown in Figure 6, was used. If the phase front of the incident energy formed a plane perpendicular to the radar beam, there would be no phase variations along the line D to -D. However, according to the theory, the phase front of the incident energy has a curvature similar to that illustrated in Figure 6. As a sphere is displaced along the line from Q to D it should cross various isophase contours. In terms of a two-member array, the measured cross section should exhibit nulls whenever the displaced sphere

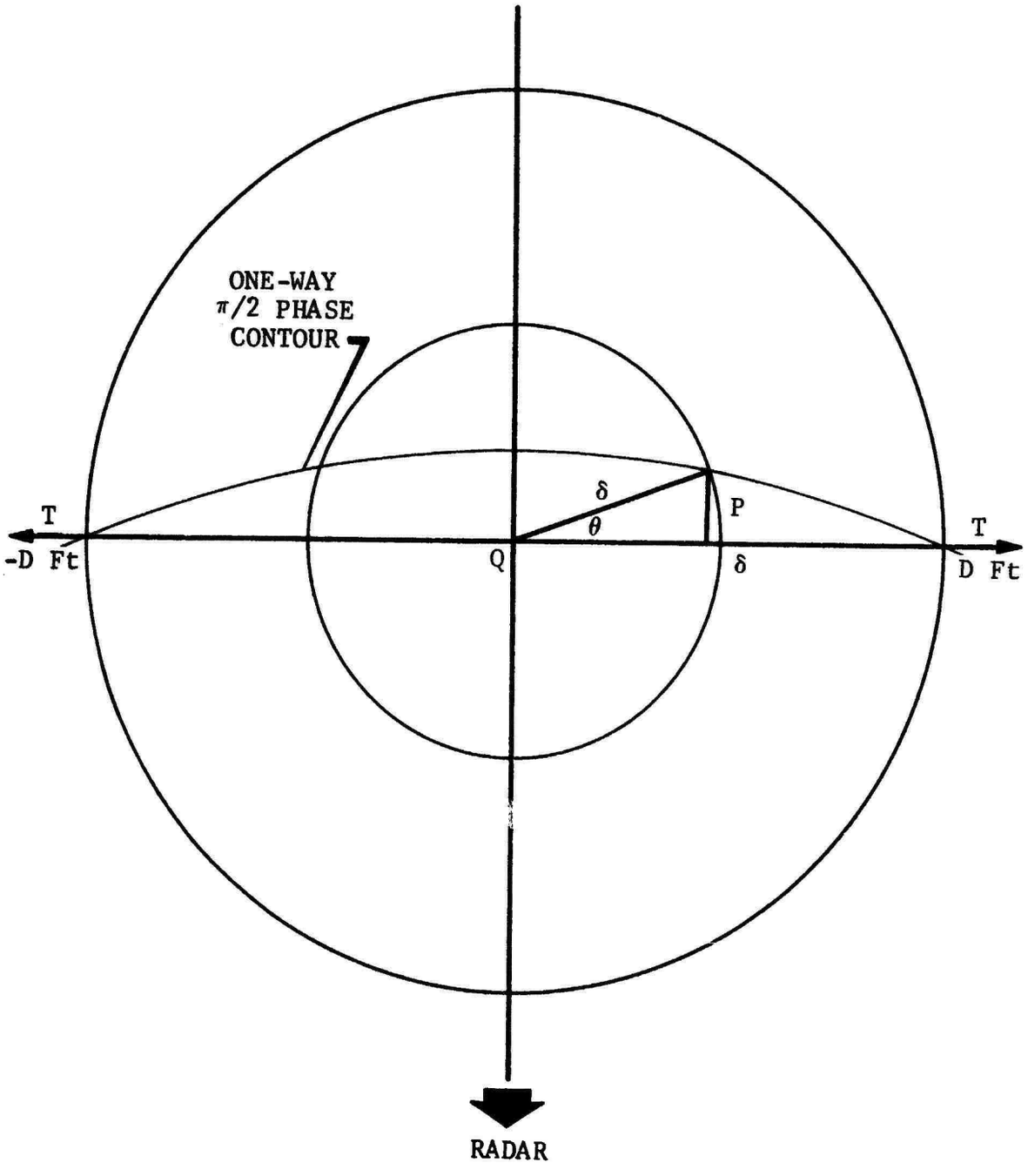

Fig. 6 HORIZONTAL PHASE PROBE GEOMETRY

crosses one-way $\pi/2$ contours relative to the sphere referenced at the fixed point Q. On this figure one such null condition corresponds to point T. If the displaced sphere were repositioned at a distance δ from the point Q, then the array must be rotated through an angle θ in order to once more locate the displaced sphere on the reference one-way $\pi/2$ contour. Knowledge of the value of the displacements P and δ allow the relative phase variation along the line D to -D to be measured. Specifically, this information is given by the relationship expressed in Equation 14.

$$\Phi_H(D) \cong kP = k\,\delta \sin\theta \,. \qquad (14)$$

In this relationship δ denotes the distance between phase centers of the spheres and D is the horizontal displacement relative to the center sphere. Errors due to extraneous illumination, calibration, and instrumentation should be negligible using this method for obtaining the horizontal phase probe.

Near Field Error

To efficiently test the proposed error models, a basic experiment was designed around a particular type of one-dimensional target. The models require a target with the characteristic that its cross section is proportional to the square of its length. A convenient target that possesses the necessary characteristics is a right circular cylinder at broadside aspect. The cross section of such a target for the frequencies of interest and for uniform illumination may be computed using Equation 15.

$$\sigma_t = k\,a\,L^2 \,, \qquad (15)$$

where

a = cylinder radius

L = cylinder length.

Hence, if the cross sections of a set of several lengths of cylinders all of the same radius are measured and compared with the above relationship, one can obtain a measure of the ratio of the empirical cross section to the theoretical cross section, or a measure of the error. If the cylinders chosen for an experiment have a sufficiently high cross section, the error being measured is essentially the error due to near field effects. On the other hand, when cylinders are chosen that exhibit cross sections so low that the various noise sources begin to have strong influence

on the error, the measured error would not necessarily be an indication of the error due to near field effects. In order to reduce the contribution of the noise to the total error, the cylinders were mounted on Styrofoam support columns in the manner shown in Figures 7 and 8. The radar return from the support columns was minimized before the target cylinders were mounted. Information on the minimization procedure and the results to be expected are discussed at length in Section 3. Vertically mounted cylinders provide a test of the vertical plane near field error model, while the horizontally mounted cylinder provides a check of the horizontal plane model. If the test cylinders are chosed such that they have a sufficiently high cross section, concern over whether or not broadside aspect is achieved can be eliminated by continuously measuring the radar cross section of a particular cylinder as it is rotated through 360 degrees of azimuth. According to the relationship in Equation 16 the peaks of the radar cross section scattering diagram would represent the value of the cylinder cross section at broadside (Reference 1).

$$\sigma_t = \frac{a\lambda}{2\pi} \frac{\cos\theta \sin^2(kL \sin\theta)}{\sin^2\theta} . \qquad (16)$$

This relationship gives the cross section of a circular cylinder illuminated by a plane wave incident at angle θ to the geometrical broadside, and the right hand side approaches ka L^2 as θ approaches zero degrees. Also, the right hand side is at its maximum value when θ is zero. The effect of extraneous illumination on the vertical cylinder measurements should be negligible. Although this is not true, in general, for a horizontally mounted cylinder, it will be shown in Section 4 (extraneous illumination error investigation) that for a broadside aspect such error sources are relatively insignificant. The effect of calibration error can be minimized by one of several approaches as will be shown in Section 5; however, such steps are usually unnecessary when spheres whose cross section is sufficiently greater than the background are used for calibration. Equation 15 represents the asymptotic limit of a more general series expression for a right circular cylinder. If cylinders are chosen such that the parameter (ka) is less than about 8.0 this relationship is no longer adequate and, for the transverse polarization case, the general expressions must be used to calculate the theoretical cross section (Reference 3). This difficulty can be avoided if the set of cylinders for any particular frequency of interest are all of the same diameter. The difference between the physical optics value and the correct value will be the same for all cylinder lengths. Hence, the measured data can be compared to the physical optics values by uniformly shifting the data to obtain

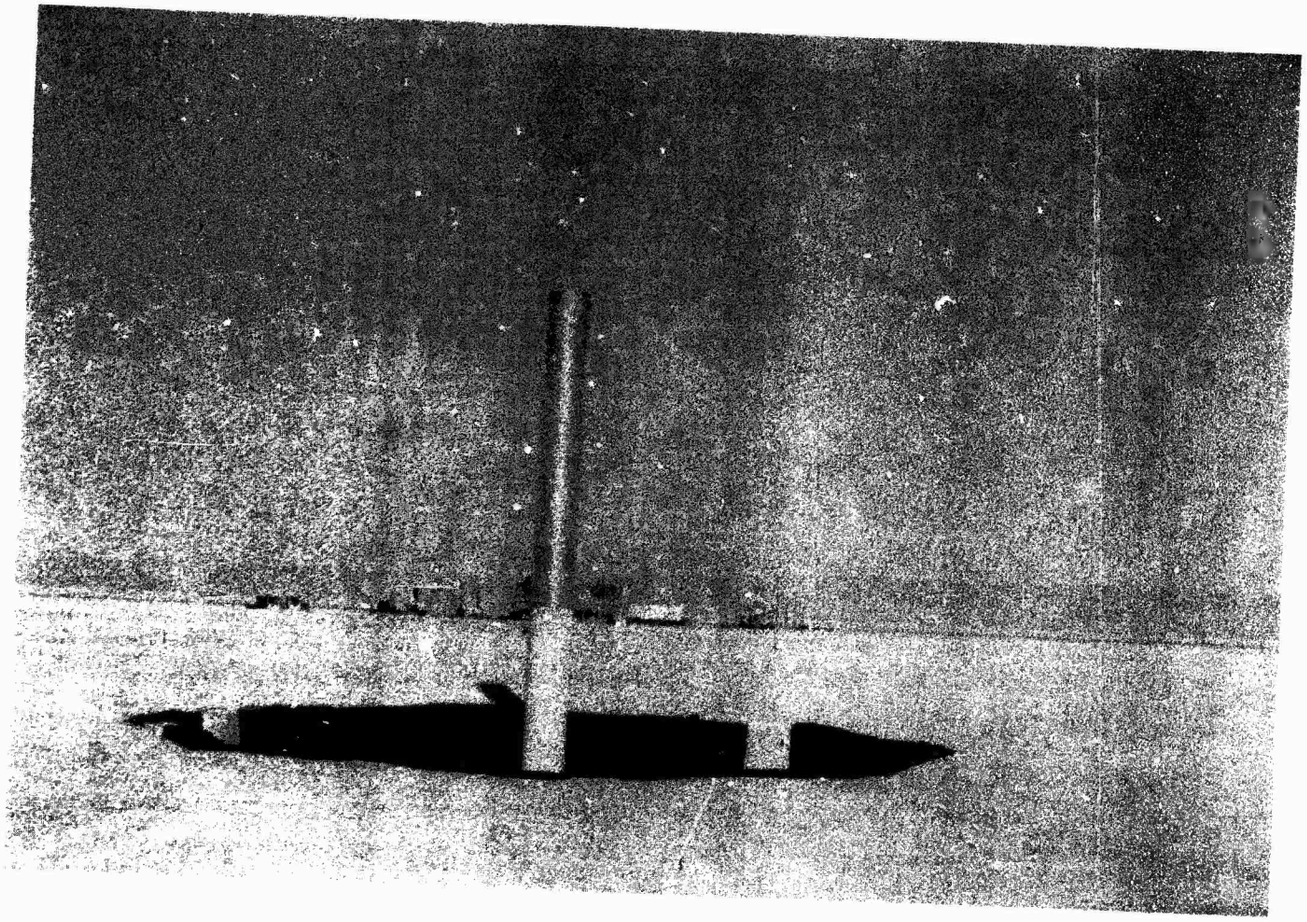

Fig. 7 VERTICAL CYLINDER MOUNTED ON STYROFOAM COLUMN

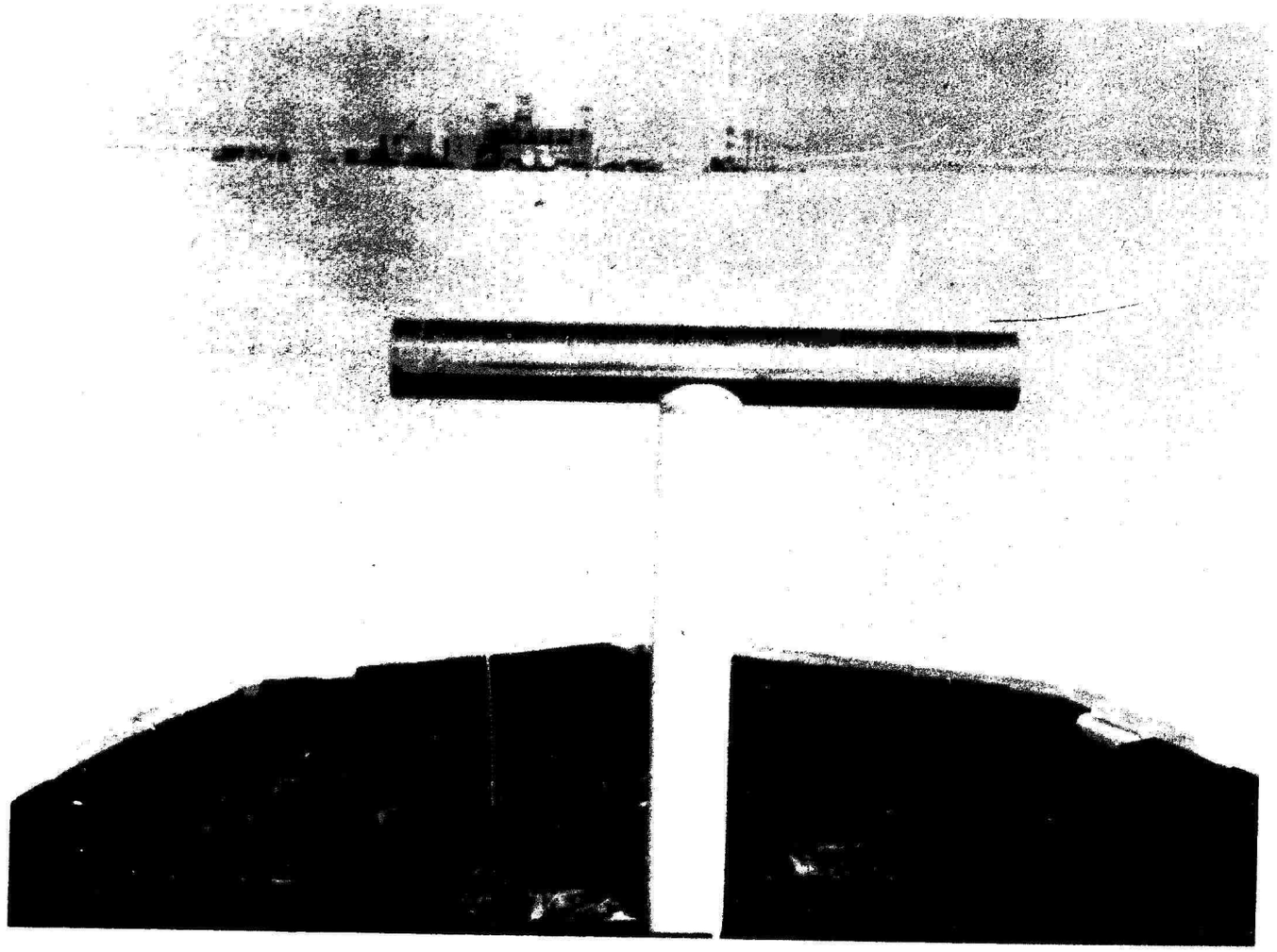

Fig. 8 HORIZONTAL CYLINDER MOUNTED ON STYROFOAM COLUMN

agreement in the no error region. (Assuming no background, etc., errors are incurred during the measurements.)

Comparison of Experiment and Theory

The results from the various experiments and the manner in which they compare with the theoretical models are presented below. To maintain the sequence of the discussion of the experiments, the amplitude probes will be discussed first.

Amplitude Probes

Figures 9 through 16 display the results from the vertical amplitude probes. The measured data are compared directly to the theoretical amplitude patterns for the several conditions of interest. Given in these figures are the measured data for the cases of horizontal and vertical polarization and the specific conditions under which each was measured. These results provide convincing evidence of the validity of the theoretical model for predicting amplitude patterns in the vertical plane when:

1. Frequency is in the range 1 to 10 gigacycles/second

2. Polarization is either horizontal or vertical.

Figure 17 displays the results from a horizontal amplitude probe. Here also the measured data are compared directly to the theoretical amplitude pattern for a uniformly illuminated circular aperature (Reference 2). Measured data for the cases of horizontal and vertical polarization are shown in Figure 17 as the conditions under which the measurements were made. Agreement between the theory and the experimental result appears to be quite good.

Vertical Phase Probe

The vertical plane phase information obtained from the measured data with the aid of Equation 13 did not initially appear to agree with the prediction given by the relationship of Equation 12. However, additional analysis revealed the existence of the following conditions:

1. The data had not been measured along a zero-degree tilt axis (axis perpendicular to the plane of the earth) as assumed, but instead at some small, unknown tilt angle θ.

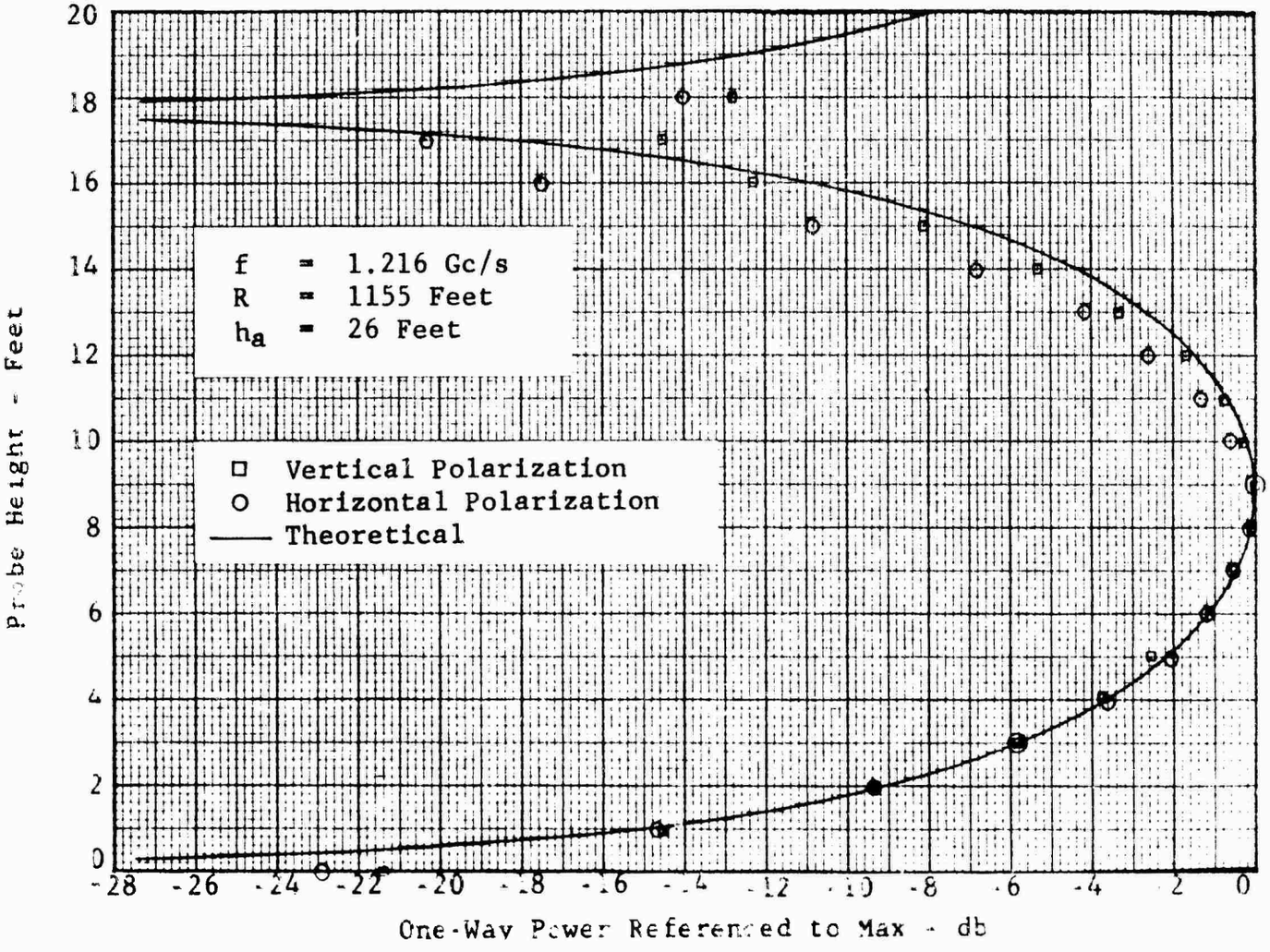

Fig 9 RESULTS FROM VERTICAL AMPLITUDE PROBE TRANSMIT ANTENNA BAND 4

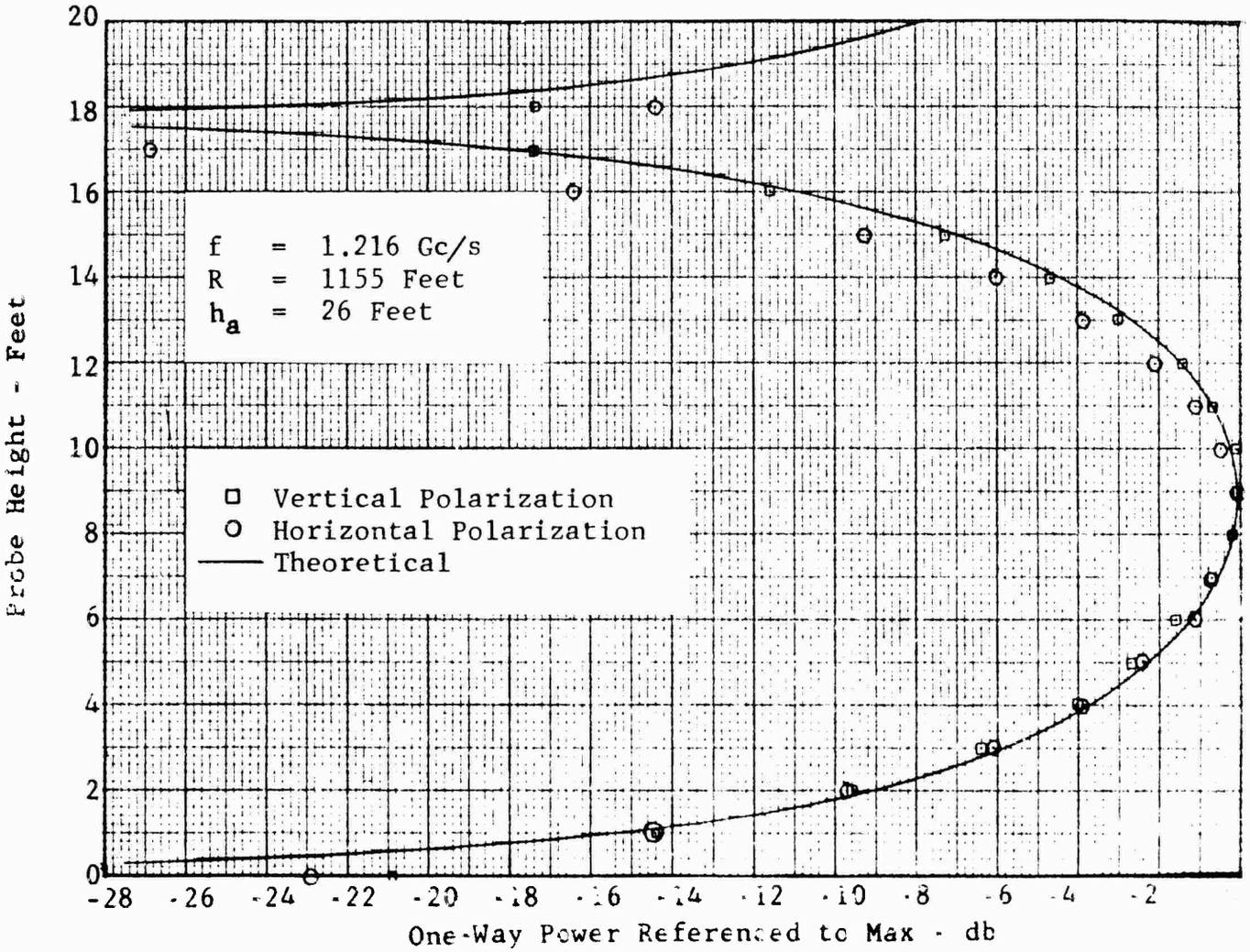

Fig 10 RESULTS FROM VERTICAL AMPLITUDE PROBE RECEIVE ANTENNA BAND 4

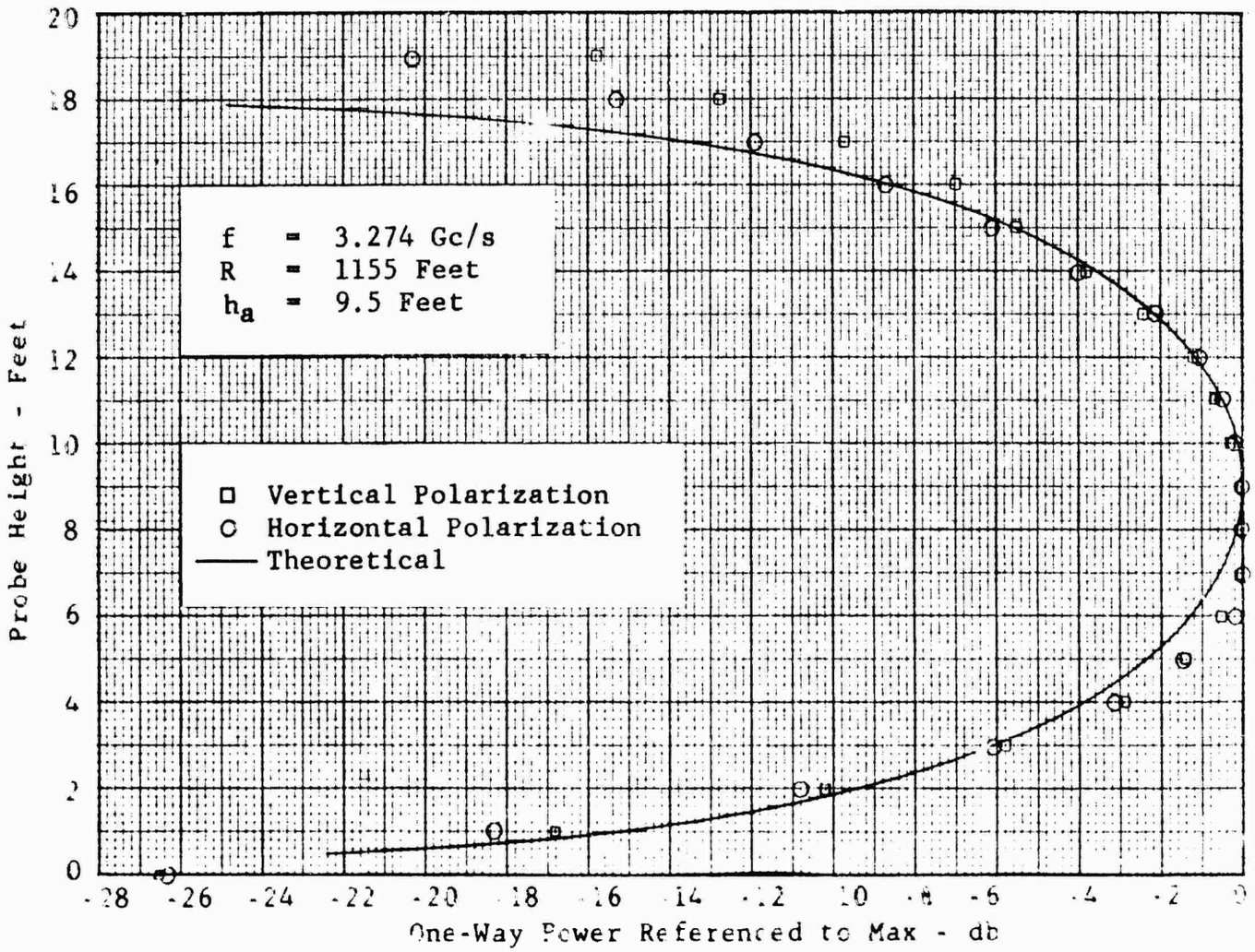

Fig 11 RESULTS FROM VERTICAL AMPLITUDE PROBE TRANSMIT ANTENNA BAND 5

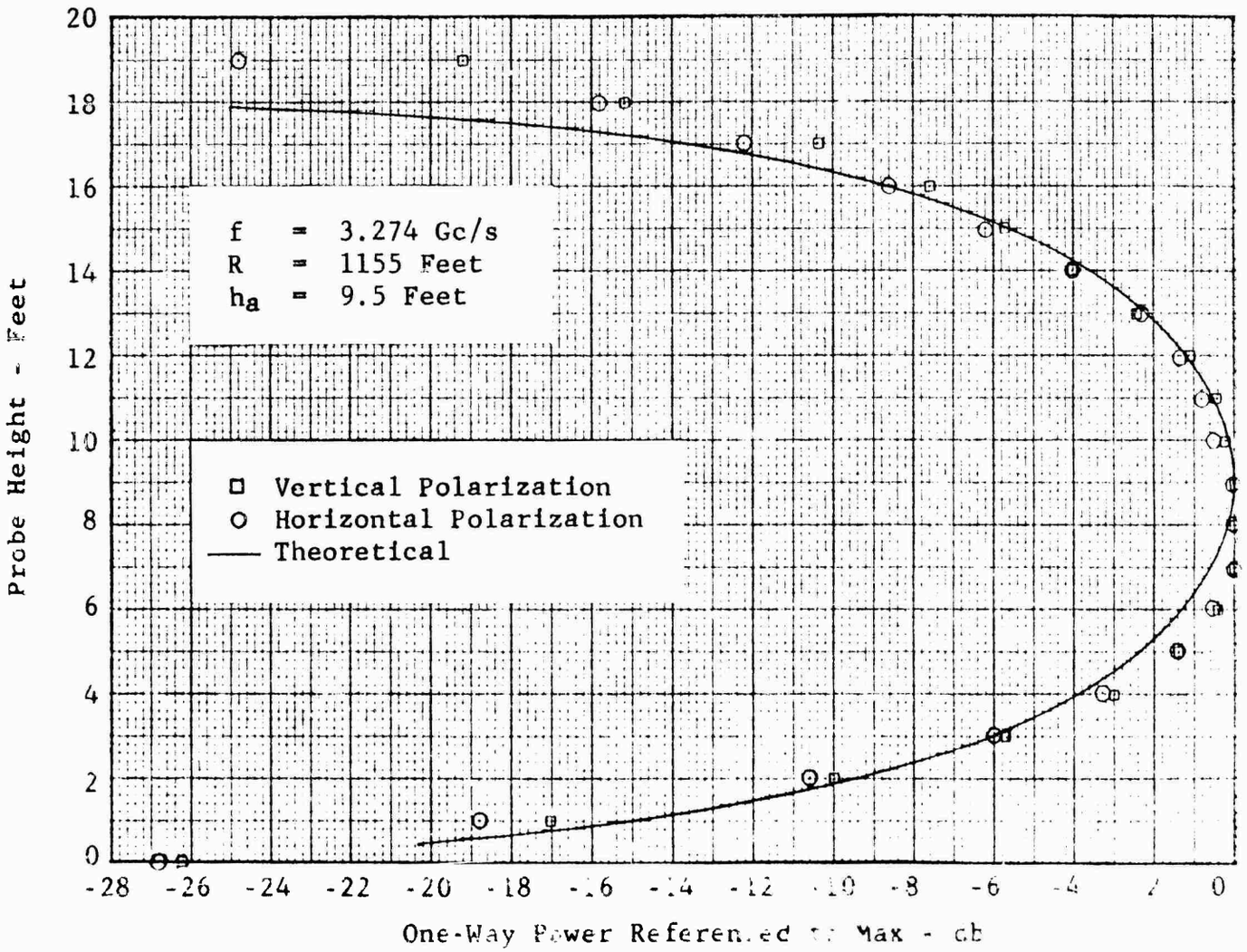

Fig 12 RESULTS FROM VERTICAL AMPLITUDE PROBE RECEIVE ANTENNA BAND 5

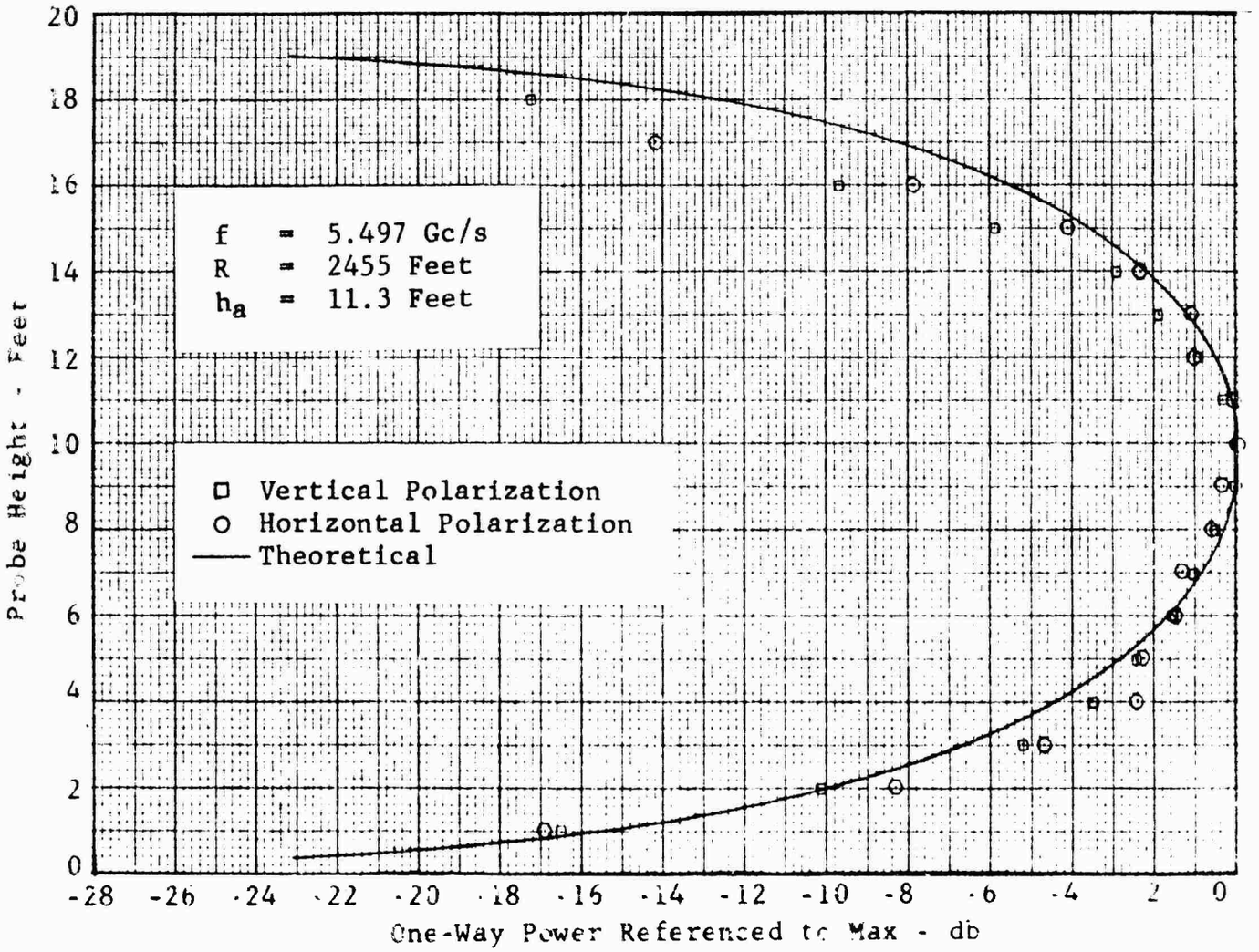

Fig 13 RESULTS FROM VERTICAL AMPLITUDE PROBE TRANSMIT ANTENNA, BAND 6

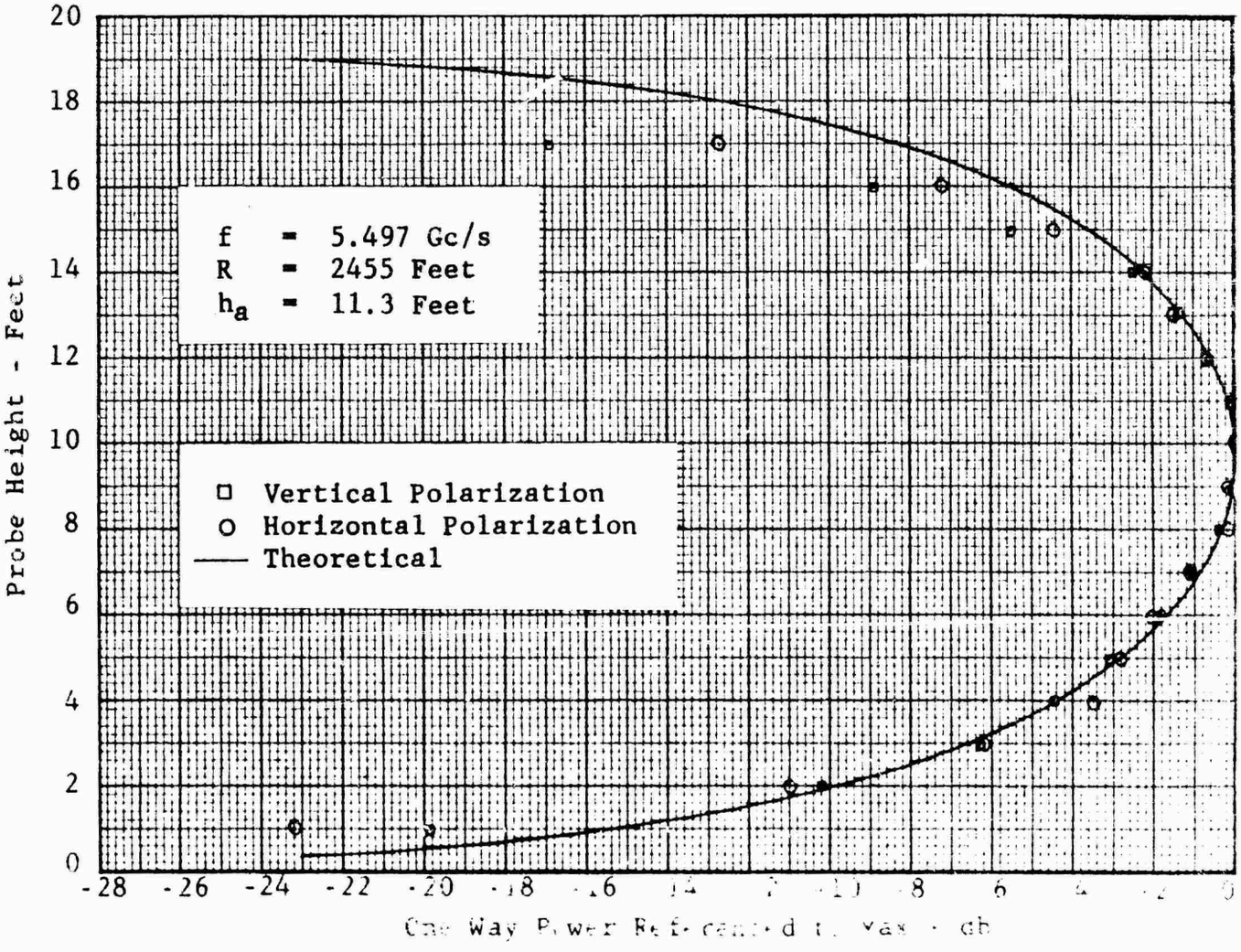

Fig 14 RESULTS FROM VERTICAL AMPLITUDE PROBE RECEIVE ANTENNA BAND b

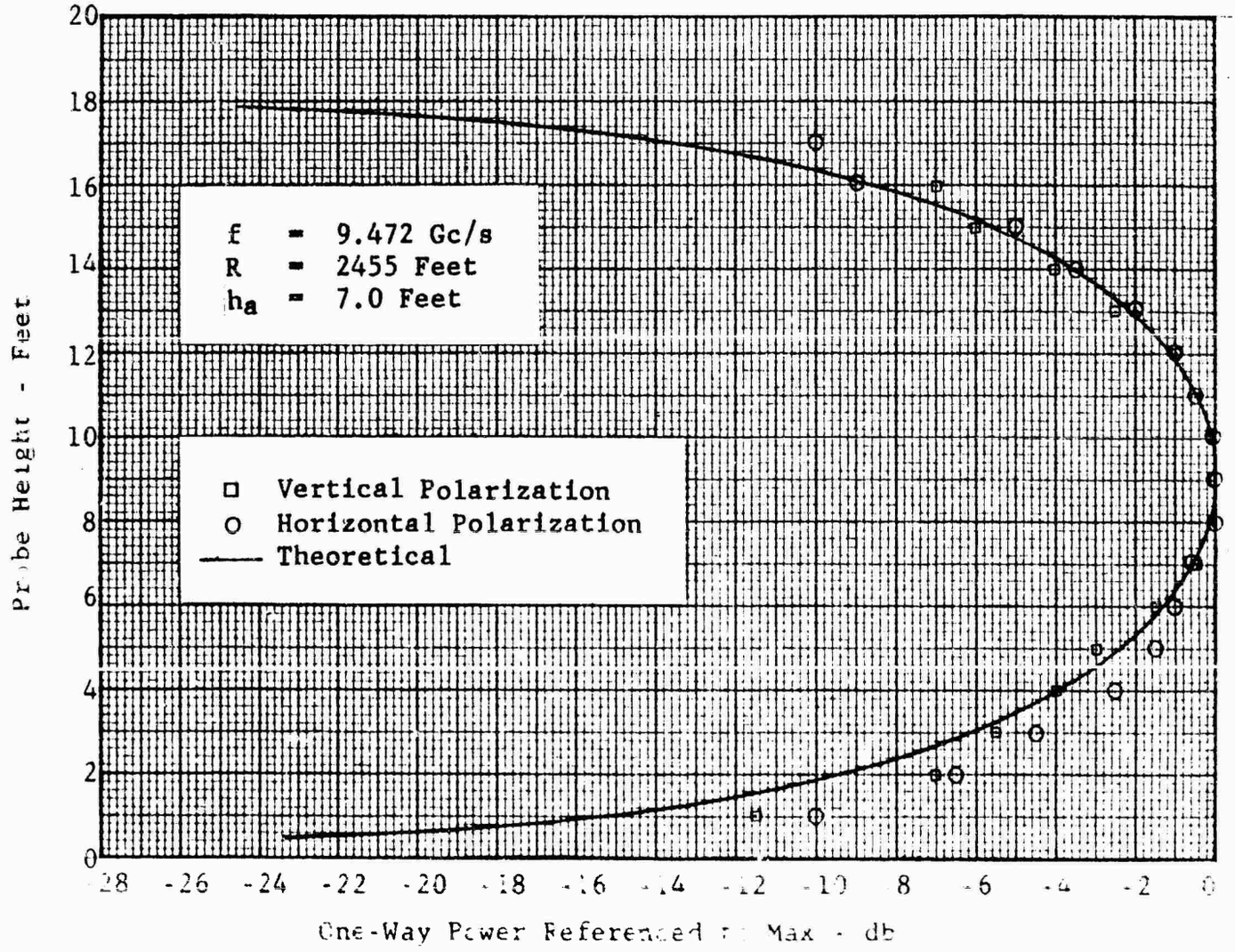

Fig 15 RESULTS FROM VERTICAL AMPLITUDE PROBE TRANSMIT ANTENNA BAND 7

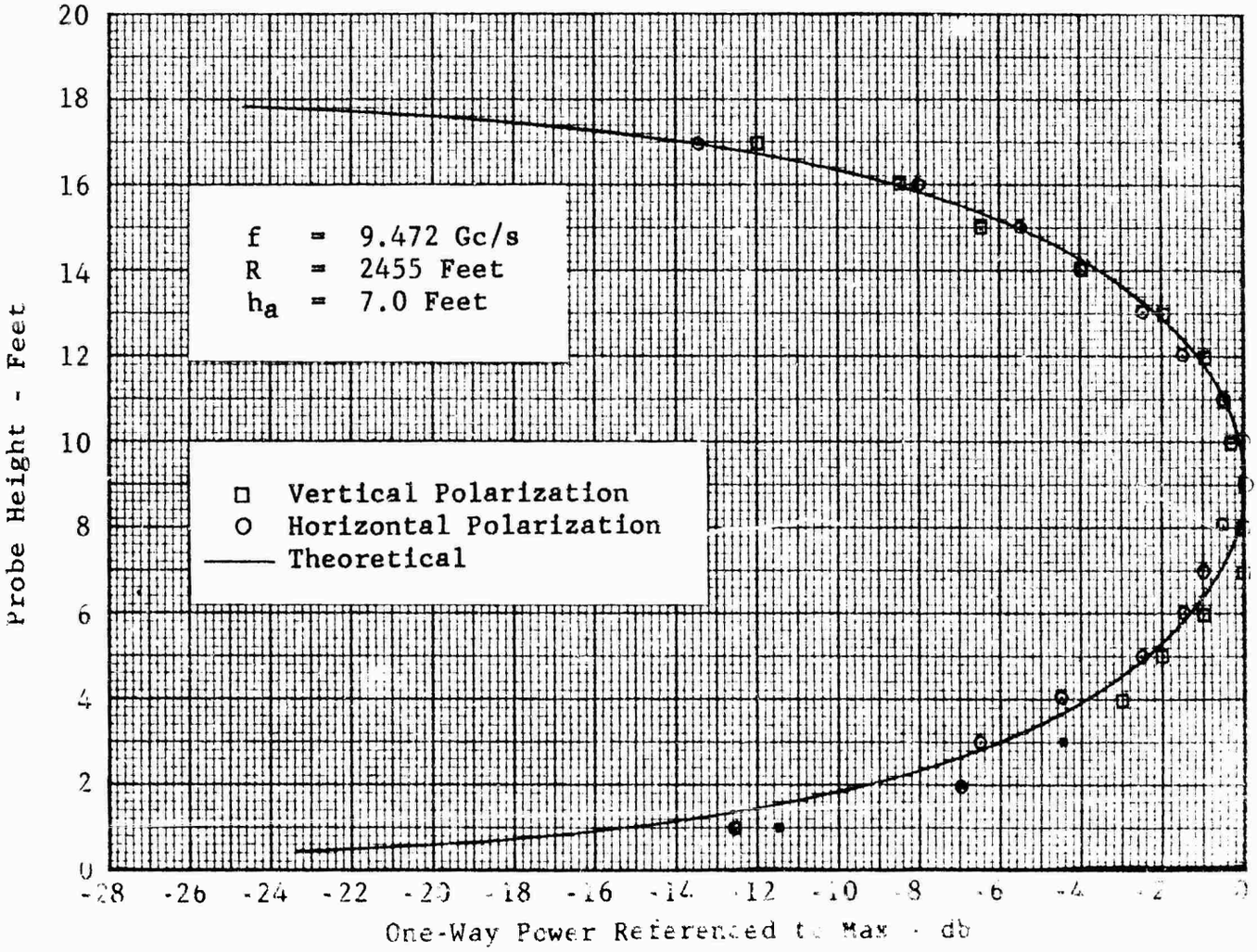

Fig 16 RESULTS FROM VERTICAL AMPLITUDE PROBE RECEIVE ANTENNA BAND 7

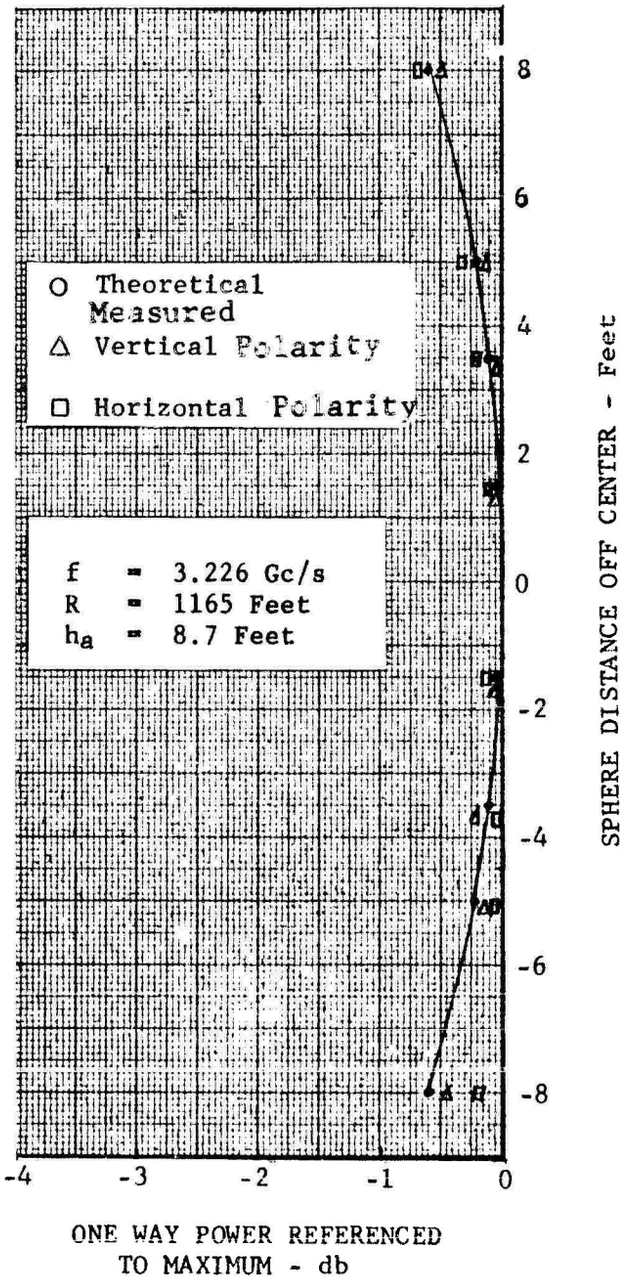

Fig. 17 RESULTS FROM HORIZONTAL AMPLITUDE PROBE

2. The two-member array had, in addition, been pitched at some unknown angle ψ (see Figure 18)

3. The phase centers of the spheres had not been aligned the same at each value of h_s (see Figure 5)

4. The interaction between the spheres and the Styrofoam support column in which the spheres were imbedded was noticeably a function of azimuth and sphere position.

In order to extract the desired information concerning the phase variation $\Phi(h_s)$, the following assumptions were made:

1. Along any tilt axis θ, as presented in Figure 18, the variation of $\Phi(h_s)$ from its true value due to a wobble (pitch) component ψ would be $\Phi(h_s) + k\Delta$ at an azimuth angle Γ and $\Phi(h_s) - k\Delta$ at azimuth angle $\Gamma + 180$ degrees. $k\Delta$ is a variation in phase from $\Phi(h_s)$ and is proportional to h_s and ψ when ψ is limited to small values.

2. Due to the physical geometry of the "sphere holder", the phase centers of the spheres had to be aligned exactly the same for each respective height h_s at 90 and 270 degrees azimuth.

3. The interaction between the spheres and their support was the same for the 90 and 270 degrees azimuth positions.

Based on these assumptions, values of $\Phi(h_s)$ may be computed by using the data obtained at azimuth angles of 90 and 270 degrees. The computed values are obtained through the use of Equation 17.

$$\Phi(h_s) = 1/2 \left\{ \left[\Phi(h_s) + k\Delta\right] + \left[\Phi(h_s) - k\Delta\right] \right\} . \quad (17)$$

Equation 17 gives $\Phi(h_s)$ along a tilt axis of unknown value. In order to compare the data obtained from Equation 17 with the theory given by Equation 12, the latter must be modified to include an arbitrary tilt angle θ. Knowing that the tilt angle in the experiment was less than 30 minutes and was toward the radar as shown in Figure 18, then the phase difference due to tilt, θ, equals $kh_s \sin\theta$, $0 \leq \theta \leq 1/2$ degree. This shift must be referenced to h_s in order to incorporate it into Equation 12. With this accomplished the new prediction is given by Equation 18.

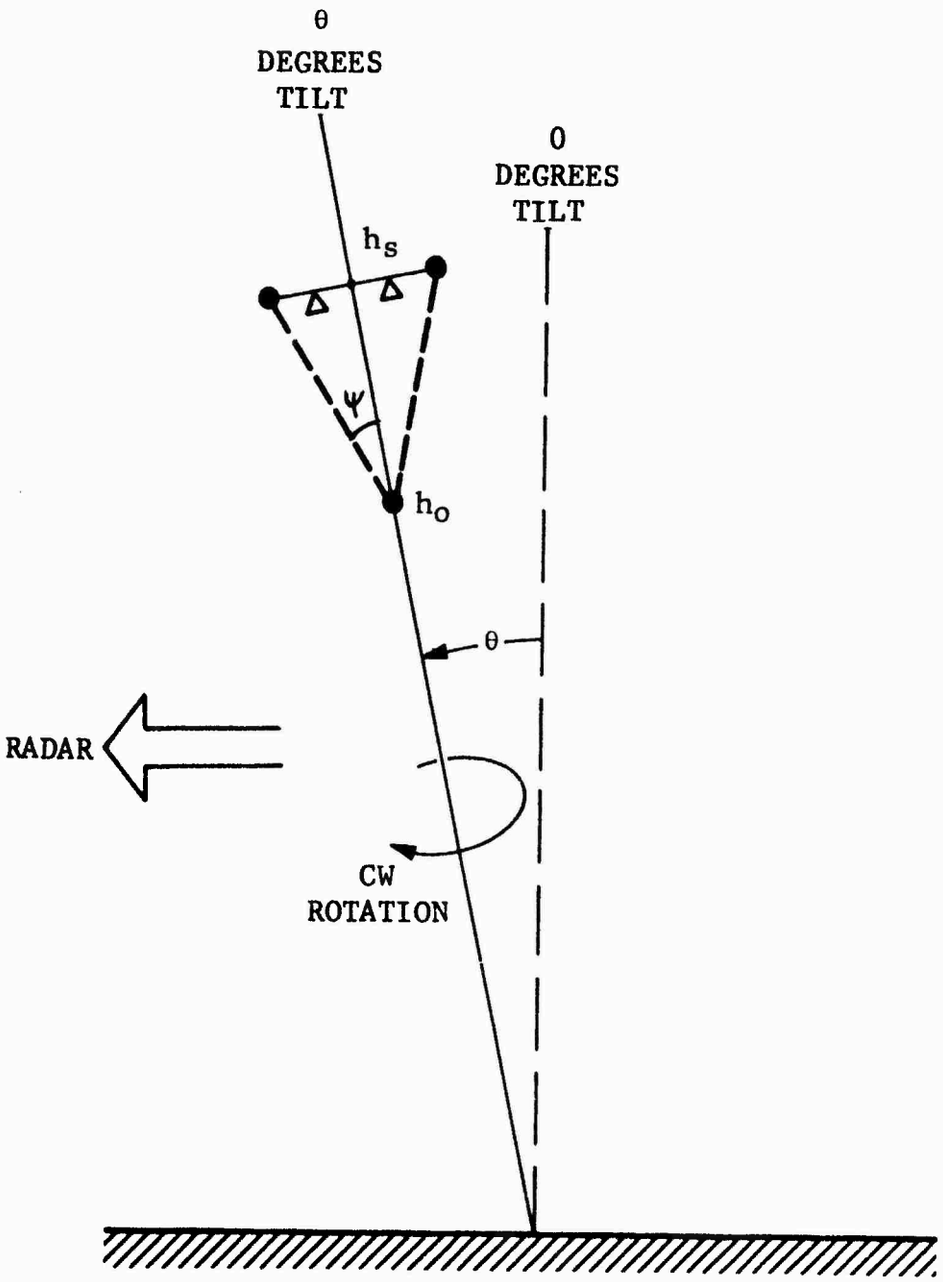

Fig. 18 TILT AND WOBBLE GEOMETRY, VERTICAL PLANE PHASE PROBE

$$\Phi(h_s) = kh_s \left(h_o/R + h_s/2R - \sin\theta\right) \qquad (18)$$

Figure 19 is a plot of $\Phi(h_s)$ as given by Equation 18 for tilt angles of 0, 10, 20, and 30 minutes. The measured data is also plotted on this figure, and it can be seen that there is good correlation between the theory and measured data for a tilt angle of about 23 minutes. This indicates that the measured phase front curvature corresponds closely to the elliptical curvature predicted by the model. By comparing Figure 19 with Figure 27 it can be seen that the choice of neglecting phase variations in the development of the vertical plane error model is backed by experimental evidence.

Figure 20 illustrates an arrangement that might be employed to obtain a vertical phase probe free of the complication that entered into the measurements discussed above. A sphere is mounted on a Styrofoam support column at the center of the rotator. A second sphere of equal cross section is fixed opposite the sphere on the rotator so that a 90-degree angle is obtained between the normal to the incident phase front and a line joining the two spheres. The rotator is then raised from an initial position h_i to a final position h_f at increments of $(h_i + \Delta h_j)$ for the horizontal and vertical polarization. This procedure would be repeated with the fixed sphere removed. With this procedure, the data obtained should be relatively free of the error sources mentioned earlier.

Horizontal Phase Probe

For the horizontal plane phase probe experiment, additional analysis was also required. The measured data indicated that the radar cross section scattering diagrams were not symmetrical around the zero-degree aspect position. In order to obtain an accurate value of θ (the azimuth angle), for the various sphere displacements, the patterns were shifted to achieve the property of symmetry. The measured data appear in Figure 21 where the theoretical data is also plotted. The cases for horizontal and vertical polarization are both presented. Again, agreement with the theory is quite good.

Near Field Error Test Data

Figures 22 and 23 illustrate the nature of the measurement results from the vertical plane experiment designed to isolate the near field error due to amplitude curvature in the vertical

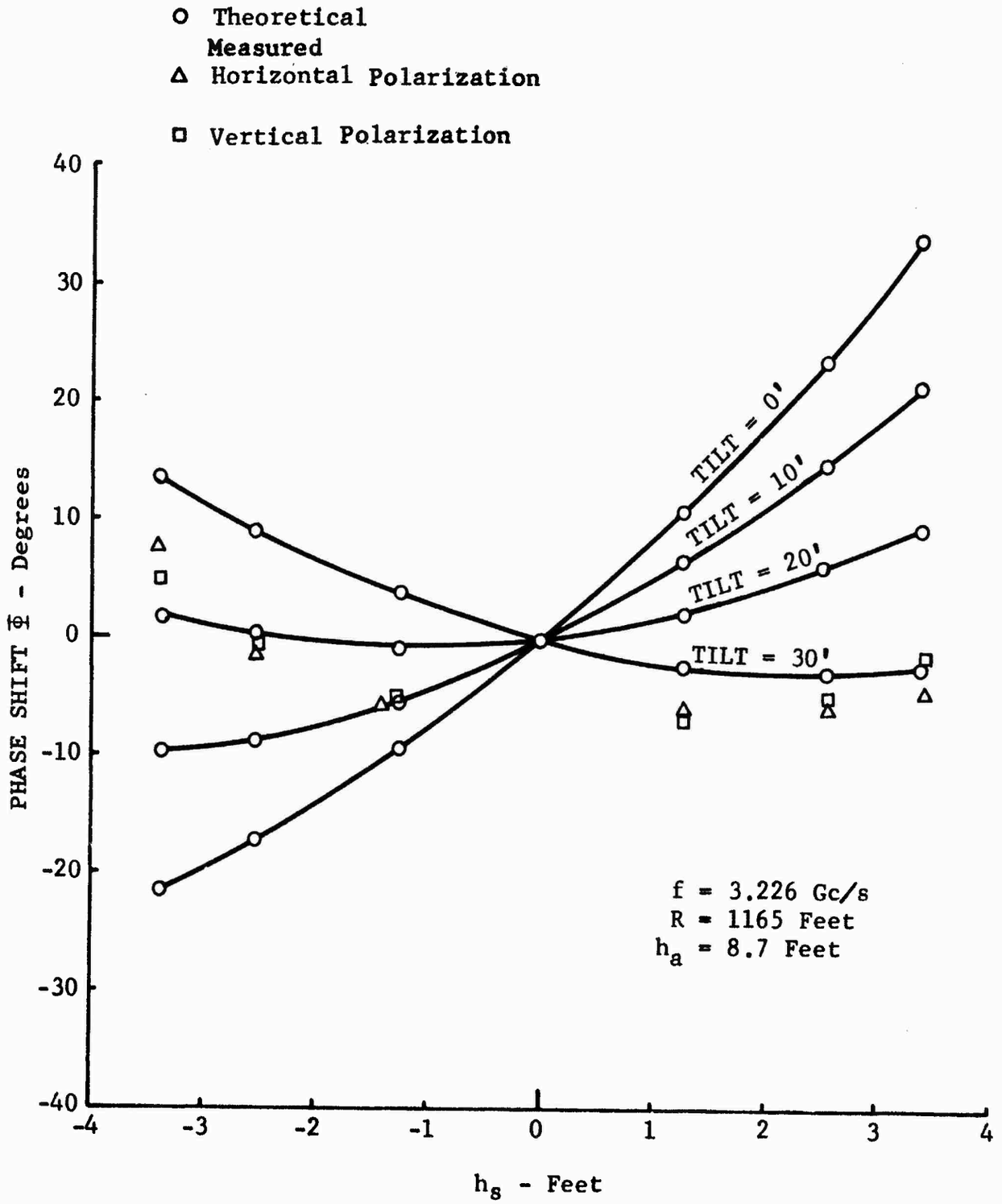

Fig. 19 RESULTS FROM VERTICAL PLANE PHASE PROBE

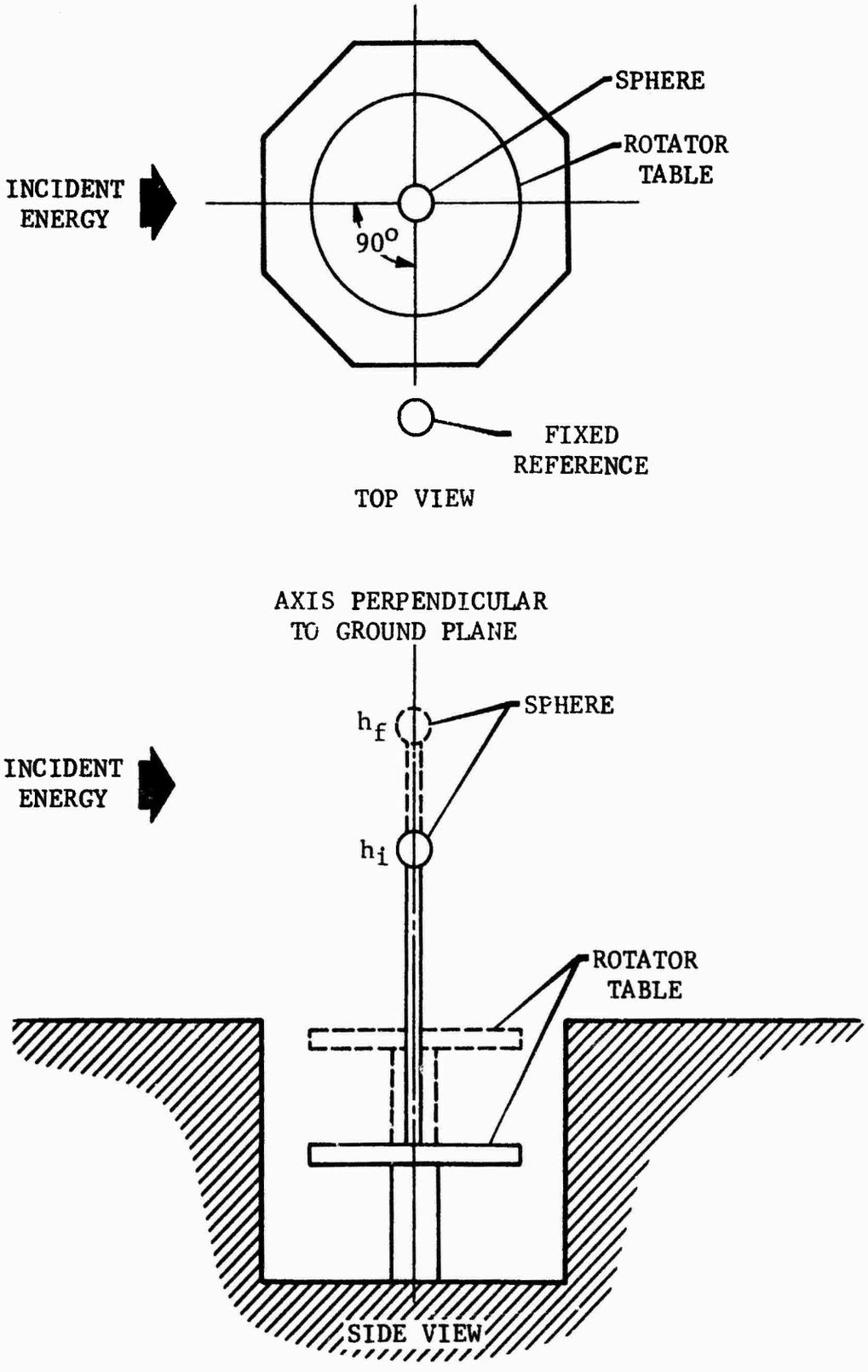

Fig. 20 MODIFIED VERTICAL PLANE PHASE PROBE GEOMETRY

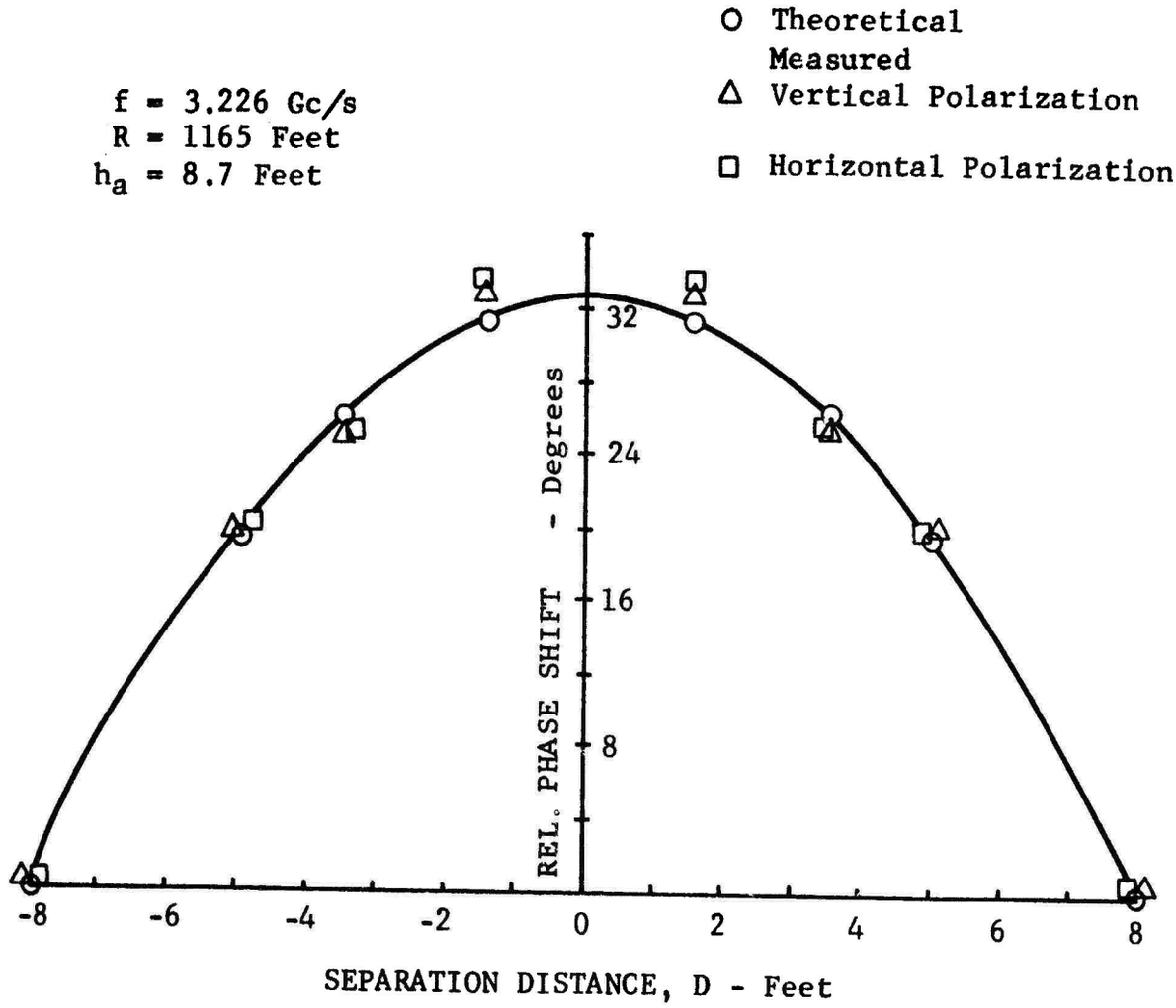

Fig. 21 RESULTS FROM HORIZONTAL PLANE PHASE PROBE

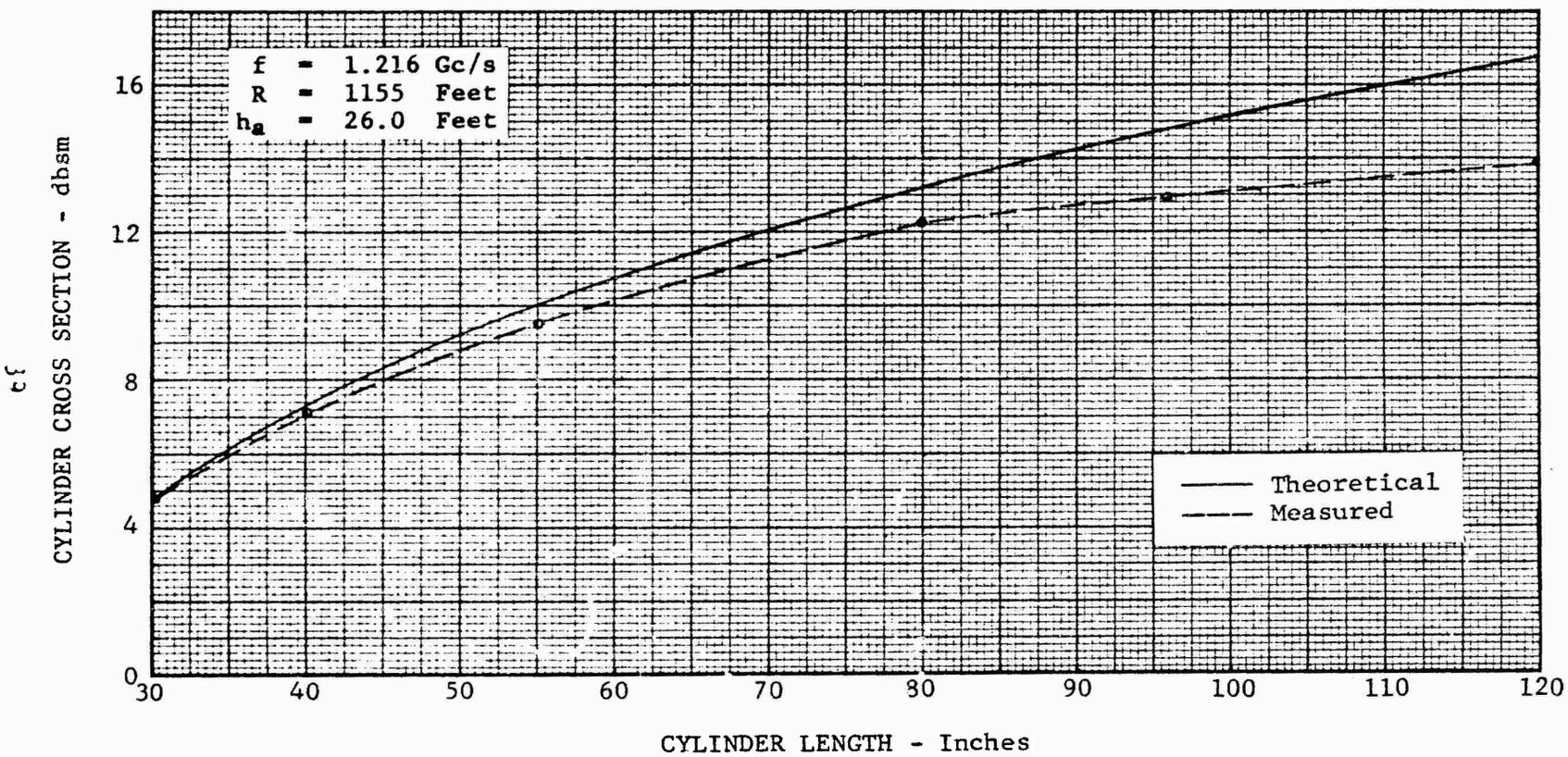

Fig 22 A COMPARISON OF THEORETICAL AND MEASURED CYLINDER CROSS SECTION, VERTICAL POLARIZATION

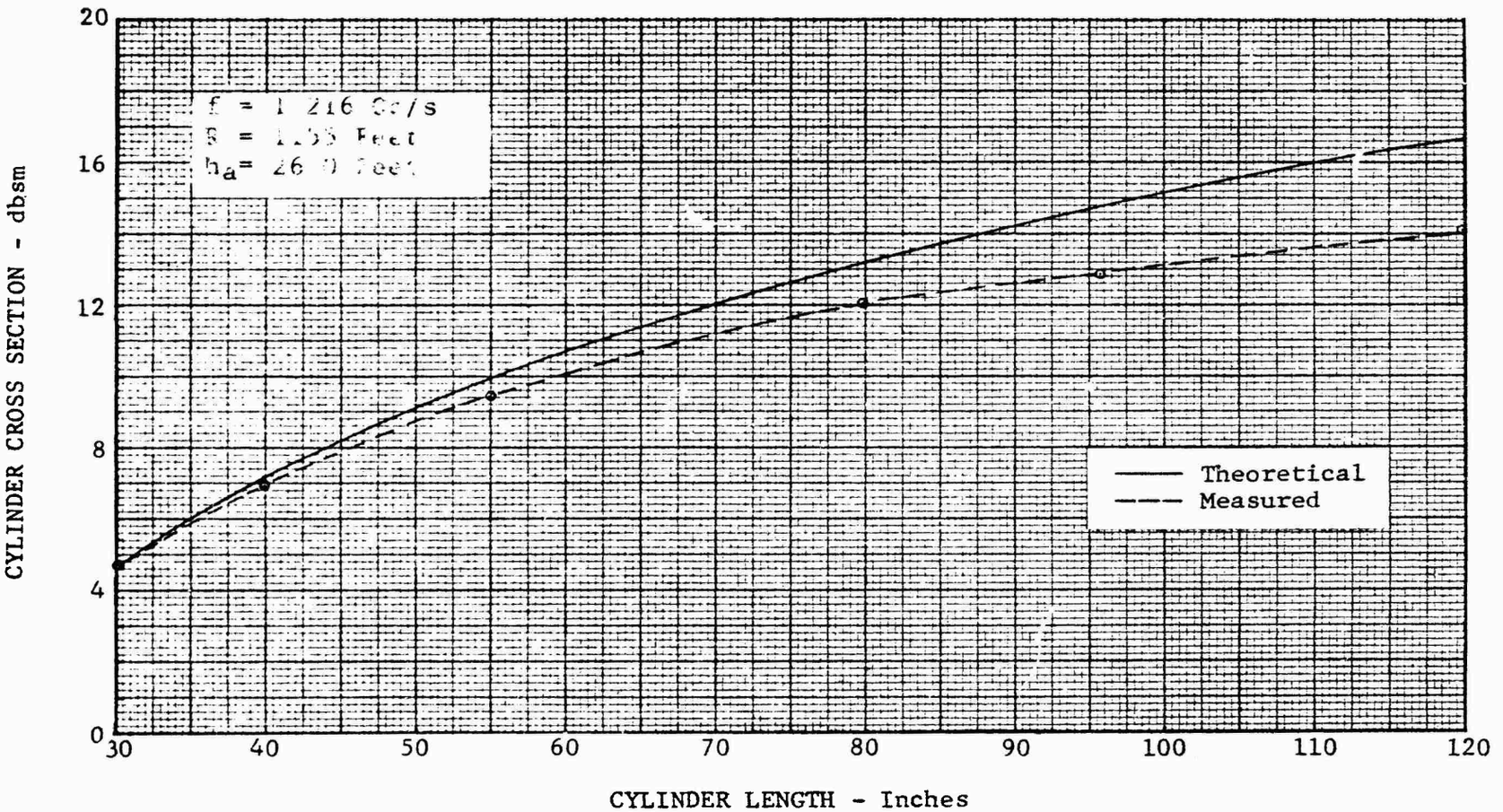

Fig 23 A COMPARISON OF THEORETICAL AND MEASURED CYLINDER CROSS SECTION, HORIZONTAL POLARIZATION

plane. Shown here for both polarization cases are the comparisons between the measured values of cylinder cross section and the theoretical values. From this information Figures 24 and 25 can be obtained. On these figures measured near field error is compared with values predicted by the theoretical relationship given in Equation 5. Since this relationship does not take into account any effect of nonuniform phase, the ordinate intercept of the best-fit line on these figures provides a good indication of the extent to which near field error has been isolated. This follows from the fact that the error predicted by the model should be less than the measured error. In both horizontal and vertical polarization the error due to sources other than near field effects was, for this experiment, about 0.25 db. Apparently Equation 5 provides a slightly better description of near field error for the case of horizontal polarization than for the case of vertical polarization. In terms of the actual target used in this test, Figures 26 and 27 illustrate the effectiveness of the theoretical relationship when it is employed to correct the near field error.

Shown in Figures 28 and 29 are the cross section scattering diagrams for a horizontally mounted ten-foot cylinder. These provide a strong indication of the validity of the near field error model for the horizontal plane. That is, the results indicate that error due to field curvature in the horizontal plane is very small in comparison to the error due to field curvature in the vertical plane for the same length target. This fact is in agreement with the theoretical error displayed in graphical form in Figures 2 and 4.

Results of Near Field Error Investigation

In summary, the near field error investigation has shown the following:

1. The vertical plane amplitude pattern given by Equation 3 provides a good first-order approximation for calculating the field patterns as a function of the range parameters h_a, h_t, R, and λ, at least in the frequency range of 1 to 10 gigacycles.

2. The vertical plane phase front pattern given by Equation 4 appears to provide a good approximation for calculating the phase distribution across a target for the range parameters discussed in this report.

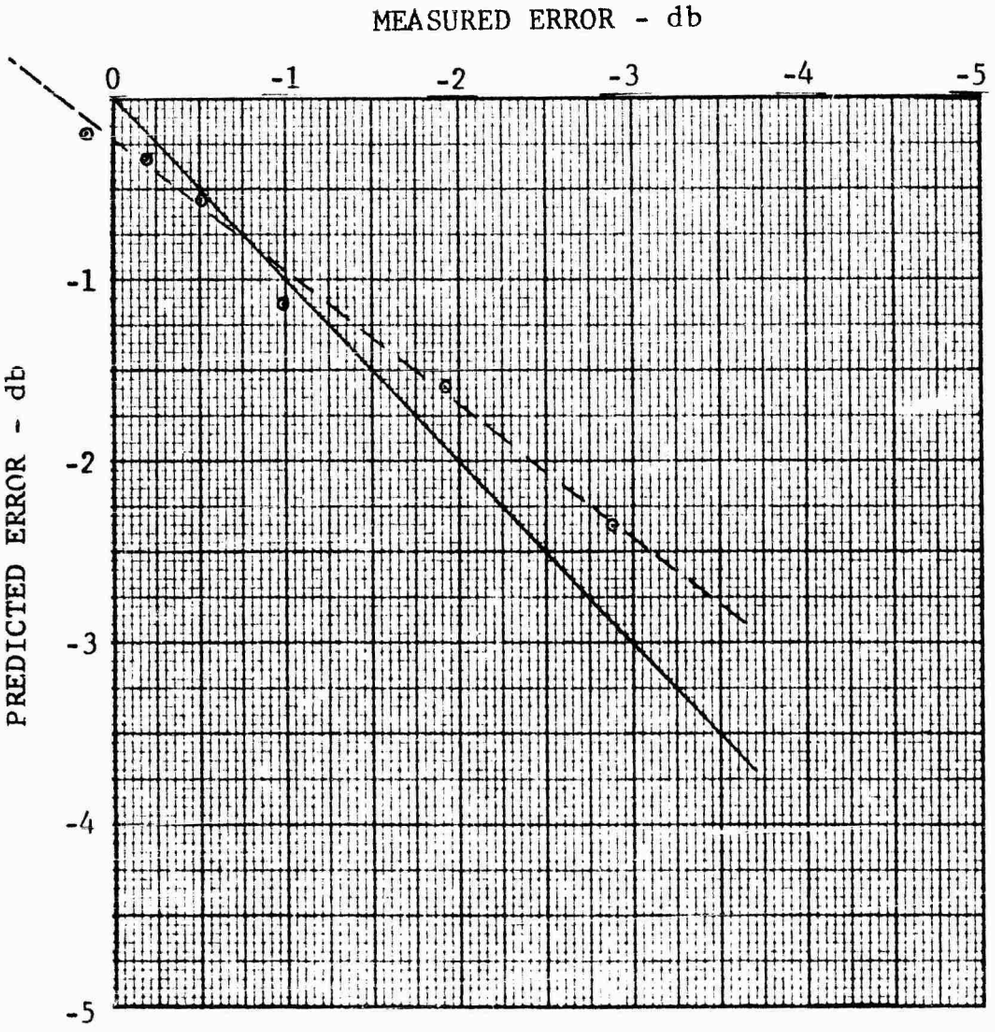

Fig 24 A COMPARISON OF PREDICTED AND MEASURED NEAR FIELD ERROR VERTICAL POLARIZATION

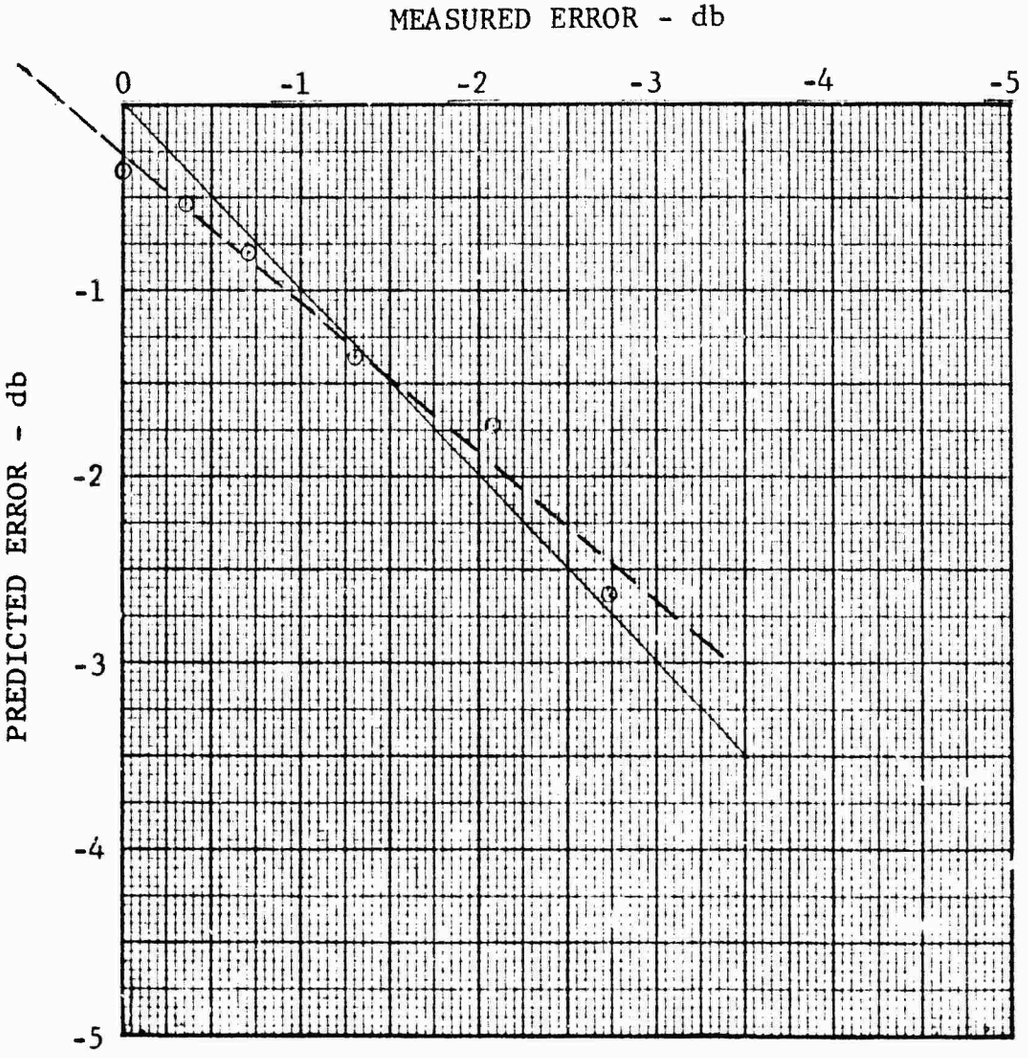

Fig 25 A COMPARISON OF PREDICTED AND MEASURED NEAR FIELD ERROR HORIZONTAL POLARIZATION

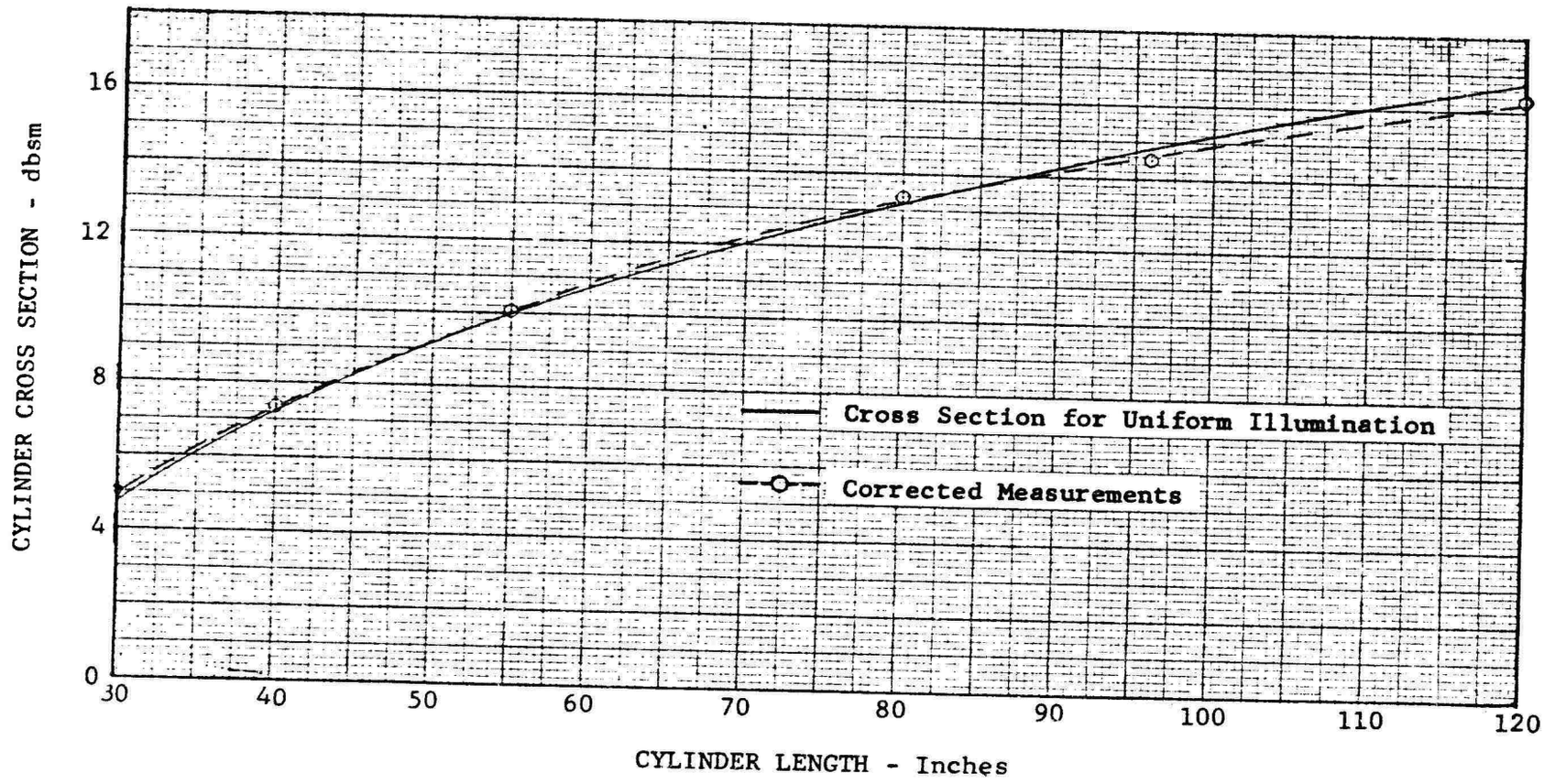

Fig. 26 A COMPARISON OF THEORETICAL AND CORRECTED MEASURED CYLINDER CROSS SECTION, VERTICAL POLARIZATION

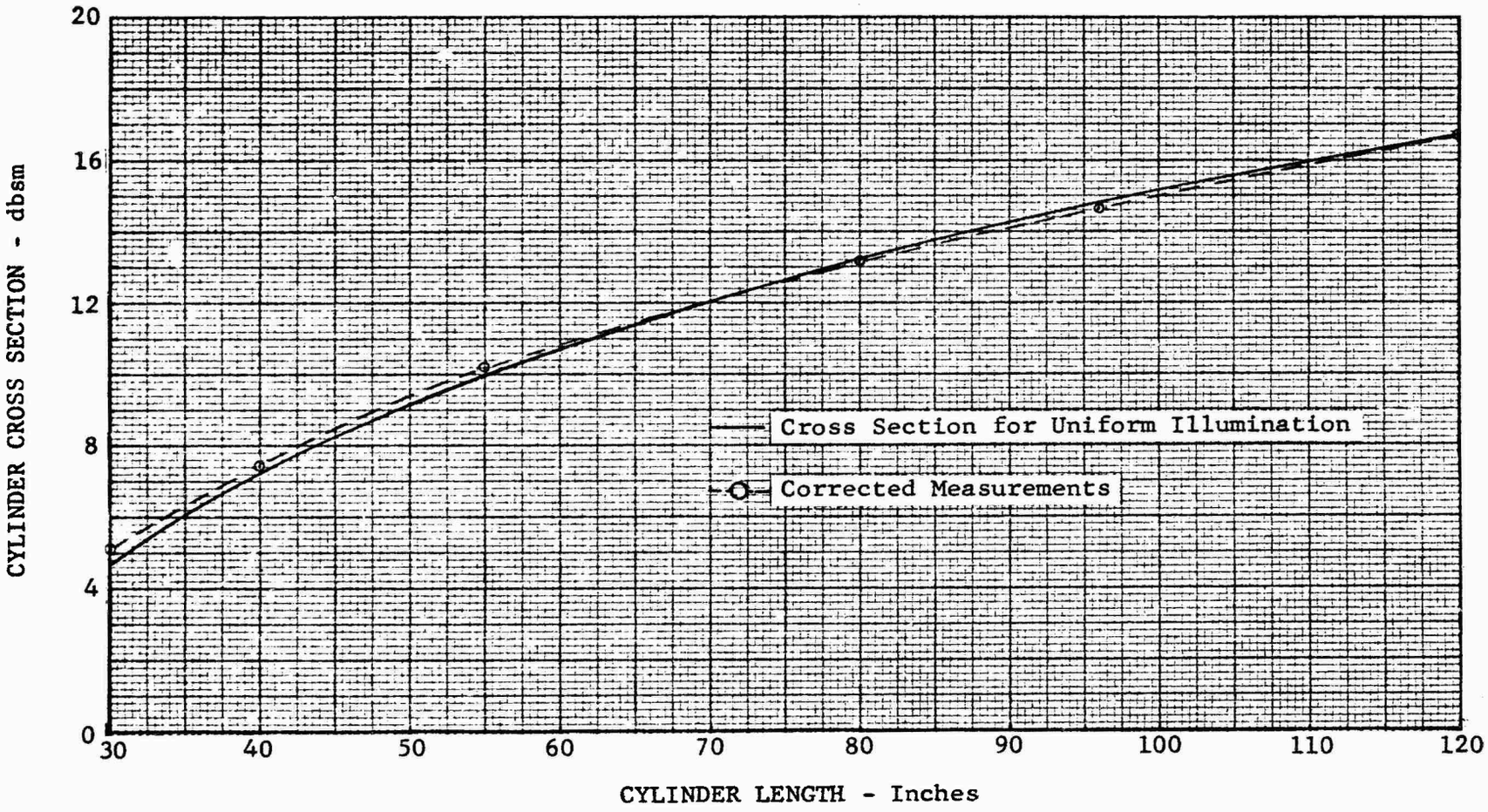

Fig. 27 A COMPARISON OF THEORETICAL AND CORRECTED MEASURED CYLINDER CROSS SECTION, HORIZONTAL POLARIZATION

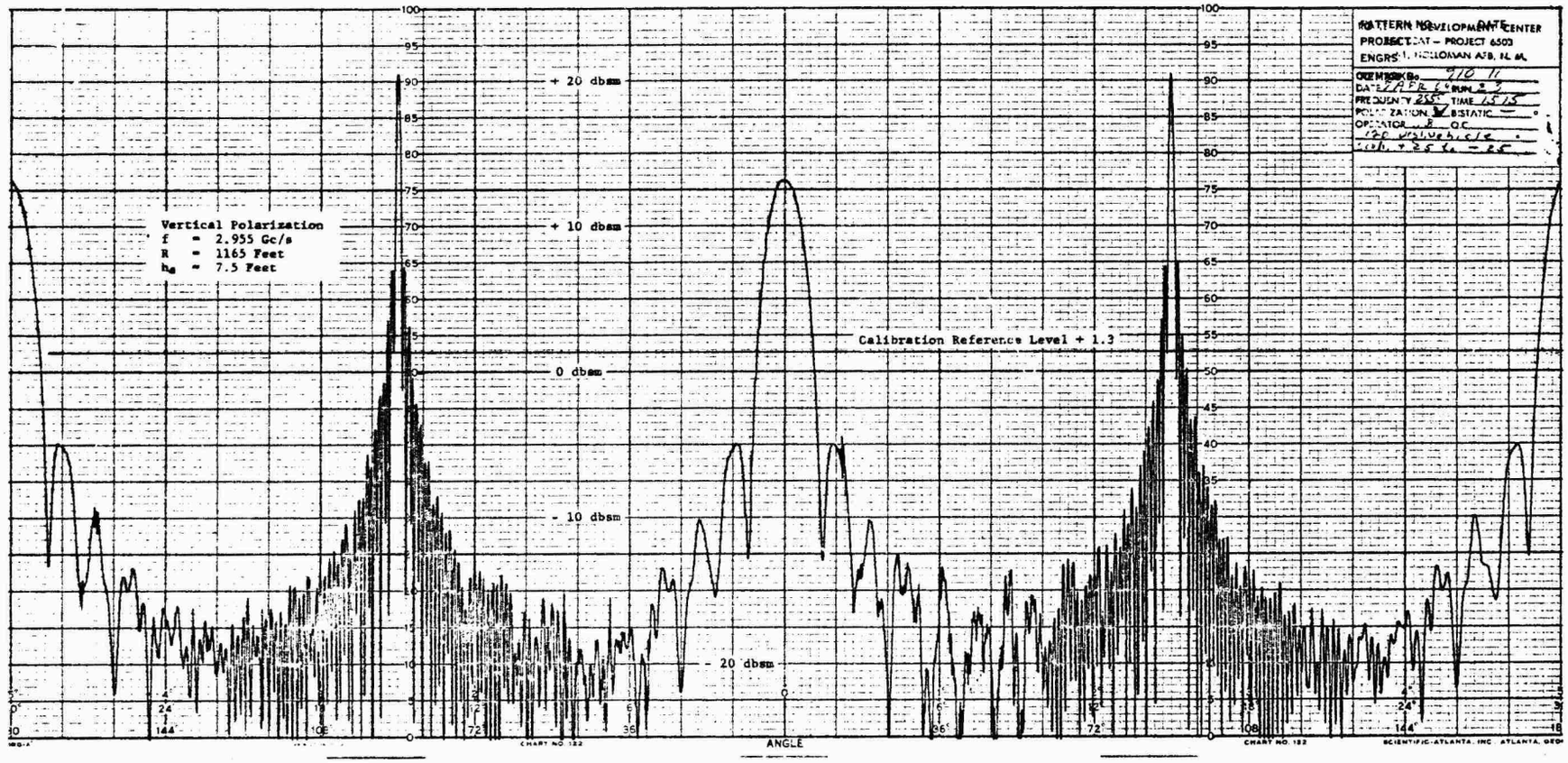

Fig. 28 RADAR CROSS SECTION SCATTERING DIAGRAM FOR A HORIZONTALLY MOUNTED 10-FOOT CYLINDER, VERTICAL POLARIZATION

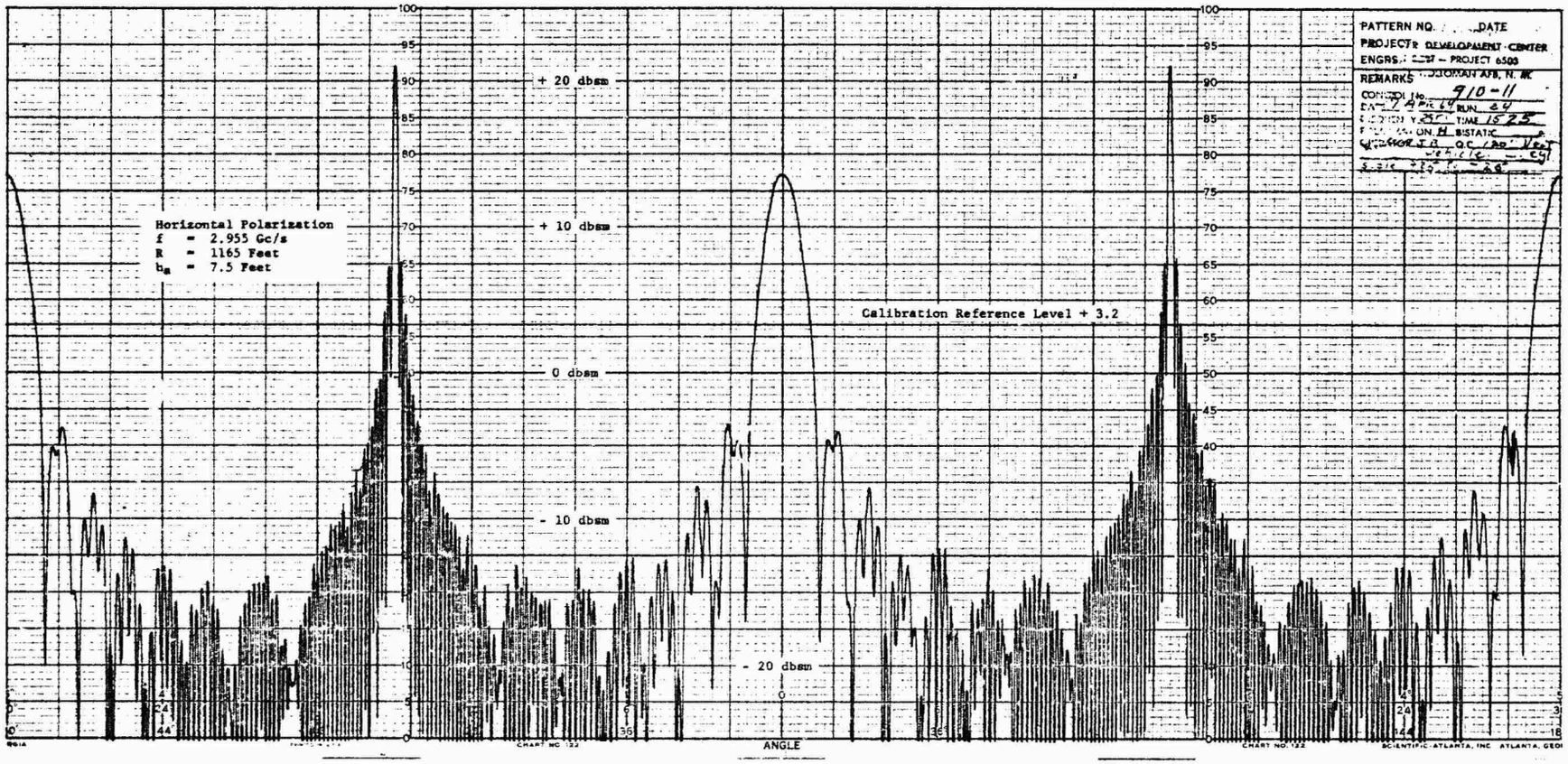

Fig. 29 RADAR CROSS SECTION SCATTERING DIAGRAM FOR A HORIZONTALLY MOUNTED 10-FOOT CYLINDER, HORIZONTAL POLARIZATION

3. The horizontal amplitude pattern closely approximates the far field amplitude expression for a uniformly illuminated circular aperture.

4. The horizontal phase variation across the target is closely approximated by Equation 7, the expression for a spherically diverging wave.

5. The vertical plane error model given by Equation 6 provides a first-order approximation for calculating the near field error for a target whose single characteristic dimension is oriented in the vertical plane.

6. The horizontal plane error model given in Equation 9 provides a first order approximation for calculating the near field error for a target whose single characteristic dimension is oriented in the horizontal plane.

7. In view of Items 5 and 6 above, the general description for near field error given in Equation 10 may be simplified to obtain the near field error incurred in the measurement of the radar cross section of a rectangular target whose cross section is proportional to the square of its area. In Equation 10 the amplitude and phase distributions can be approximated by the distributions in Equations 5 and 8, respectively, as indicated in Equation 19.

$$E'_{nf} = \left| \int_0^1 \int_0^1 A^2(D'_V) \; \epsilon^{-i2\phi(D'_H)} \; dD'_H \, dD'_V \right|^2 . \quad (19)$$

Inspection of this relationship reveals that it can be simplified further into the form given by Equation 20. Here the total near field error is expressed in db

$$E_{nf} = (E_{nf})_v + (E_{nf})_h , \quad (20)$$

where

$(E_{nf})_v$ = vertical plane near field error as given by Equation 6

$(E_{nf})_h$ = horizontal plane near field error as given by Equation 9.

Figure 30 represents plots of constant near field error contours in the (K_H, K_V) plane. This curve provides an upper bound type estimate of the near field error for targets distributed more of less uniformly in the horizontal and vertical plane (i.e., obviously there are special case targets such as three spheres for which the two-dimensional distribution is not uniform). The use of the curves requires only that the maximum vertical and horizontal dimensions of the normal plane projection of the target be known, along with the pertinent range parameters λ, R, and h_a.

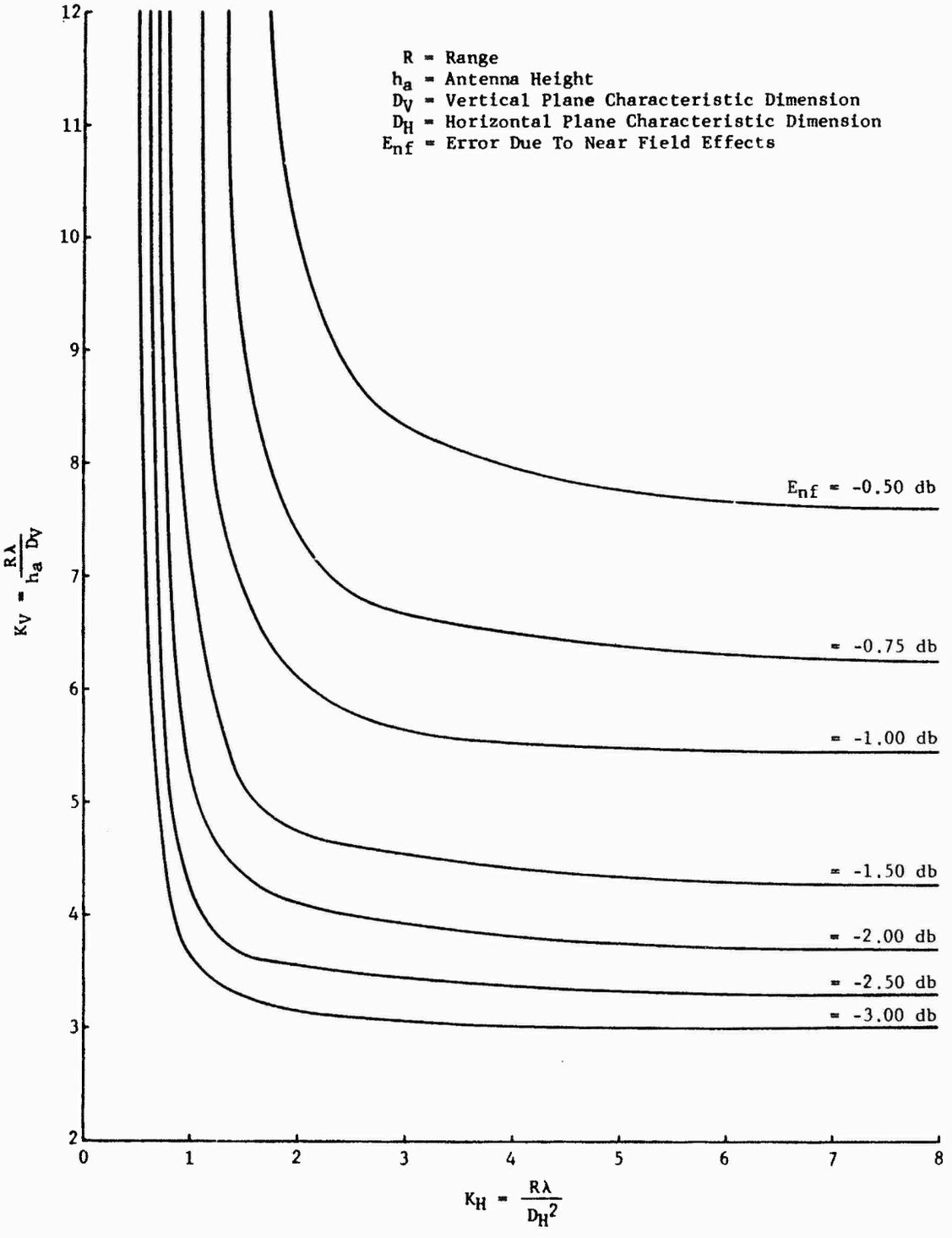

Fig. 30 NEAR FIELD ERROR ESTIMATE FOR AN ARBITRARY TARGET

SECTION 3

BACKGROUND ERROR INVESTIGATION

General

During the process of radar cross section measurements the presence of noise signals anywhere in the system will alter the measured data. Since the presence of a certain amount of noise is apparently inevitable, the practical approach to the situation (once the noise has been minimized) is to try to establish those conditions under which the errors due to noise become serious. If this can be accomplished these conditions can be either avoided or appropriately considered; hence, the concern over errors due to noise is reduced. It is convenient to separate the types of noise that occur into two groups; (1) noise that originates in the propagation path of the system and (2) noise that originates in the receiver section of the system. Noise signals of the first type must be carefully defined in order to distinguish them from propagation path error sources described in Section 4 (Extraneous Illumination Error Investigation). Of interest in this section is the background noise which can be defined as the radar return from the target support system as measured without a target. The receiver noise will be discussed in Section 5 (Calibration and Instrumentation Errors).

Theoretical Model

It is convenient to consider the amplitude and the phase of the background return as random variables. In fact, this becomes necessary if any general error analysis is to be undertaken. Here general error analysis denotes one applicable to a significantly large class of targets, ideally the class of all targets. Thus, the sort of information one can obtain on background error will necessarily be statistical in nature. This information should, however, be sufficient to establish the conditions under which the noise is of interest.

Neglecting coupling errors, the error due to background noise is defined in Equation 21.

$$E_b = \frac{\sigma_m}{\sigma_t} = 1 + \frac{\sigma_b}{\sigma_t} + 2\sqrt{\frac{\sigma_b}{\sigma_t}} \cos \Delta\phi \,, \qquad (21)$$

where

σ_m = measured value of cross section

$\sqrt{\sigma_t}$ = target return

$\sqrt{\sigma_b}$ = background return

$\Delta\phi$ = phase of $\sqrt{\sigma_b}$ with respect to $\sqrt{\sigma_t}$.

E_b is a random variable since it is a function of random variables. That is, from the definition in Equation 21, E_b is seen to be a function of σ_t, σ_b, and $\Delta\phi$. None of these are, in the general sense, subject to exact prediction. The density for E_b can theoretically be obtained if the necessary probability densities involving these three quantities are known. Unfortunately the density of σ_t for the class of all targets is not readily available. This difficulty can be avoided, however, if the error density is to be found for a given target level. With this condition the following assumptions were chosen as being the most appropriate:

1. σ_b and $\Delta\phi$ are statistically independent

2. $\Delta\phi$ is equally likely to take on any discernible value, specifically, $\Delta\phi$ is uniformly distributed on the range $-\pi$ to $+\pi$ radians

3. Empirical background noise information obtained in the absence of an actual target can be used to generate the density of σ_b for a fixed type of target support.

On the basis of these assumptions, it can be shown that the probability density function for background error E_b is given be Equation 22 (Reference 4).

$$p_{E_b}(E_b') = \frac{1}{\pi} \int_{K_{min}}^{K_{max}} p_K(K') \left| J(K', E_b') \right| dK' , \quad (22)$$

where

K = σ_b / σ_t, relative background noise for fixed target level σ_t

$p_K(K')$ = probability density for K

$J(K', E_b')$ = Jacobian transform between the random variables K, $\Delta\phi$ and K, E_b.

Integration of Equation 22 with respect to E_b' yields the cumulative density function for background error as shown in Equation 23.

$$P(E_{b_1} \leq E_b' \leq E_{b_2}) = \int_{E_{b_1}}^{E_{b_2}} p_{E_b}(E_b')dE_b' \quad . \qquad (23)$$

Thus, for a given target level, the limits on the background error between which any specified percentage of all possible background errors lie, can be estimated. Here, then, is a model that permits the examination of conditions under which the errors caused by noise become serious.

Test Program

The nature of the assumptions used to arrive at a model for the error due to background noise restricts the extent to which the model can be tested. However, the validity of the model is obviously most dependent on whether or not the background noise density exhibits statistical regularity. To induce statistical regularity the type of, and conditions for, measurement of the target support were of primary concern in designing the test program.

Particularly important in an experiment of this type is the degree of control of the "fixed" parameters involved (i.e., parameters which are normally fixed during target cross section measurement). For this experiment, background noise data was recorded under the following conditions:

1. The geometry of the target support system was fixed for each frequency of interest in that the target supports were circular Styrofoam columns, 16 inches in diameter.

2. The state of the D/λ parameter was fixed for each frequency of interest in that the target support systems were tuned to achieve minimum radar return (D denotes column diameter).

3. The relative column illumination was fixed for each frequency of interest in that the peak of the first lobe was placed at the top of the target support column.

4. The state of the target aspect control system was fixed for each frequency of interest in that the perimeter of the pit and the rotator table were covered with RAM; also, the table was tilted to place the support column at broadside aspect.

5. The polarization states of the illuminating field were fixed for each frequency in that data were taken only for horizontal and vertical polarization.

The degree of statistical regularity exhibited by the background noise is largely determined by the extent to which these conditions are controlled. If no attempt is made to keep such conditions fixed, then very large samples of noise will be required to establish the desired probability density. In certain other data, one of the above conditions has been intentionally varied in an attempt to include its variation in the overall statistics of the background noise. That condition was the relative column illumination level. It is of interest because the illumination level of the support column cannot be considered to be constant for every actual measurement of a target cross section. If the noise densities for several illumination levels exhibit the same characteristic shape then one could reasonably conclude that the primary effect of varying column illumination level is varying the mean value of the density.

A history of the background noise for a given frequency can be conveniently generated by sampling the background return as the aspect of the target support system is varied. The number of samples of noise that can be taken during a 360-degree aspect variation is limited only be the rate capability of the sampler employed. For this experiment, the limit was ten samples per degree of aspect change and the data was digitally recorded on punched paper tape.

The gathering of such samples requires that background noise be as completely isolated as possible. The error source due to receiver noise cannot be conveniently removed from the experiment.

However, as shown in Section 5 (Calibration and Instrumentation Errors), this error source was relatively unimportant in comparison to the background error.

Test Results

Noise densities and error densities were generated by using the samples of the background noise obtained in the manner described in the previous section. Noise densities and means were generated from appropriate samples with the aid of a finite density approximation and the standard estimate for mean. The operation indicated in Equation 22 was carried out be approximating the integral with a finite summation. Adding to the convenience of such an approximation is the fact that the actual noise density is readily available only in the form of an array of ordered pairs. Likewise, the operation on the right side of Equation 23 was conveniently approximated by the use of finite summation. Each of the three basic steps listed above, as well as numerous other minor steps, were described in Fortran IV and carried out with the aid of an IBM 7090 Digital Computer.

Shown in Figures 31 through 38 are background noise densities in log space along with the appropriate cross section plots from which the densities were generated. These figures show the distributions of background noise in db after shifting to a position of zero mean. Shown on each figure are the operation conditions under which the cross section data was generated. Also shown are the mean levels of the noise. These curves were all generated under the system of experimental control previously outlined. Figures 39 and 40 represent noise densities that were generated under the altered condition mentioned earlier. The column illumination level, which was used to generate the data shown in Figure 31, was allowed to vary. This variation was used in an effort to determine the effect that this parameter would impose on the shape of the noise density curve. Also shown in Figures 39 and 40 are the corresponding curves for the fixed illumination level of Figure 31. Figures 41 through 44 illustrate the final form of the results obtained from the described analysis. These figures are descriptively termed percentile error curves. They represent the bounds, for specific conditions, within which the background errors lie (worse case curves) and the bounds within which 90 percent of the errors lie.

To examine the statistical regularity of the data in a manner different than that described above, the mean levels of the background (for fixed column illumination level) as a function of frequency were compared with the theoretical variation derived in a separate investigation. In Figure 45 values of the measured

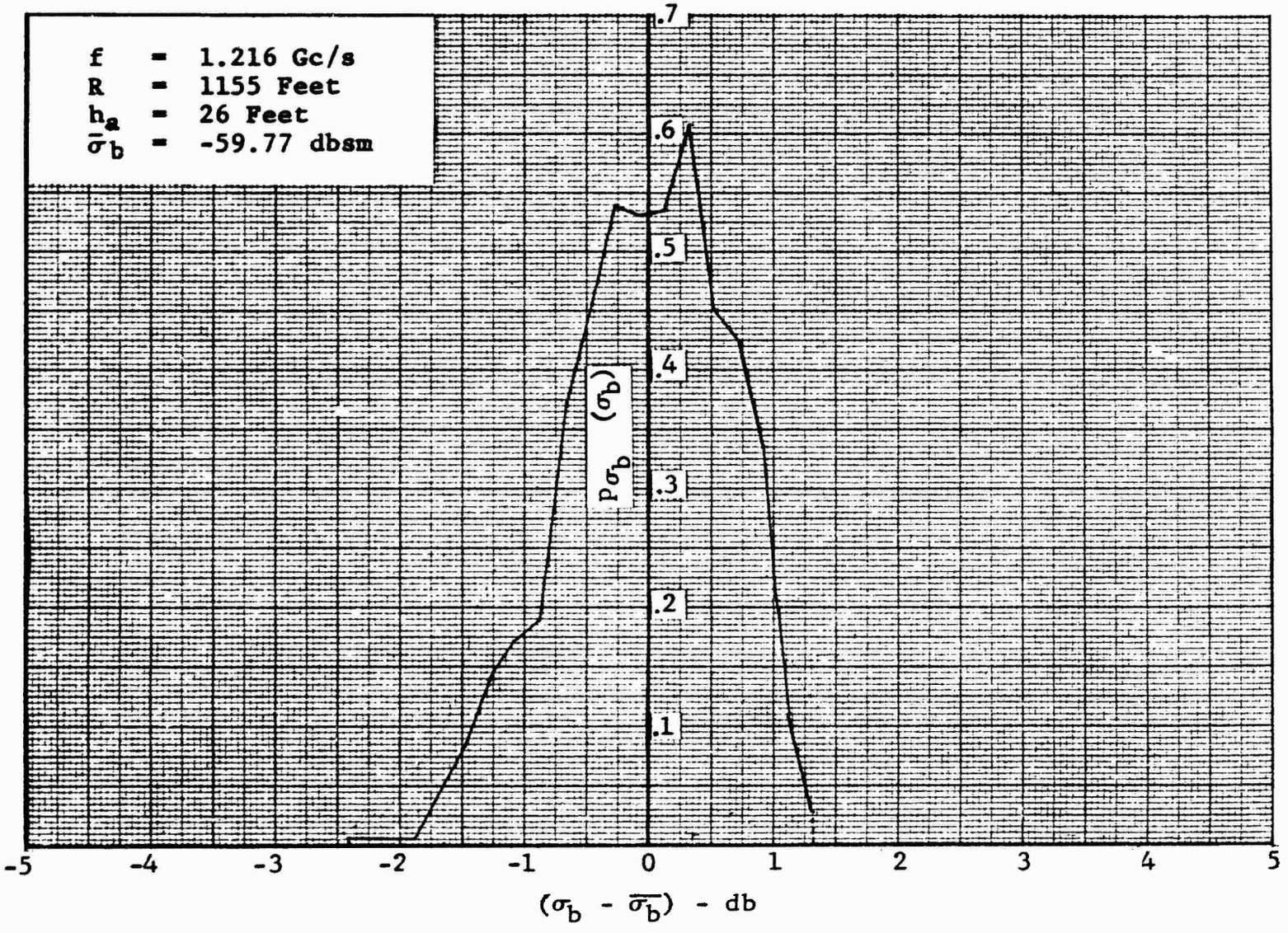

Fig. 31 BACKGROUND NOISE DENSITY, BAND 4, VERTICAL POLARIZATION

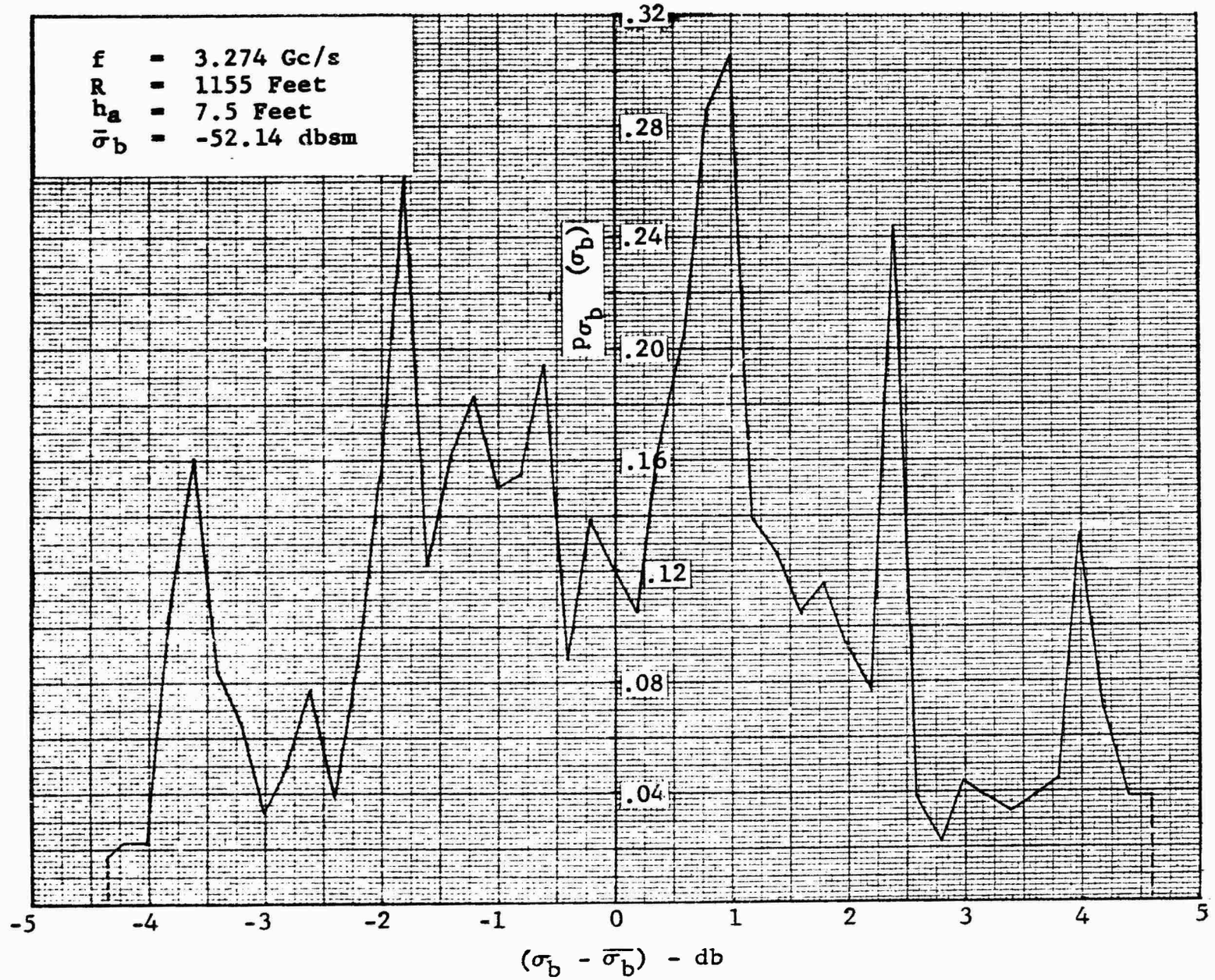

Fig. 32 BACKGROUND NOISE DENSITY, BAND 5, HORIZONTAL POLARIZATION

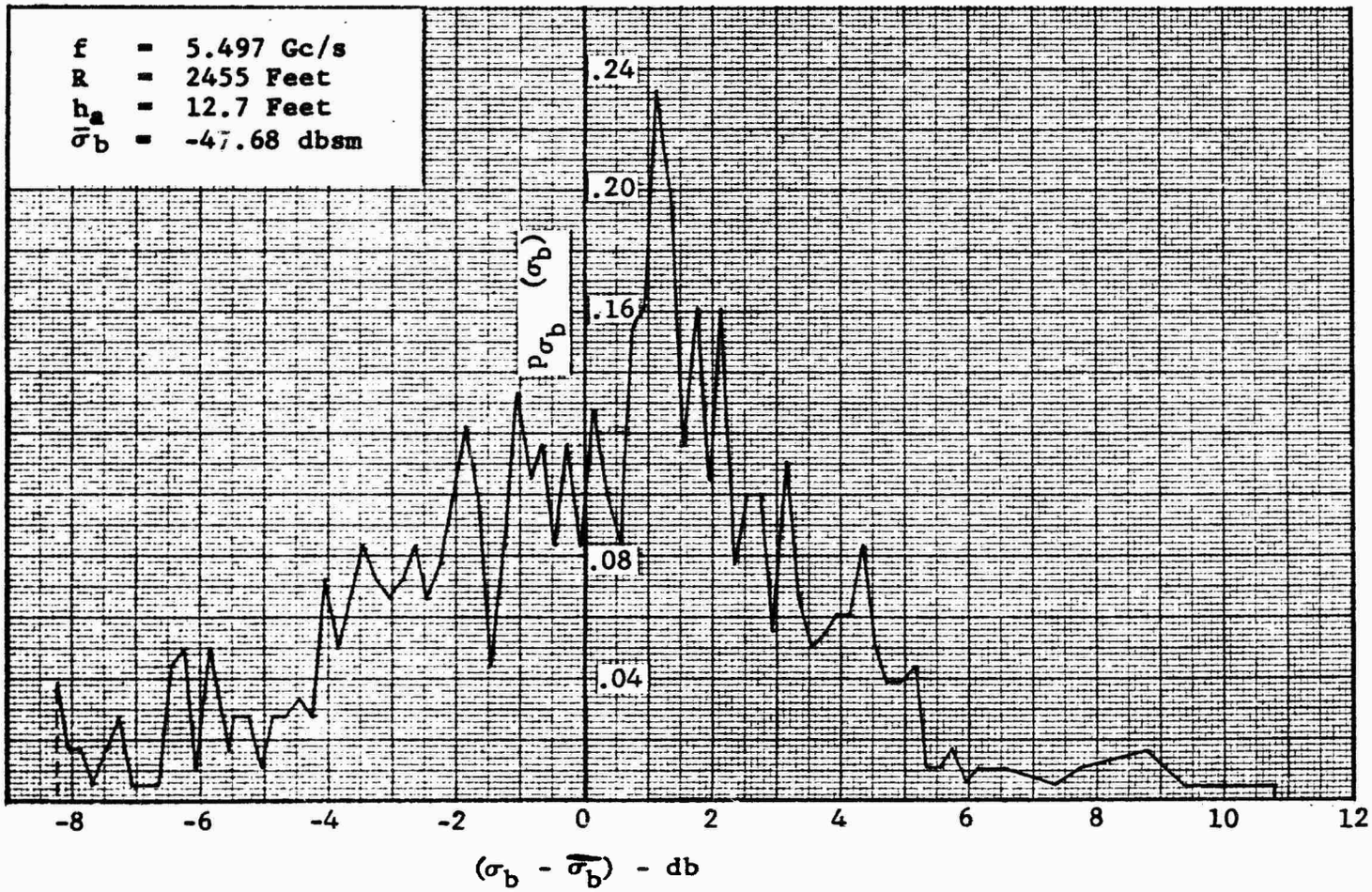

Fig. 33 BACKGROUND NOISE DENSITY, BAND 6, VERTICAL POLARIZATION

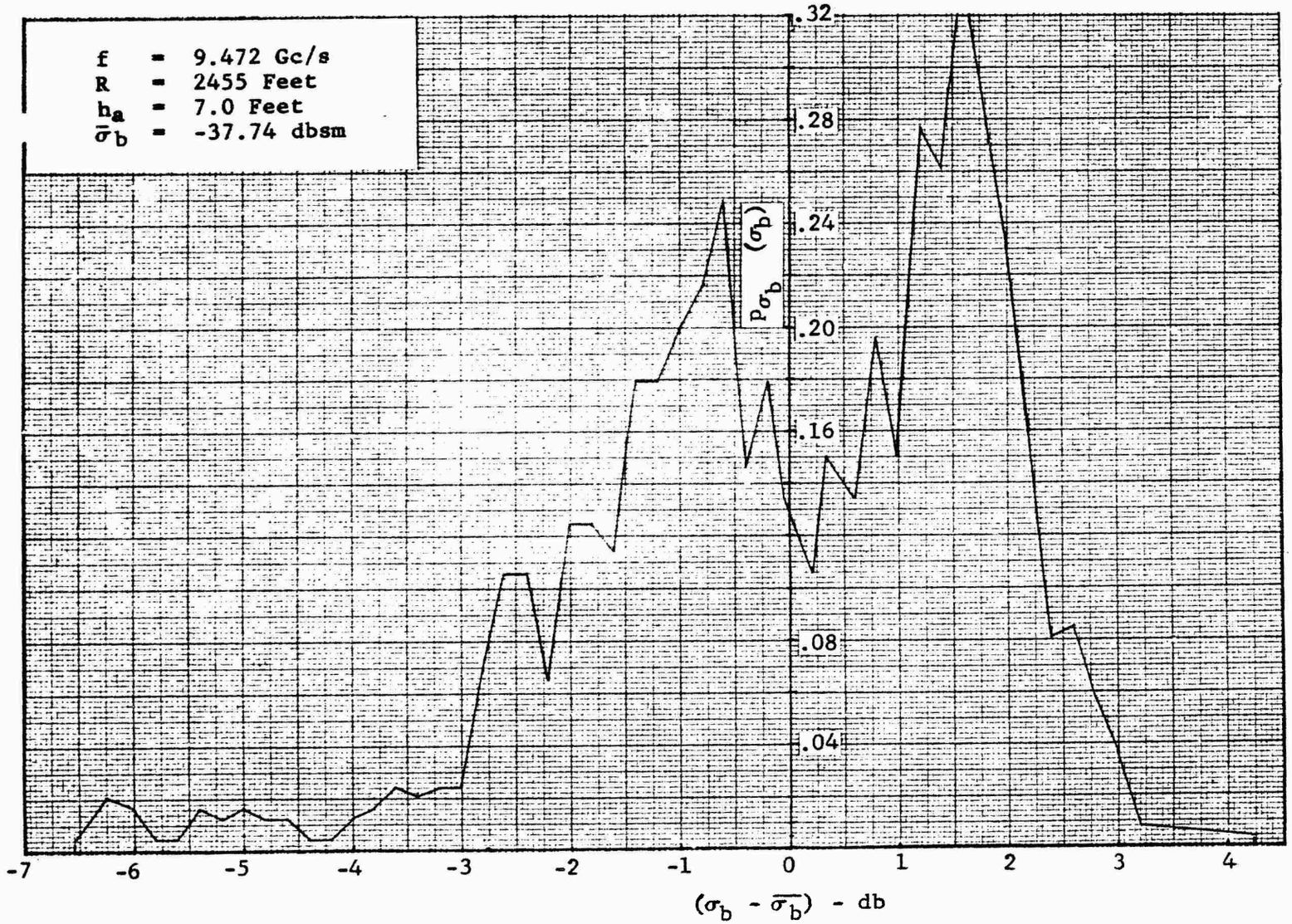

Fig. 34 BACKGROUND NOISE DENSITY, BAND 7, HORIZONTAL POLARIZATION

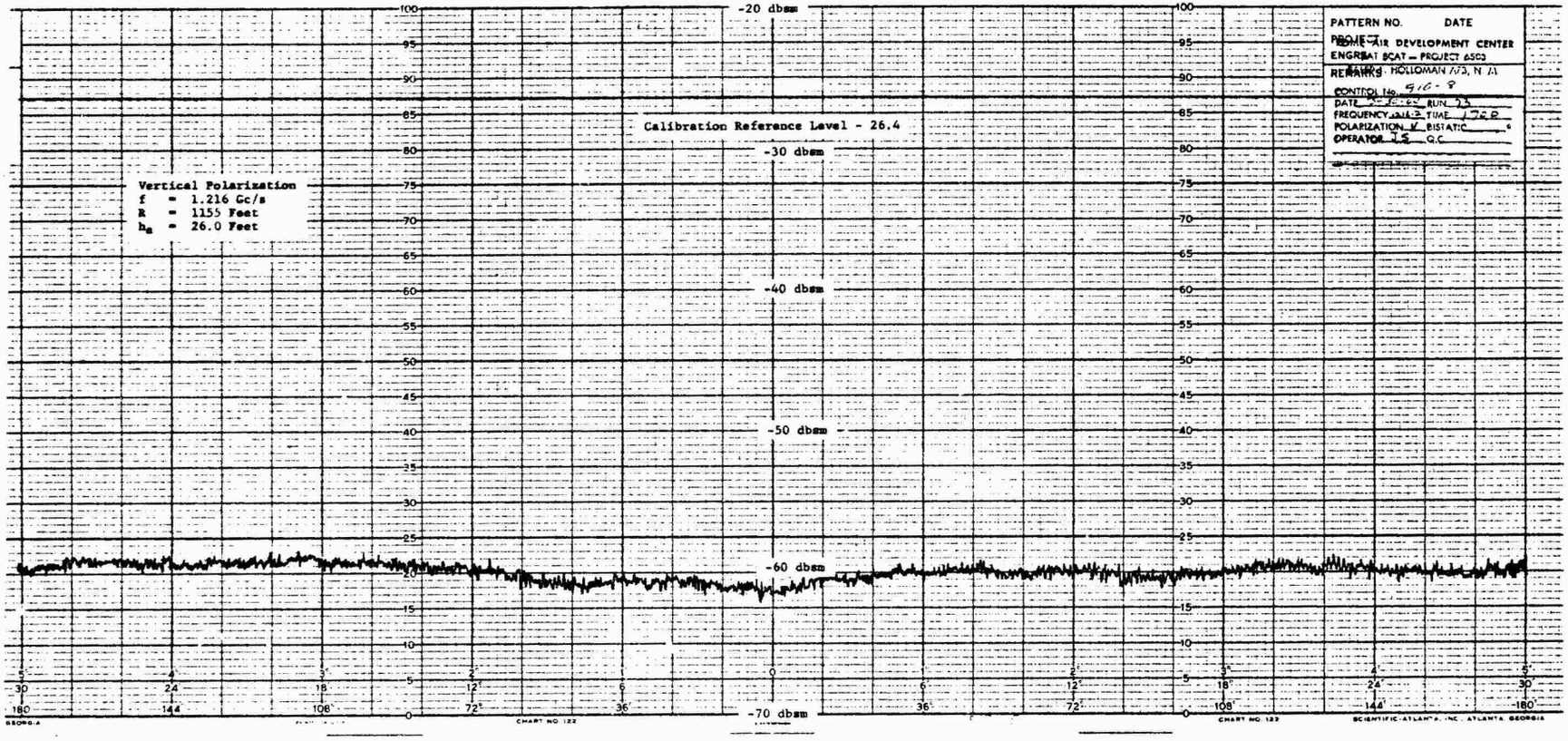

Fig. 35 ANALOG RECORD OF BAND 4 BACKGROUND NOISE, VERTICAL POLARIZATION

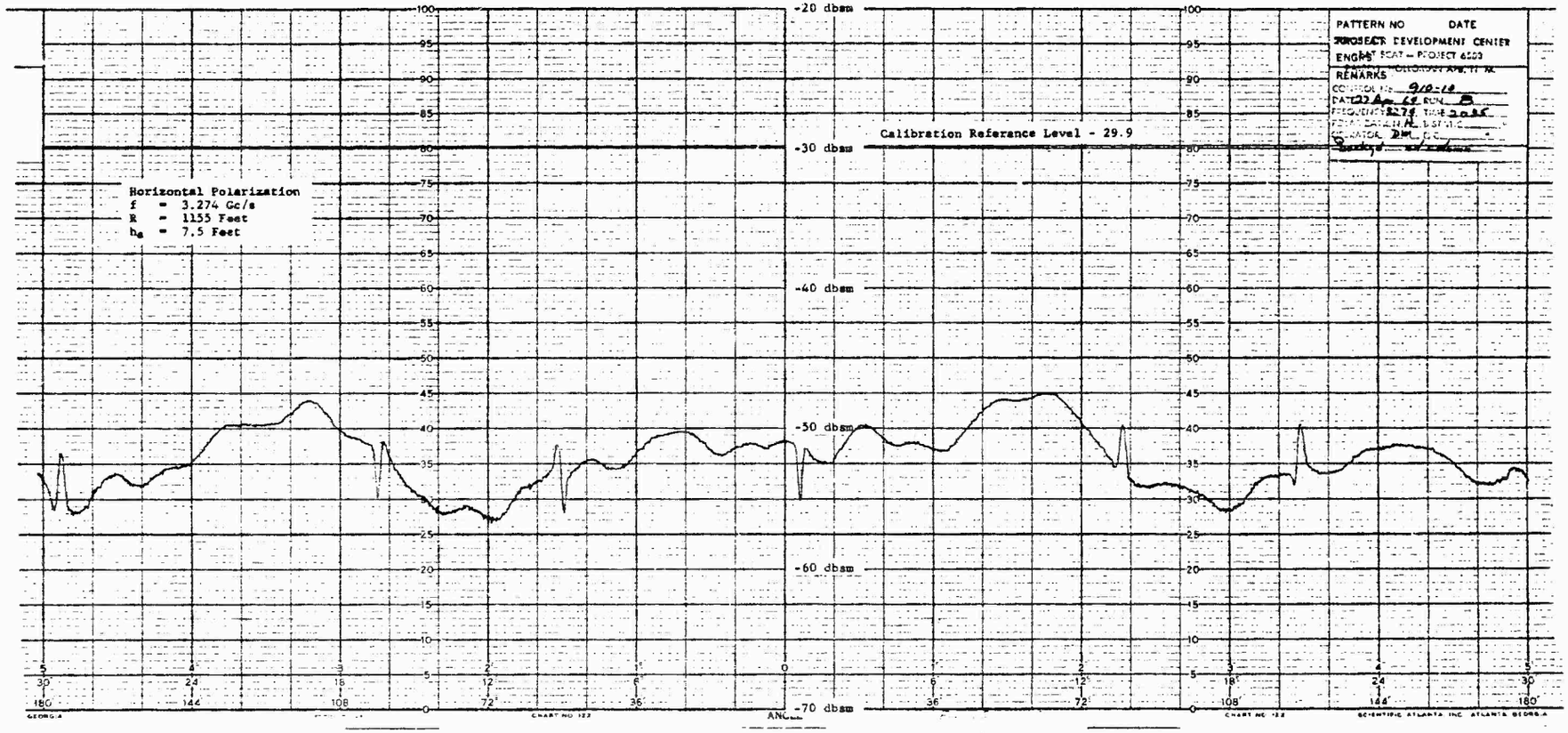

Fig. 36 ANALOG RECORD OF BAND 5 BACKGROUND NOISE, HORIZONTAL POLARIZATION

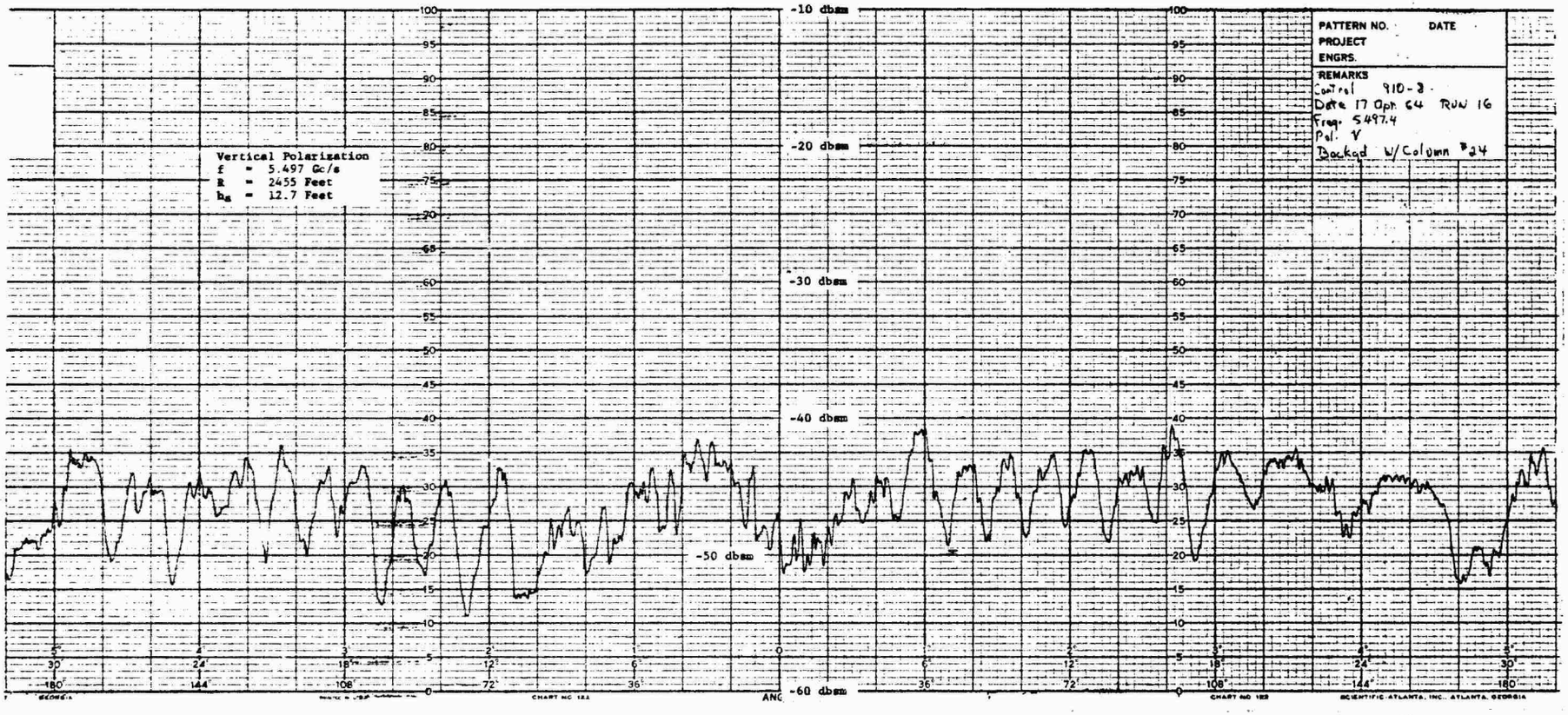

Fig. 37 ANALOG RECORD OF BAND 6 BACKGROUND NOISE, VERTICAL POLARIZATION

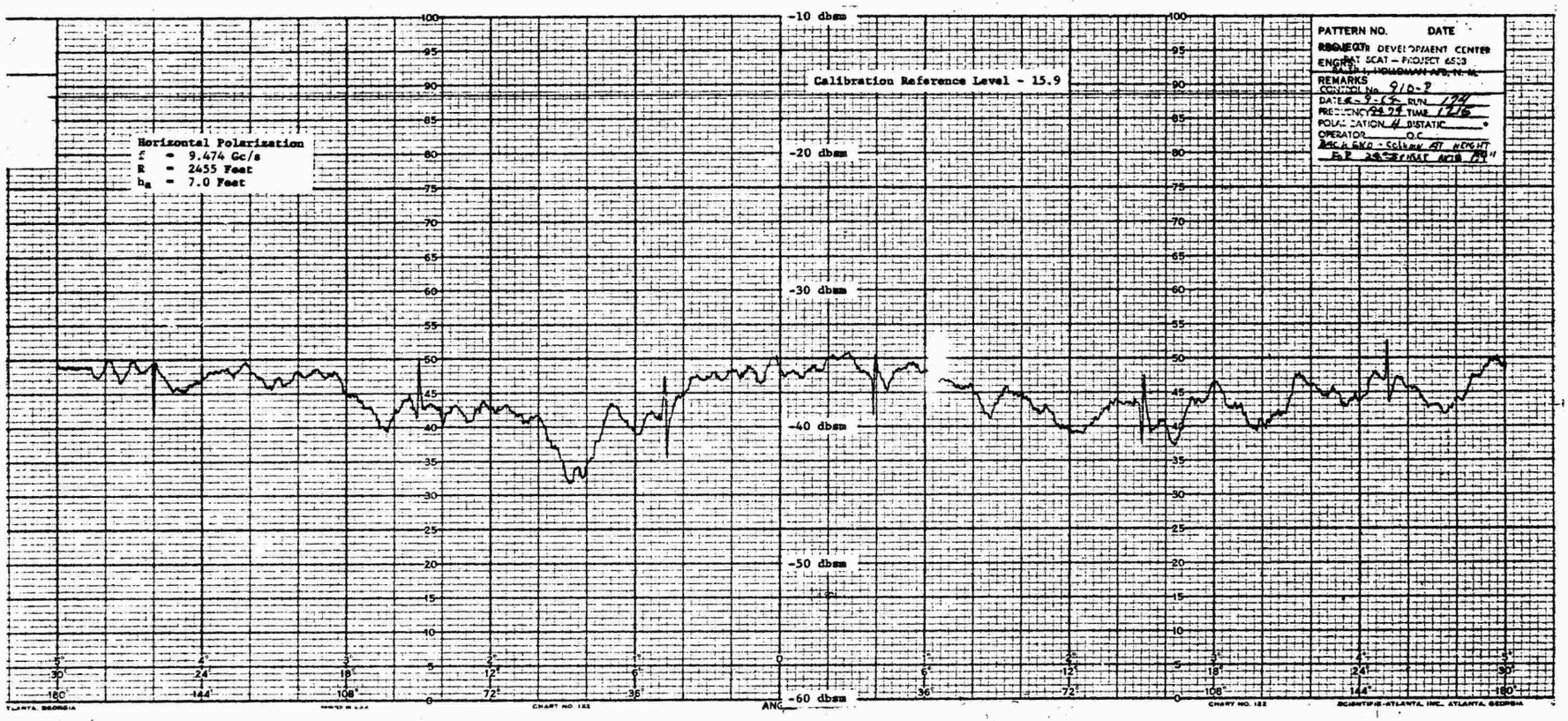

Fig. 38 ANALOG RECORD OF BAND 7 BACKGROUND NOISE, HORIZONTAL POLARIZATION

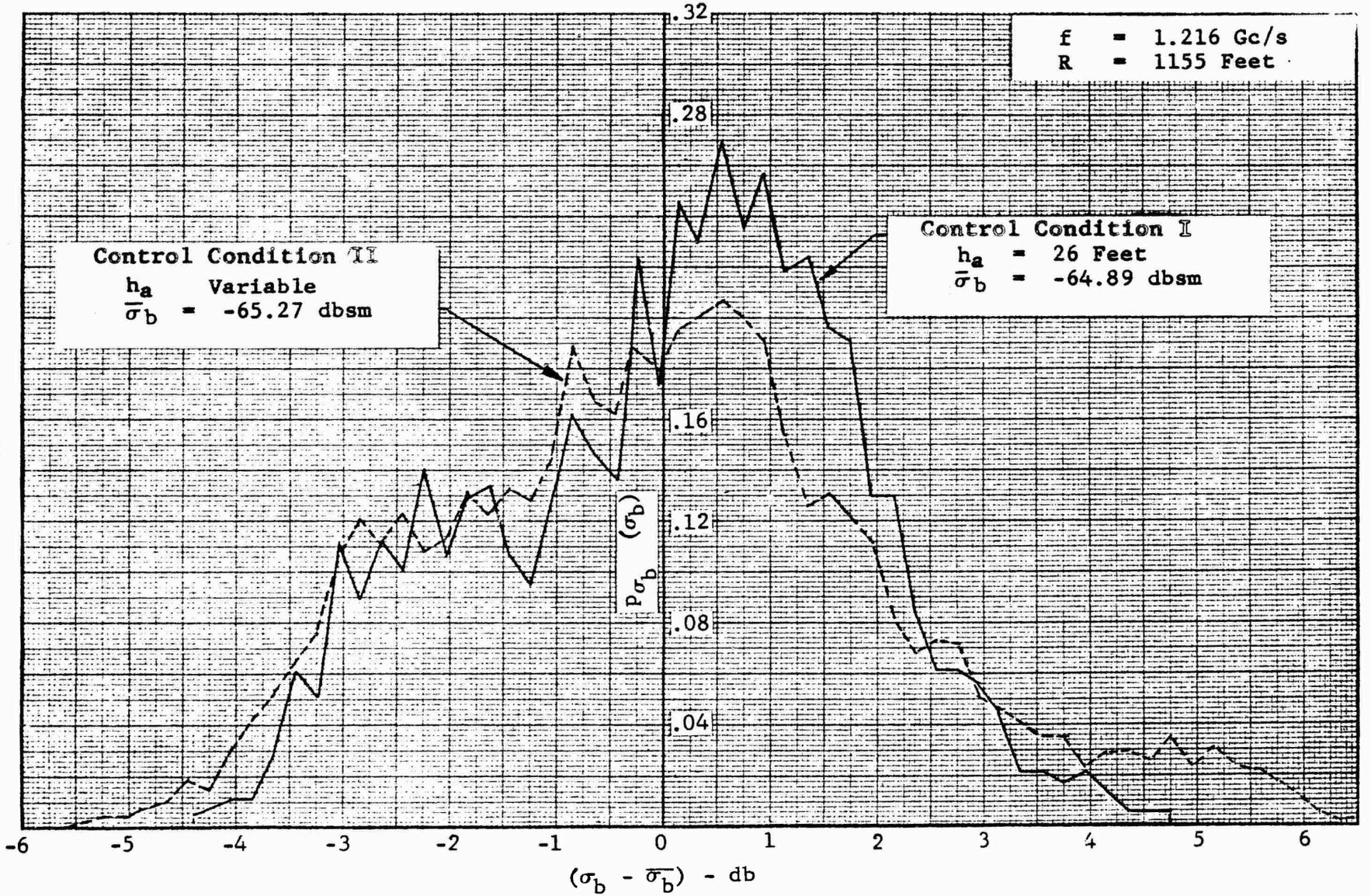

Fig. 39 COMPARISON OF BACKGROUND NOISE DENSITIES FROM CONTROL CONDITIONS I AND II, HORIZONTAL POLARIZATION

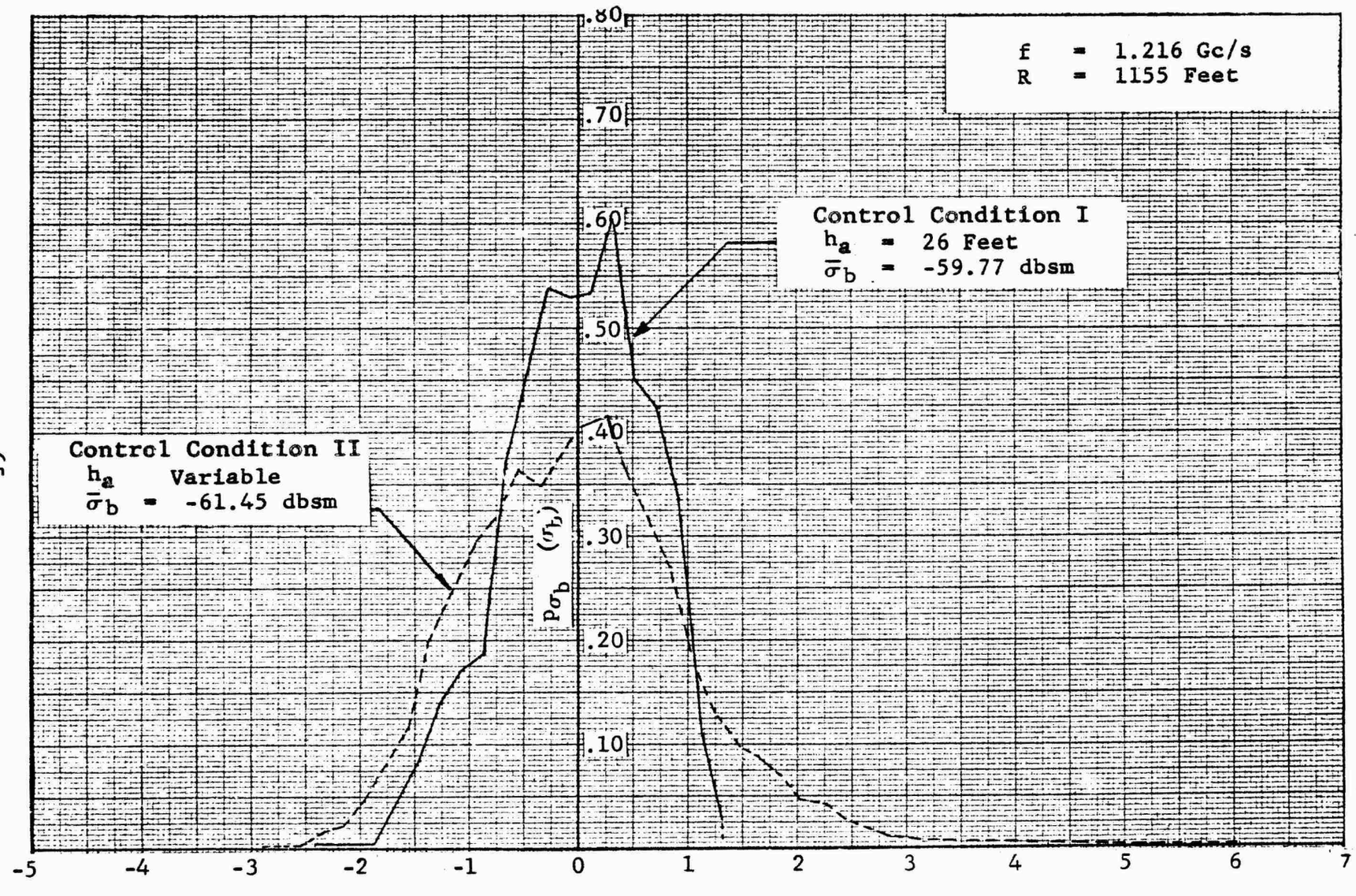

Fig. 40 COMPARISON OF BACKGROUND NOISE DENSITIES FROM CONTROL CONDITIONS I AND II, VERTICAL POLARIZATION

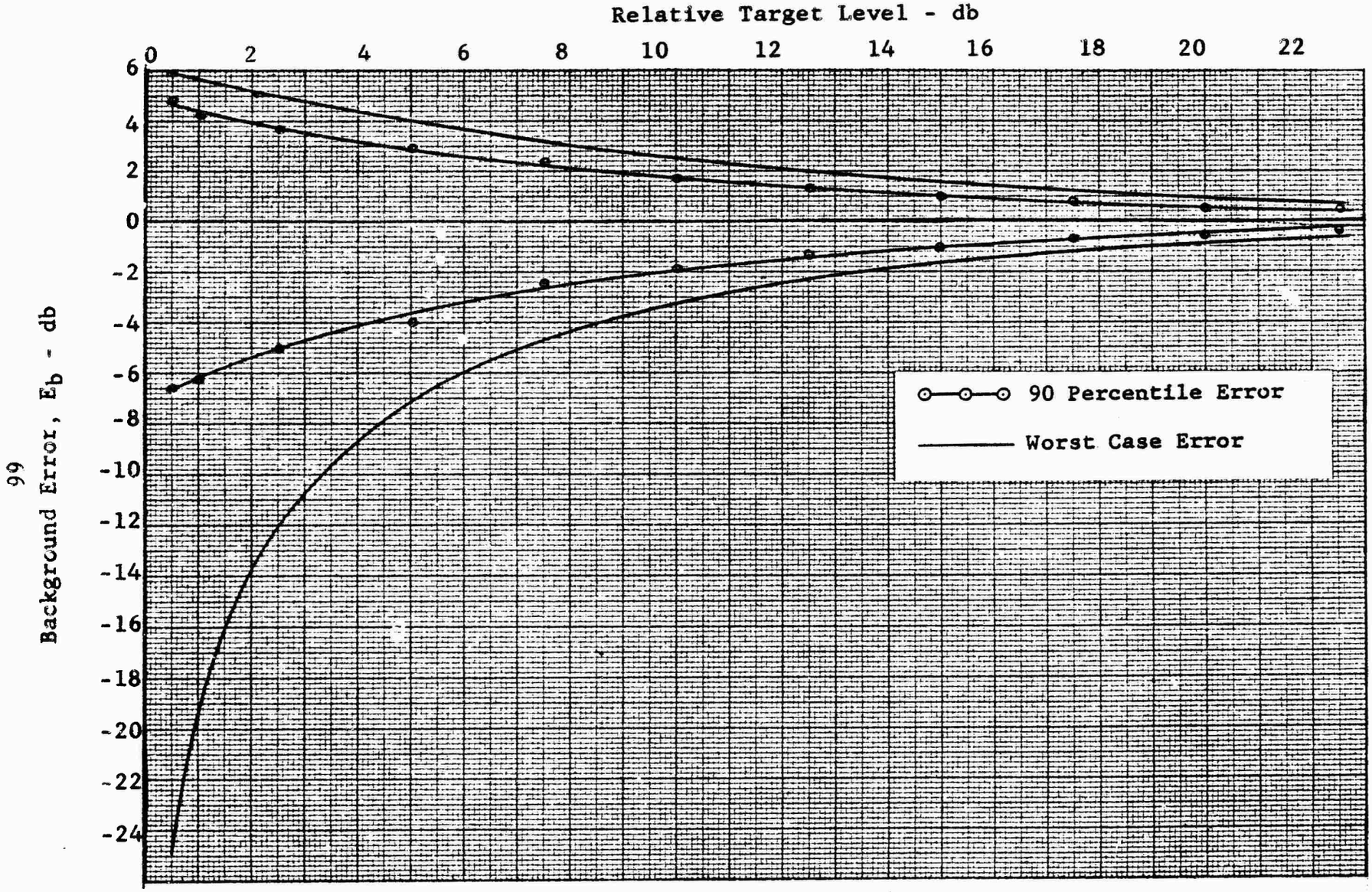

Fig. 41 NINETY-PERCENTILE ERROR CURVE, BAND 4, HORIZONTAL POLARIZATION

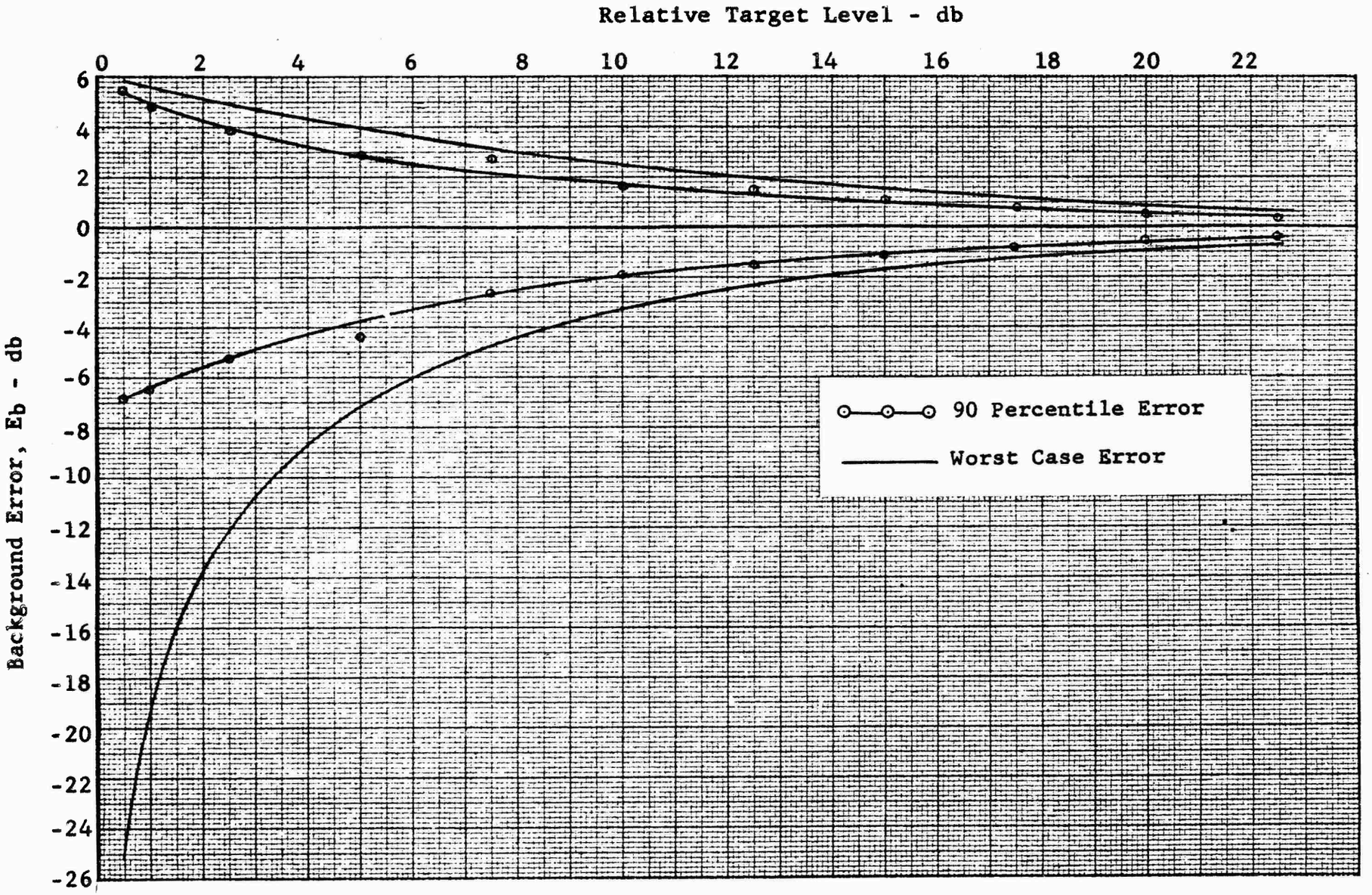

Fig. 42 NINETY-PERCENTILE ERROR CURVE, BAND 5, HORIZONTAL POLARIZATION

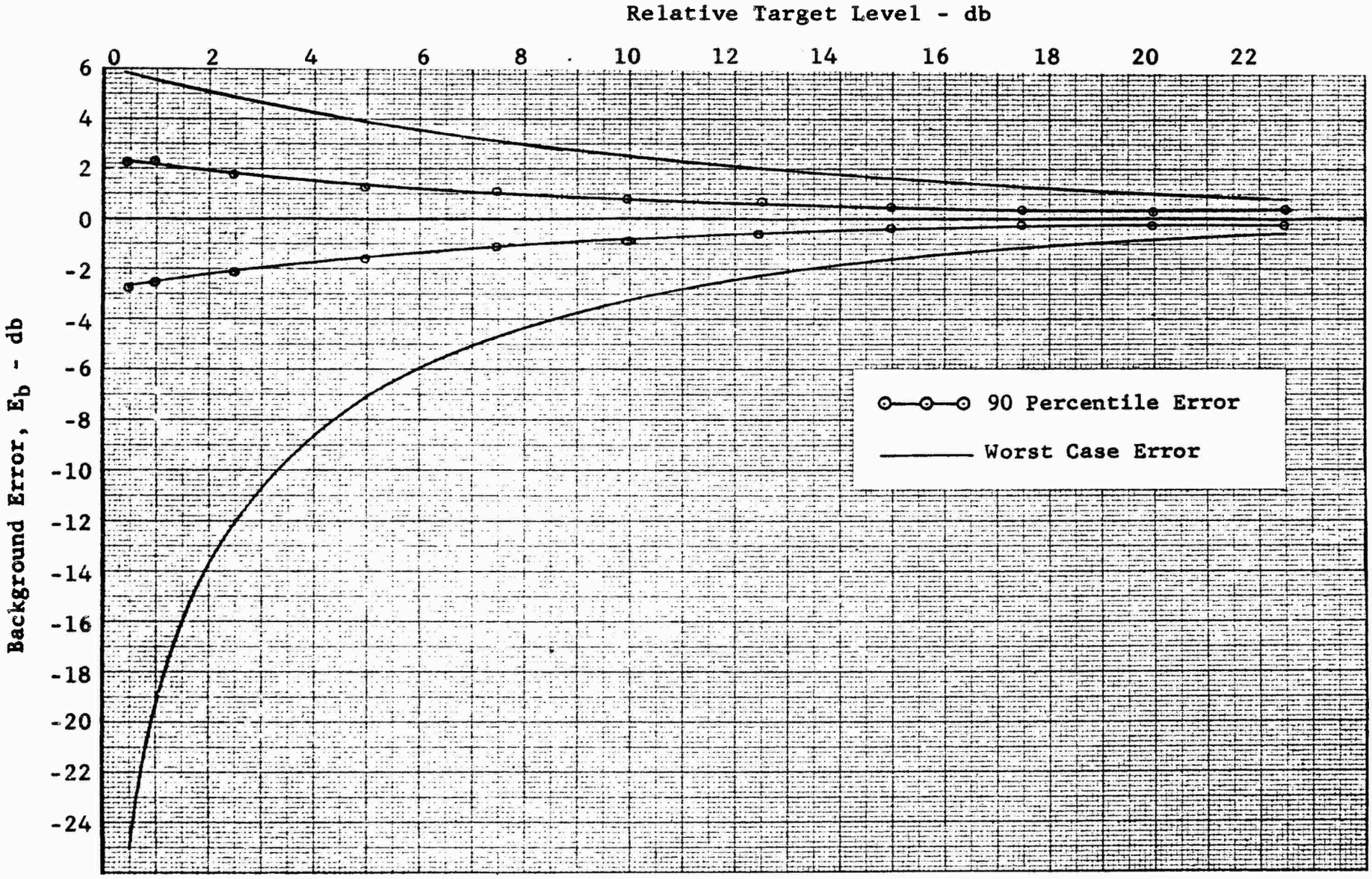

Fig. 43 NINETY-PERCENTILE ERROR CURVE, BAND 6, HORIZONTAL POLARIZATION

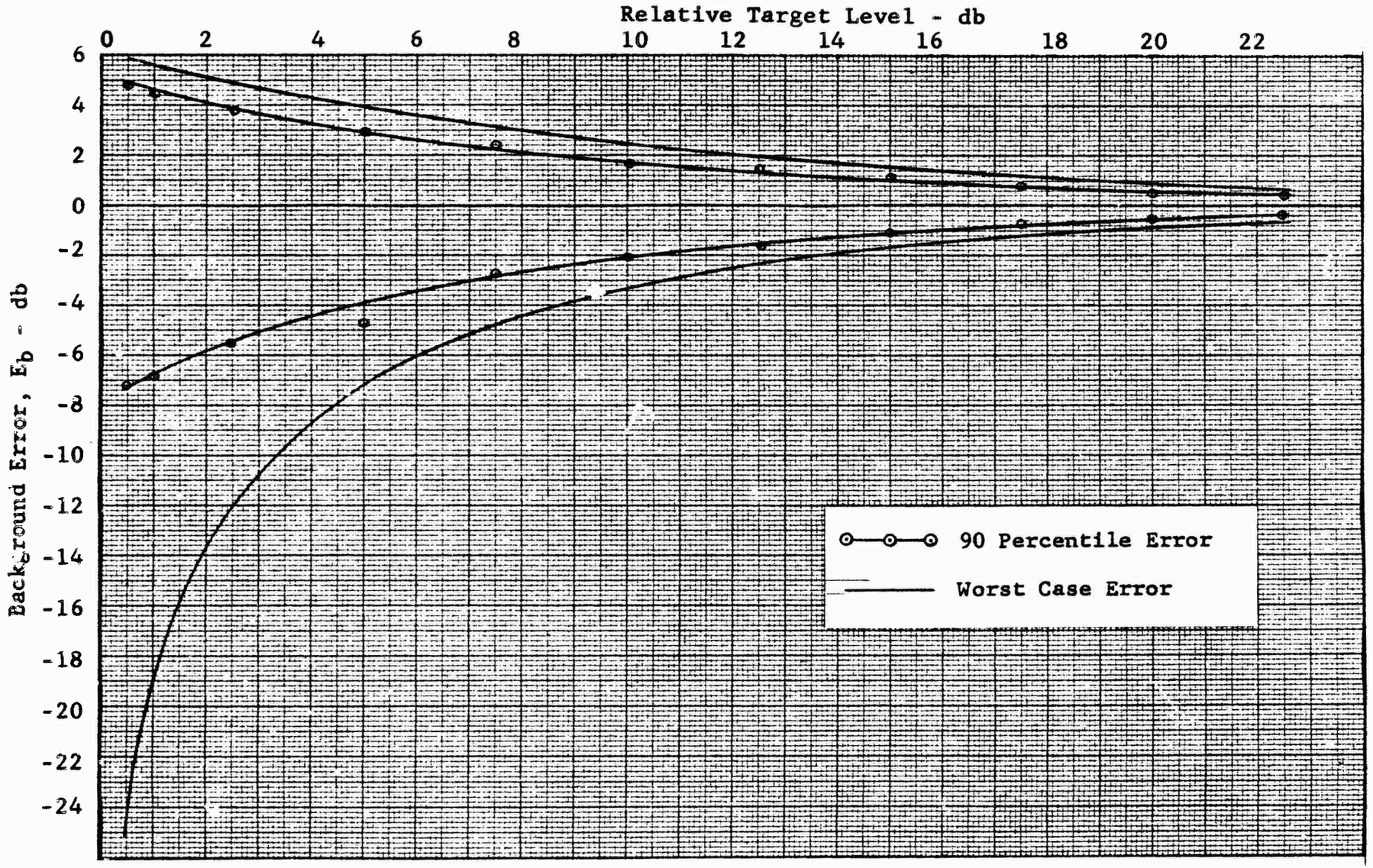

Fig. 44 NINETY-PERCENTILE ERROR CURVE, BAND 7, HORIZONTAL POLARIZATION

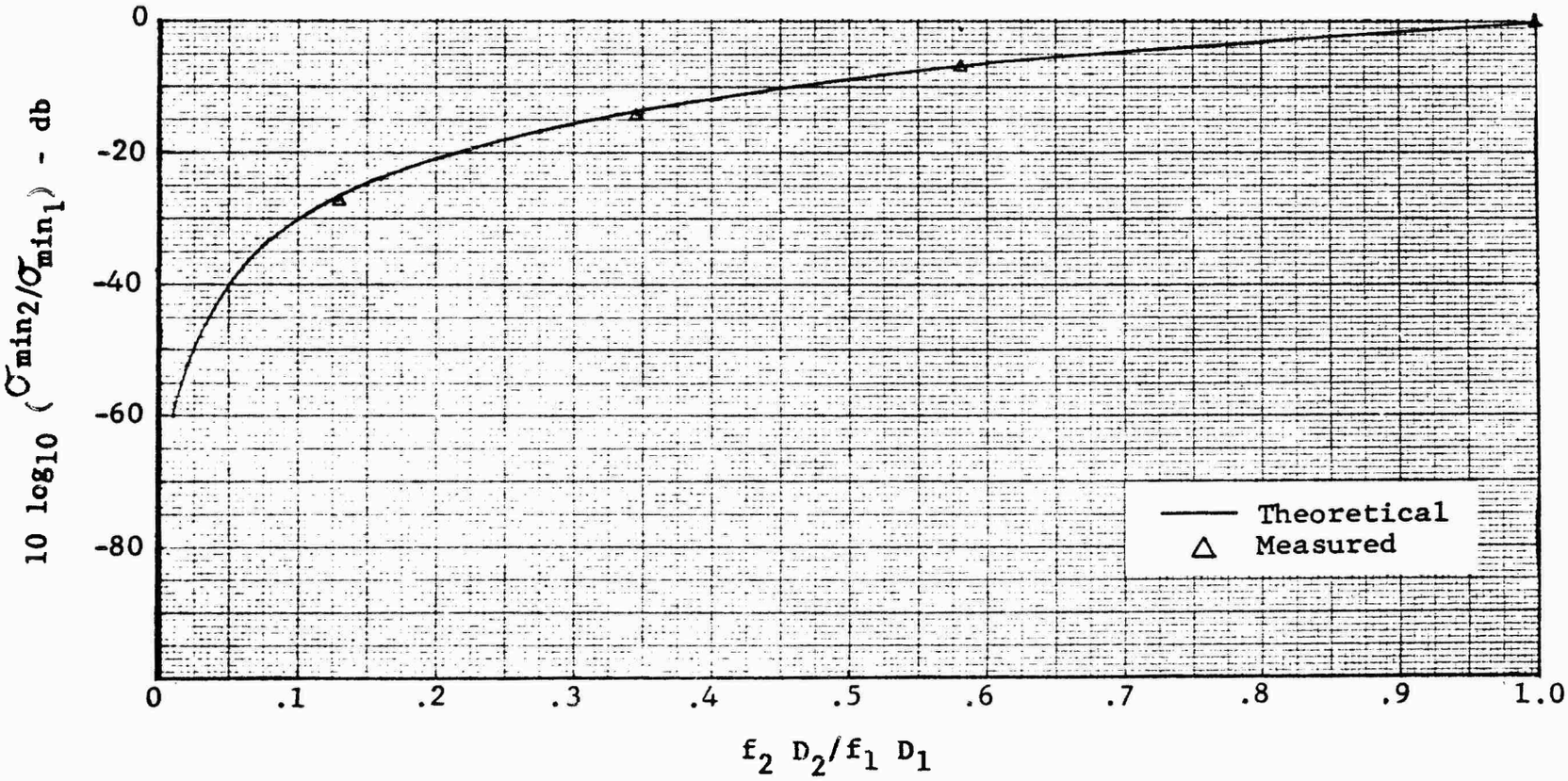

Fig. 45 COMPARISON OF BACKGROUND MEANS WITH TUNED COLUMN MODEL, HORIZONTAL POLARIZATION DATA

background mean of tuned columns are plotted against the theoretical mean variation as predicted by studies under the Cellular Plastic Support Task of the RAT SCAT Research and Development Program (Reference 5). The model in Reference 5 predicts the locus of the local minimums of the cross section per unit length for uniform illumination of a tuned Styrofoam column as a function of frequency.

Results of Background Error Investigation

Estimates of errors, due to target supports of the type described in this report using the model developed, appear justified. The general shape of the background density was quite regular even though insufficient histories and/or control of test parameters apparently caused variations in the shape of several of the densities. Figure 46 shows a comparison of the worst case and the 95-percentile case for each of the frequencies investigated. The error curves here are plotted against the actual target level instead of the relative level employed previously. An additional generalization has also been applied to these curves on the basis of the agreement between the measured and theoretical mean variation as indicated in Figure 45. Instead of a comparison strictly on the basis of frequency, the curves can be taken to represent a comparison of the background error for several conditions of the parameter D/λ where D is the diameter of the Styrofoam support column. Thus, an estimate of the error due to background noise can be obtained from this figure if the D/λ parameter and the target level of interest are supplied. Specifically, if the target weight (and hence the column diameter), the frequency, and the target cross section level are known, an estimate of the magnitude of the background error within which 95 percent of the background errors lie is available.

The background errors indicated in Figure 46 are representative of the errors to be expected for a nominal Styrofoam column length of 10 feet. The estimate is somewhat conservative since the analysis was carried out for target levels down to and including the level of the peak background noise rather than mean levels. It is for this lower limit of target level that the worst case error approaches $-\infty$. Figure 46 also provides a convenient means for the determination of realistic specifications concerning allowable error due to background noise.

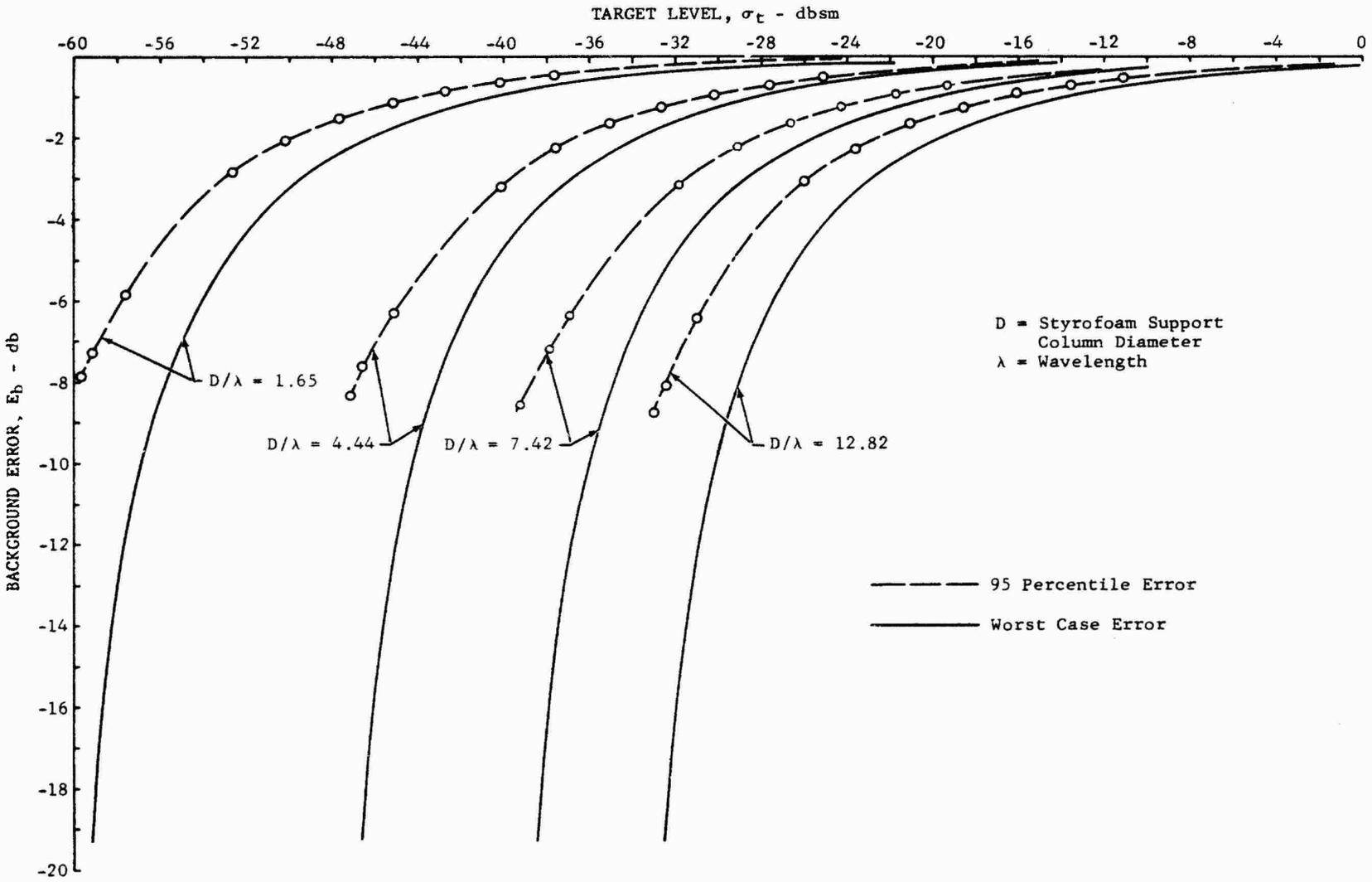

Fig. 46 BACKGROUND ERROR LIMITS VERSUS TARGET LEVEL

SECTION 4

EXTRANEOUS ILLUMINATION ERROR INVESTIGATION

General

Extraneous illumination can be defined in general as the energy which strikes the target by radiation from sources other than direct and ground path energy from the transmitter and is returned to the receiver. The major sources of extraneous illumination are indicated in Figure 47.

Figure 47(a) contains a sketch of the extraneous illumination which is due to energy reflected from extraneous scatters inside the range gate ellipse. In this connection, the ellipse, the scatterers, and the reflected energy must not be considered as being related to the ground plane path which is regarded as a part of the normal target illuminating path. Figure 47(b) contains a sketch of the extraneous illumination caused when the target is excited by reflections from its own radiation pattern.

On the RAT SCAT range, the region enclosed by the range gate ellipse is controlled to avoid sizeable scatterers in this region. For this reason, the extraneous illumination of this nature is assumed to be negligible in comparison to that of the type represented in Figure 47(b).

The extraneous illumination caused by reradiation from the target is also limited to regions covered by the range gate. For this reason, the major contributor is assumed to be the pit area. In particular, since the rotator platform has a 17-foot diameter, the major contributor was anticipated to be reflection from the rotator platform.

Method For Evaluating Error Due To Extraneous Illumination

The primary objectives in connection with extraneous illumination are (1) measure extraneous illumination error as a function of polarity and (2) measure the effectiveness of using radar absorbent material (RAM) in the pit. The mathematical model selected to accomplish the above tasks was of a statistical nature. This type of model appeared appropriate due to the large number of indeterminate parameters inherent in the measurement program. The particular model selected utilizes the difference between measured and theoretical cross section values of a "worst case"

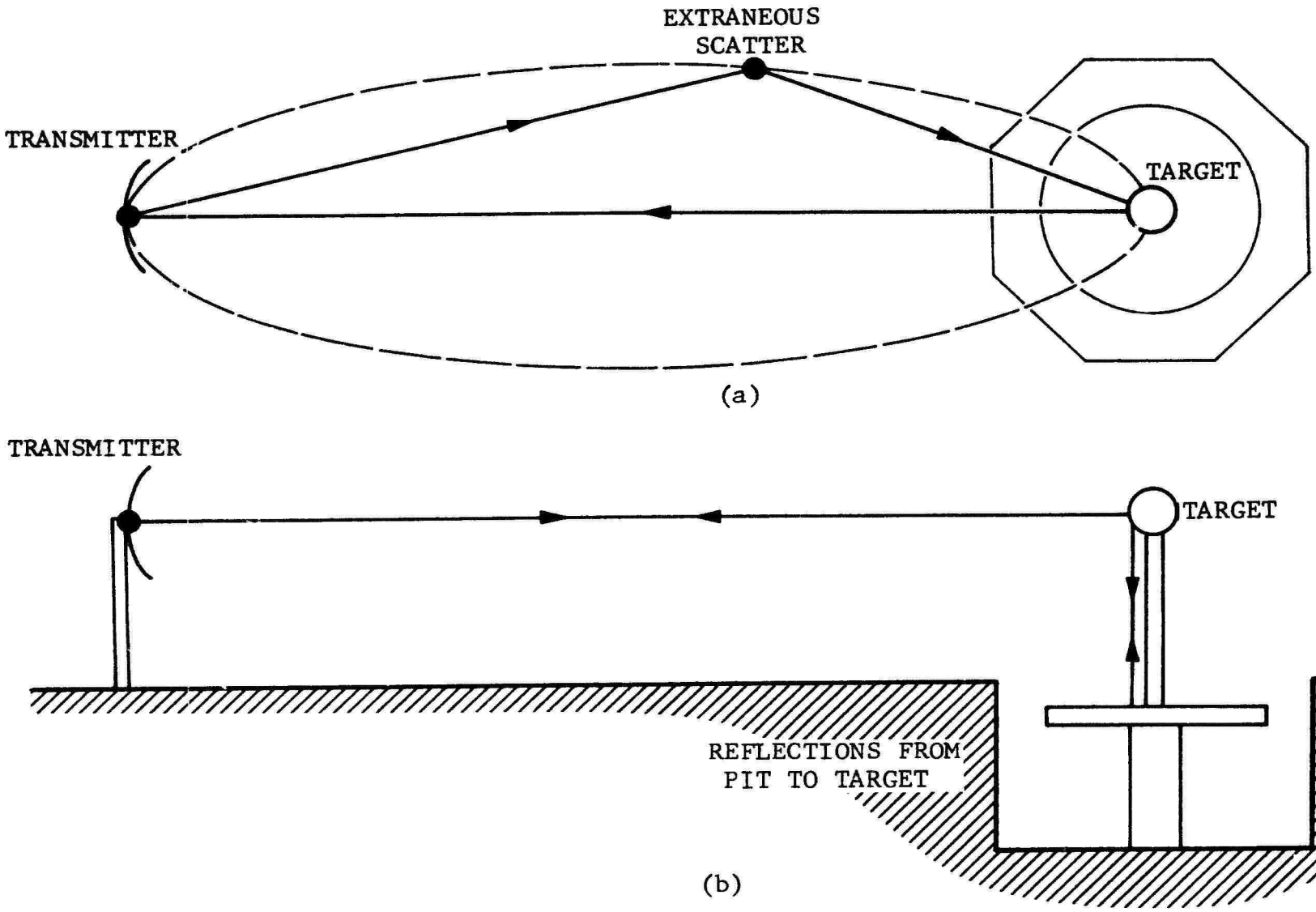

Fig. 47 SOURCES OF EXTRANEOUS ILLUMINATION

type target. In particular, the dispersion between the measured and theoretical cross section values of a horizontally mounted cylinder under various measurement conditions is used to develop an error measure. In order to place a numerical value on the amount of dispersion, the variance and its square root, the standard deviation is computed using the main lobe, first side lobe, second side lobe, etc. of the measured data. A normalized error function can then be defined as a function of this standard deviation. The development of the error model used in processing the measured data is developed below.

Let σ_{ji}^{PR} equal the i^{th} cross section value of the j^{th} side lobe of a cylinder which is measured using polarization P and pit RAM condition R. Let σ_{ja} equal the j^{th} side lobe theoretical value of the cylinder under the above conditions and the variation in measured cross section with i is such that the mean value is equal to the theoretical. The formula for sample variance as a function of polarity P, RAM condition R, side lobe j, and the number of cross section values N may then be written as Equation 24.

$$\left(\mathbf{U}_j^{PR} \right)^2 = \sum_{i=1}^{N} \frac{(\sigma_{ji}^{PR} - \sigma_{ja})^2}{N} \quad . \tag{24}$$

Hence, the standard deviation is

$$\mathbf{U}_j^{PR} = \sqrt{\frac{1}{N} \sum_{i=1}^{N} \left(\sigma_{ji}^{PR} - \sigma_{ja} \right)^2} \quad . \tag{25}$$

$\mathbf{U}_j^{PR}$ is a significant measure of extraneous illumination since the measured cross section σ_{ji}^{PR} will be in the range $\sigma_{ja} \pm \alpha \mathbf{U}_j^{PR}$, γ percent of the time if the measured cross section is assumed to have a distribution with finite variance (e.g., assuming a normal distribution $\alpha = 2$, $\gamma = 95.5$). By using the value of $\mathbf{U}_j^{PR}$ calculated in Equation 25, and average deviation $\bar{\mathbf{U}}^{PR}$ for the main lobe and first k consecutive side lobes may be defined as

$$\bar{\mathbf{U}}^{PR} = \frac{1}{M} \sum_{j=1}^{M} \mathbf{U}_j^{PR} \quad , \tag{26}$$

where M equals the total number of lobes averaged (M = k+1). The values of $\mathbf{U}_j^{PR}$ calculated in Equation 25 can also be used to compute a measure of a normalized average error denoted by E_{jn}^{PR} and defined as

$$E_{jn}^{PR} = \frac{\mathbf{U}_j^{PR} + \sigma_{mL}}{\sigma_{mL}} , \tag{27}$$

where σ_{mL} is the theoretical value of the cross section of the main lobe of the cylinder. An average error function $\bar{E}^{PR}$ may then be computed by using Equations 26 and 27 as

$$\bar{E}^{PR} = \frac{\bar{U}^{PR} + \sigma_{mL}}{\sigma_{mL}} . \tag{28}$$

σ_{mL} was used as the normalizing factor since the error in the side lobes caused by extraneous illumination is dependent on the energy of the primary radiator. In this case the primary radiator is assumed to be the main lobe of the cylinder. Therefore, E_{jn}^{PR} was computed using the broadside formula for a perfectly conducting cylinder. The values of E_{jn}^{PR} represent a normalized measure of the average error caused by extraneous illumination. This illumination is expressed as a function of polarity and RAM

The normalized average error E_{jn}^{PR} may be redefined in a form denoted by E_j^{PR}, which corresponds to a more standard definition of average error, as

$$E_j'^{PR} = [\sigma_{mL} E_{jn}^{PR} - \sigma_{mL} + \sigma_{ja}] \frac{1}{\sigma_{ja}} , \tag{29}$$

or

$$E_j'^{PR} = \frac{\mathbf{U}_j^{PR} + \sigma_{ja}}{\sigma_{ja}} . \tag{30}$$

$E_j'^{PR}$ indicates the amount of extraneous illumination error in the return from the j^{th} side lobe normalized to the theoretical value of the j^{th} side lobe.

Test Program

The amount of extraneous illumination which strikes a given target depends on several parameters. An important parameter is target geometry. This being the case, a test program designed to give a measure of cross section measurement error, which results from the extraneous illumination that strikes an arbitrary target, is exceedingly difficult. However, a test program for estimating the upper bound to this type error is feasible and should yield information with which a reasonable estimate of the extraneous illumination error associated with a given target may be made.

RAM is another of the important parameters indicated above and has been used at the RAT SCAT Site to reduce the illumination from the rotator platform. Measurements were made with and without RAM in the pit in order to estimate the effectiveness of the RAM.

The measurement program initially conceived was planned for the measurement of the radar cross section of flat plates at various tilt angles and heights ranging from h_i to $h_i + \lambda/2$ in $\lambda/8$ steps. The ratio of the cross section measured from the forward canted side of the plate to that measured from the rearward canted side of the plate was to be used as a measure of the effects of extraneous illumination. These tests were to be conducted first without absorbent material installed in the pit and then with absorbent material installed in the pit.

This original plan was modified by replacing the flat plate with a horizontally mounted cylinder. The change was made for two primary reasons. It was originally assumed that the more significant extraneous illumination would originate from a measurable and defined area of the pit. Instead, flat plate measurements in Bands 5 and 7 indicated that the extraneous illumination appeared to be randomly distributed over the whole pit area. Also, the use of the flat plates in the experiment introduced more parameters than had been expected. The variance of these parameters, such as tilt angle change with height setting, had to be accounted for in an analysis of the data. Consequently, any attempt to isolate and define the effects due to extraneous illumination was suspect.

A 40-inch cylinder with a radius of 8 inches was measured at a frequency of 5497.4 megacycles. The axis of the cylinder was parallel to the ground and measurements were made in steps of $\lambda/8$ from the initial height to the initial height plus $\lambda/2$.

Also, the cylinder was displaced horizontally with respect to the center of the rotator in order to detect phasing between the main target return and the return due to extraneous illumination. An RCS pattern was obtained at each respective position at both horizontal and vertical polarity. With these measurements sixteen values were obtained for each side lobe and for each polarization for evaluation of Equation 24. This procedure was repeated under the three following RAM conditions:

1. RAM in pit and on perimeter

2. RAM in pit and no RAM on perimeter

3. No RAM on perimeter or in pit.

Test and Program Results

Figures 48 through 50 contain three RCS patterns obtained under the following three RAM conditions with the cylinder at the same height:

1. RAM in pit and on perimeter

2. RAM in pit and no RAM on perimeter

3. No RAM on perimeter or in pit.

The graphs in Figure 51 are plots of U_o^{PR} (standard deviation of main lobe), U_4^{PR} (standard deviation of fourth side lobe), and $\bar{U}^{PR}$ (average deviation for M equal to 5). Figure 52 contains graphs of E_o^{PR} (normalized average error of main lobe, E_4^{PR} (normalized average error of fourth side lobe), and $\bar{E}^{PR}$ (average for M equals 5 in Equation 26). Figure 53 contains graphs of average error E_o^{PR} (average error of main lobe) and E_4^{PR} (average error of fourth side lobe).

Analysis of the data presented in the form of graphs in Figures 51 and 52 indicates that both standard deviation and normalized error increase as RAM is removed from the pit area in all cases and that the greatest increase occurs when the RAM is completely removed from the rotator table. The overall average value of error normalized to the cylinder main lobe, $\bar{E}$, for the main lobe and the first four side lobes varies from 0.055 db in the most favorable condition to 0.164 db in the worst condition (analysis was limited to the main lobe and first four side

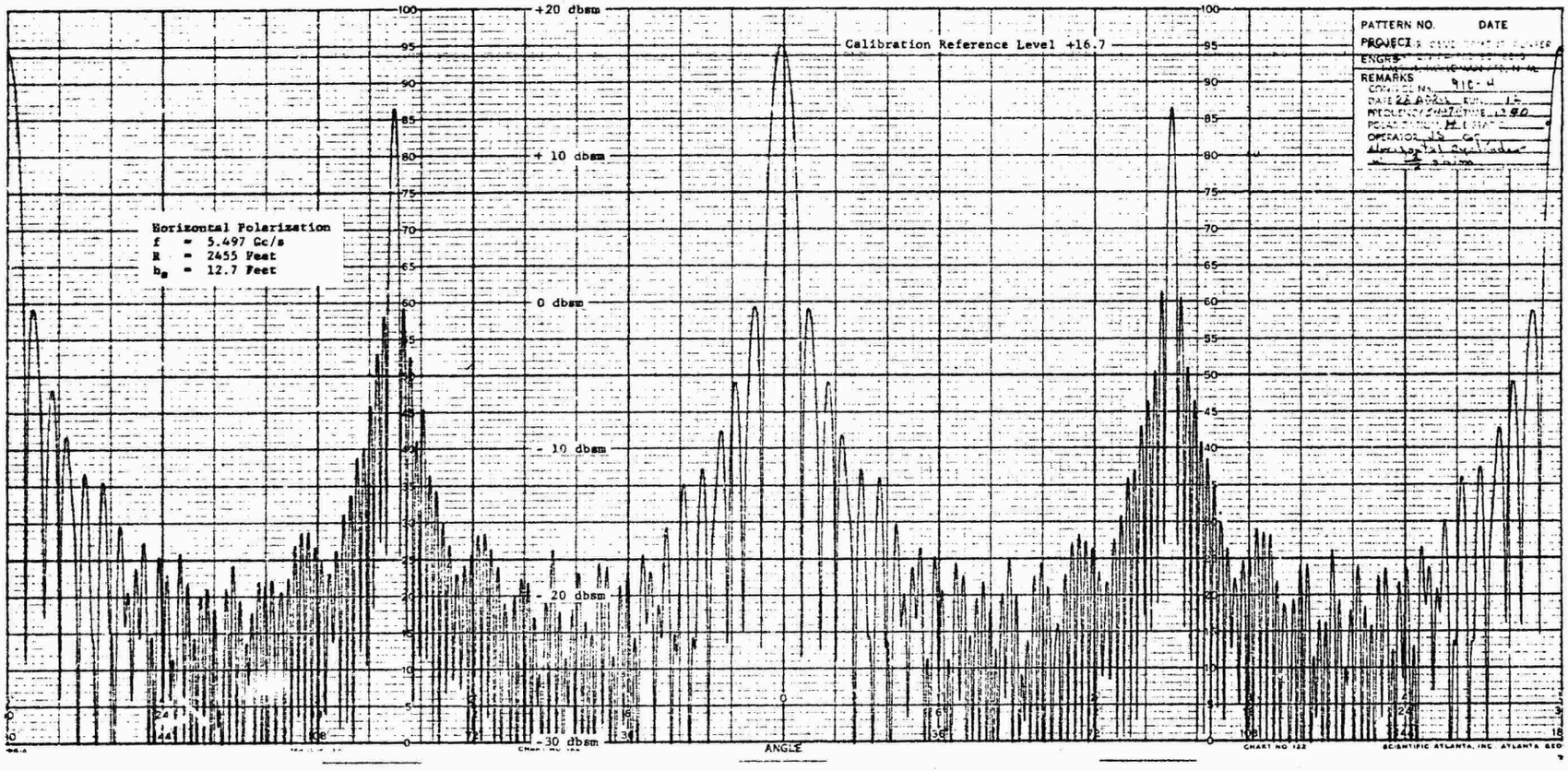

Fig. 48 CROSS SECTION RETURN FROM CYLINDER (WITH RAM)

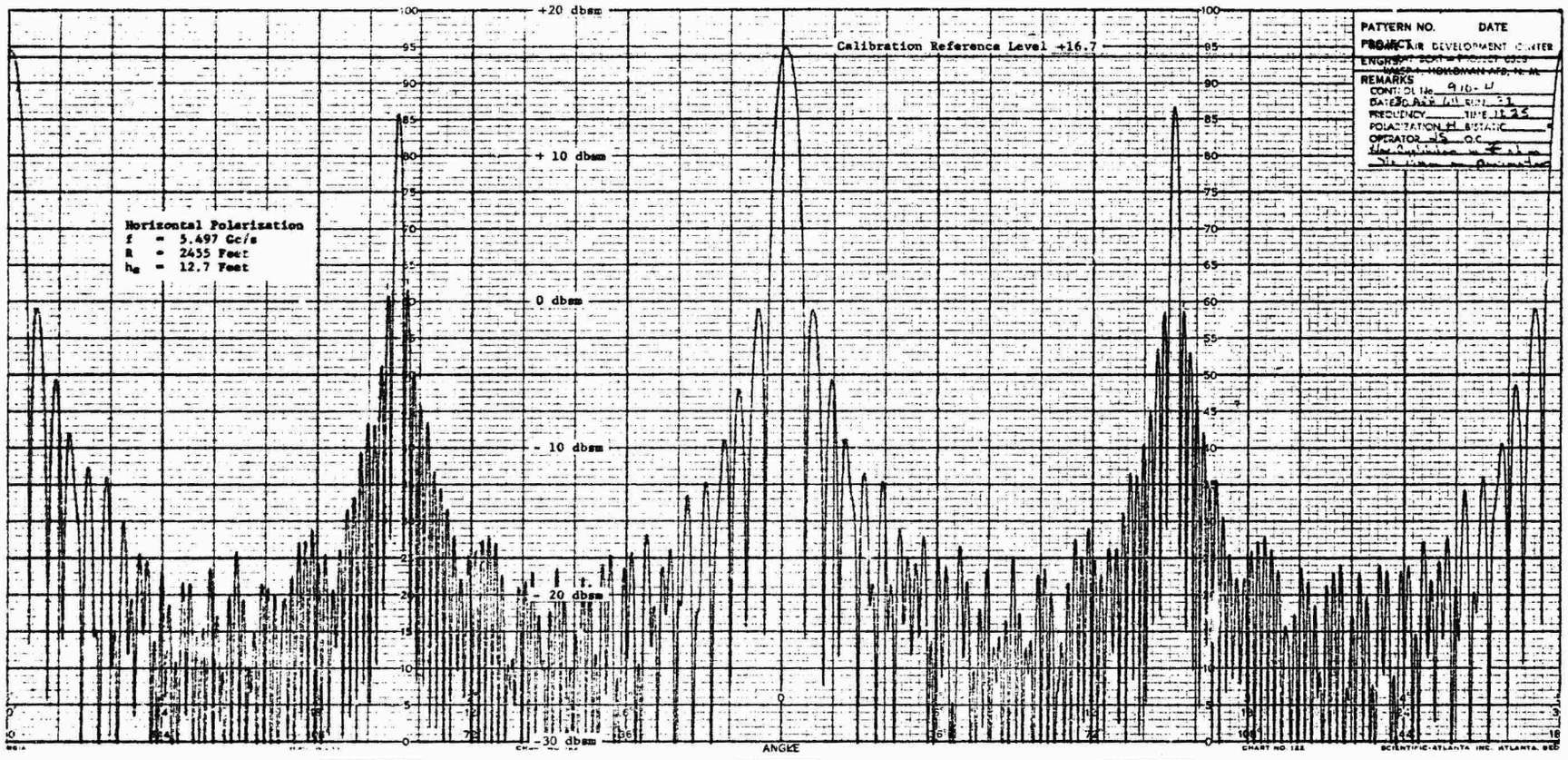

Fig. 49 CROSS SECTION RETURN FROM CYLINDER
(WITH RAM REMOVED FROM PIT PERIMETER)

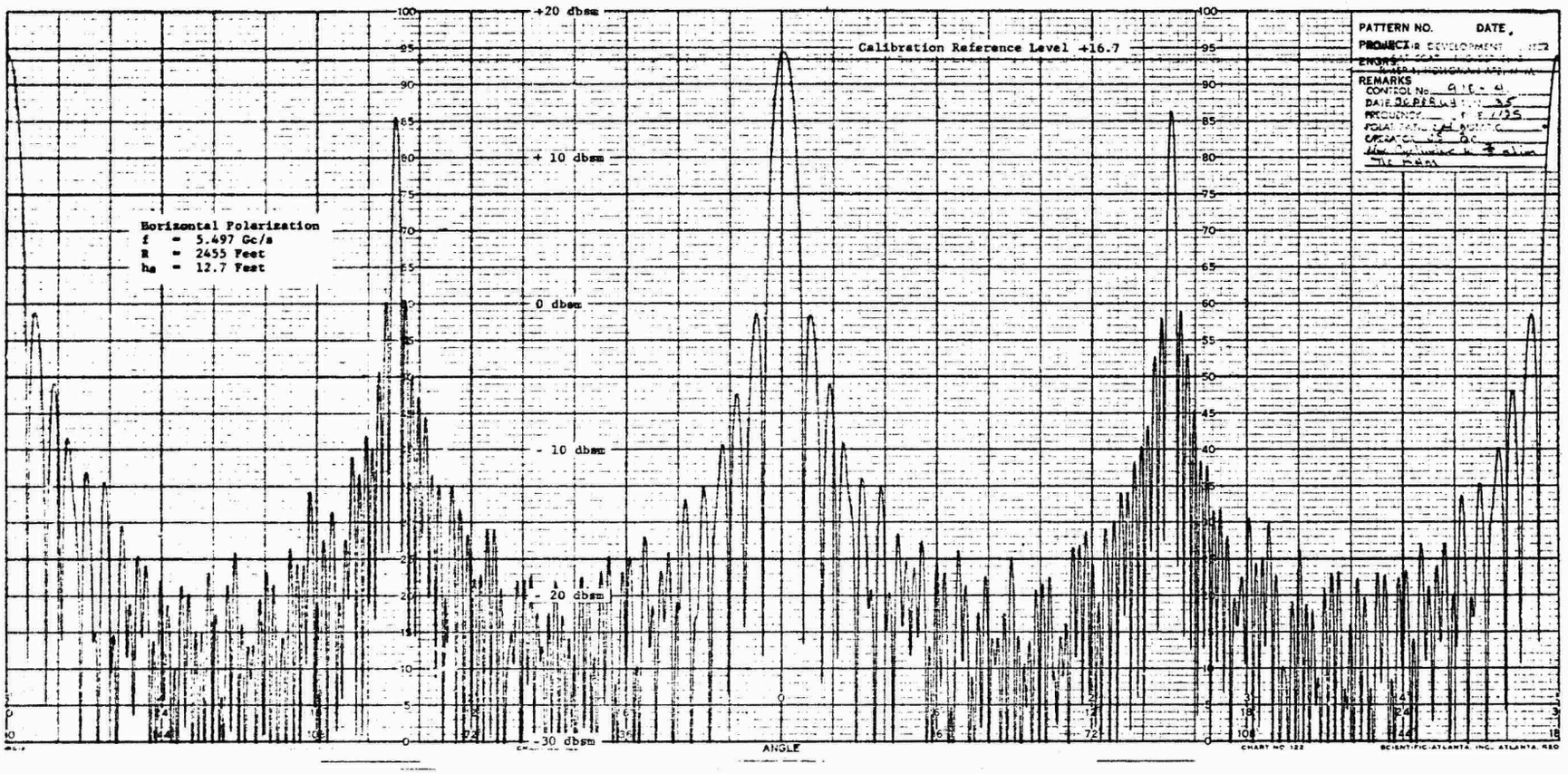

Fig. 50 CROSS SECTION RETURN FROM CYLINDER (WITHOUT RAM)

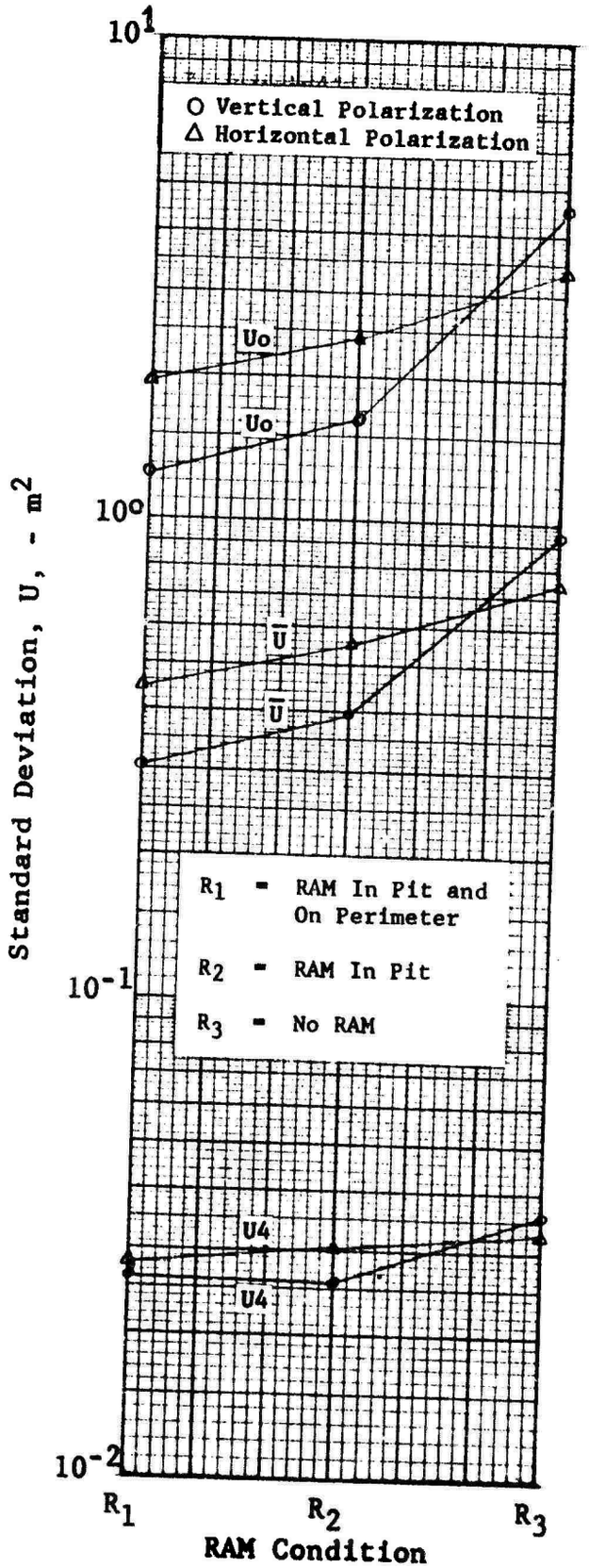

Fig. 51 STANDARD DEVIATION, U, VERSUS RAM CONDITION

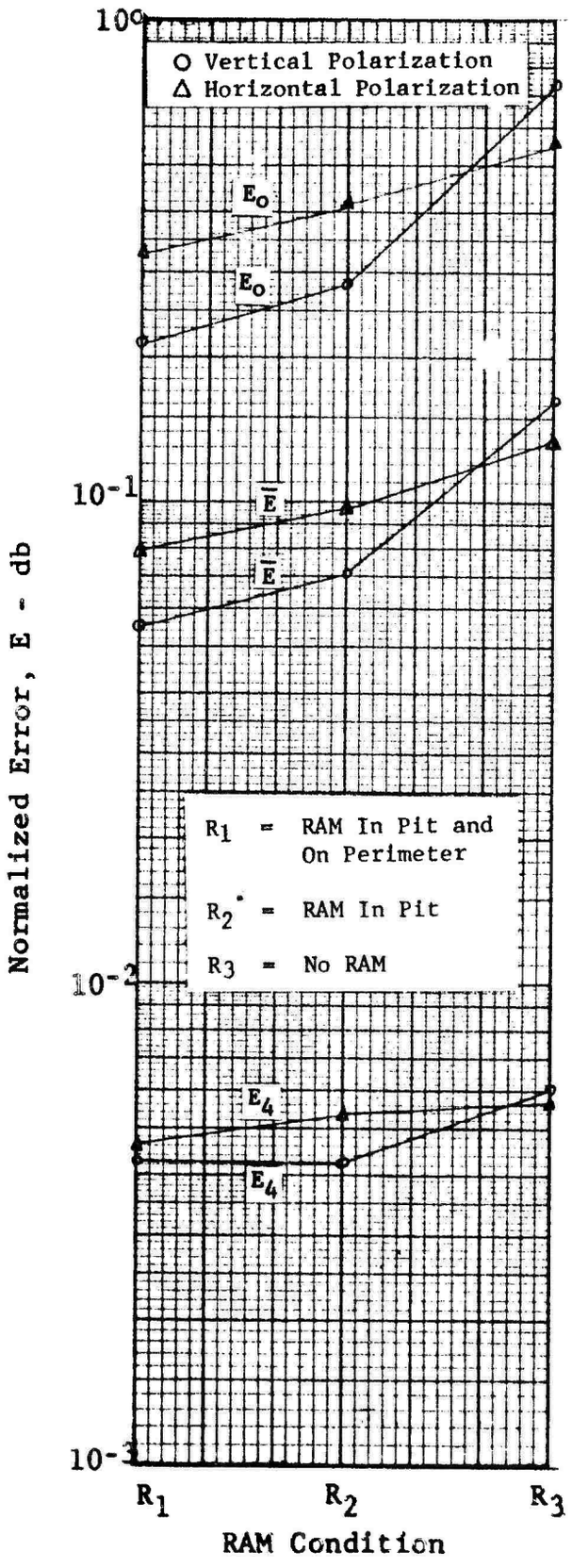

Fig. 52 NORMALIZED ERROR, E, VERSUS RAM CONDITION

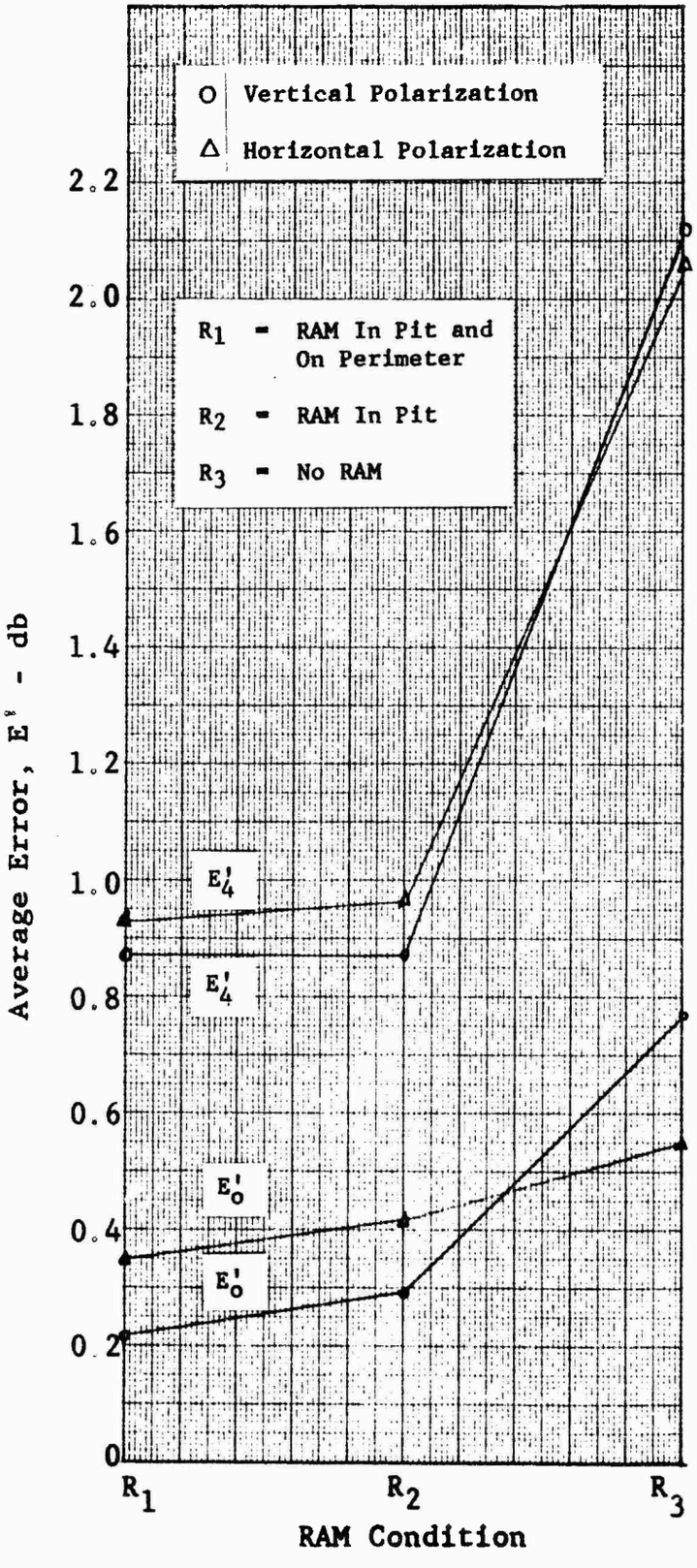

Fig. 53 AVERAGE ERROR, E', VERSUS RAM CONDITION

lobes due to limitations imposed by the validity of (1) the theoretical formula for calculation of cross section of a cylinder and (2) the data once the side lobes were 25 db down from the main lobe). Analysis of Figure 53 shows that the values of E_{jn}^{PR} for the main lobe are the same as the values of E_j^{PR} for the main lobe, as expected due to the fact that both E_{jn}^{PR} and E_{jn}^{PR} are normalized to σ_{mL}. Further investigation of Figure 53 yields the fact that E_j^{PR} increases as j increases, and that E_j^{PR} rapidly increases when RAM is removed from the rotator. The extraneous illumination investigation may be summarized noting the following:

1. In all cases all errors increase as RAM is removed from the pit, especially from the rotator

2. The error due to extraneous illumination contained in the cross section measurements of the main lobe of the cylinder is insignificant

3. The error contained in the cross section measurements of the side lobes becomes significant as j increases.

Therefore, in order to reduce the extraneous illumination errors which occur, particularly if the target side lobe structure is of interest, in cross section measurements, RAM should be used on the rotator platform and around the perimeter of the pit.

SECTION 5

CALIBRATION AND INSTRUMENTATION ERROR INVESTIGATION

Calibration Error

The radar return from a spherical target provides a convenient means of establishing an absolute reference level for the cross section measurement system. Theoretical radar cross sections of spherical targets have been accurately calculated for a wide range of the parameter (d/λ) where d is sphere diameter. Hence, if the frequency of the illumination and the sphere size are known then the receiver output (which is proportional to the received power) can be defined to be the theoretical cross section level of the sphere and the system is said to be calibrated. Such a procedure requires the positioning of the sphere at the point of interest for each calibration and then a subsequent removal of the sphere in order to measure the cross section of some target of interest. To reduce the time required per measurement a secondary standard in the form of a mid-range corner reflector is employed. This is easily accomplished by first calibrating the system as above and then assigning a level to the return from the corner by comparing this return to the return from the sphere. The secondary standard does not have to be removed from the range for each measurement because it can be lowered into the ground null of the illumination pattern, and, in addition, the direct return from the corner can be gated out electrically.

With the above description of the calibration process in mind, various ways in which errors can enter into the process are listed as follows:

1. The wavelength of the illumination may not correspond exactly to the wavelength used to determine the theoretical cross section of the sphere.

2. The diameter of the sphere used for calibration may not correspond exactly to the diameter used to determine the theoretical cross section.

3. The target used for calibration is not necessarily spherical in shape; hence its assumed cross section may not correspond to the actual cross section.

4. The calibrating sphere may not be located at the intended target center point.

5. The level of the secondary standard may not remain constant during the time a series of measurements are being made. Since the time of such a change is, in general, unknown, all of the measured data must be considered to be in error.

6. The various error sources that are discussed elsewhere in this report may be present to an appreciable extent.

Of these items, the first five are appropriately termed systematic errors in that they can be almost completely eliminated if enough precision in the calibration procedure is attained. The last item, on the other hand, serves to lump together most if not all of the inherent error sources in the calibration procedure. In this report it has been shown that if the sphere support column is properly tuned the inherent errors become of concern only for those spheres that exhibit rather low cross sections. Under these conditions, the calibration procedure can become strongly influenced by the presence of background noise. However, this problem can be virtually eliminated as will be shown.

Test Program and Results

Figures 54 and 55 provide an indication of the calibration errors to be expected for both polarization cases when the degree of precision used in the calibration procedure is as it has been in the past at the RAT SCAT facility. These figures were arrived at by taking all the sphere cross section measurements from the RAT SCAT Qualification Tests and operating on them with statistical techniques. The total range of the measured data in dbsm was divided into 5.0 db increments and each succeeding increment overlapped the last 2.5 db. All of the measured data within each increment were shifted in a linear fashion to the increment mid-point. With the data aligned at common levels the mean and standard deviation of the measured cross sections were computed for each level and plotted against the theoretical cross section level (the increment mid-point). If there were no calibration errors present the mean values would all lie along the 45-degree lines on the figures. Hence, the displacement of a mean value from a 45-degree line should be a measure of the calibration error to be expected at that cross section level.

Figures 56 and 57 represent the results for both polarizations from an experiment designed to demonstrate the accuracy that is

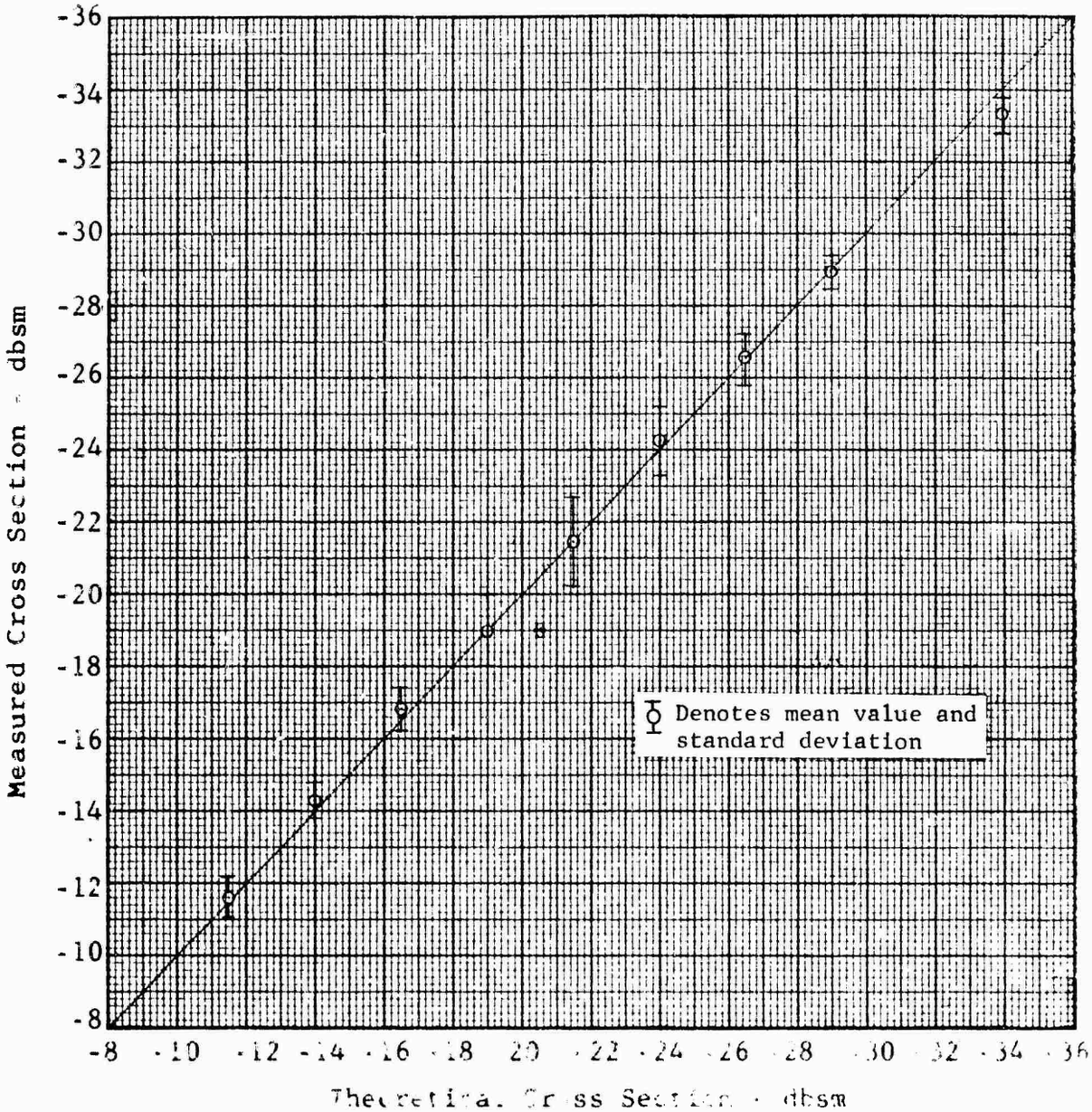

Fig 54 EXPECTED CALIBRATION ERROR BASED UPON QUALIFICATION TEST DATA HORIZONTAL POLARIZATION

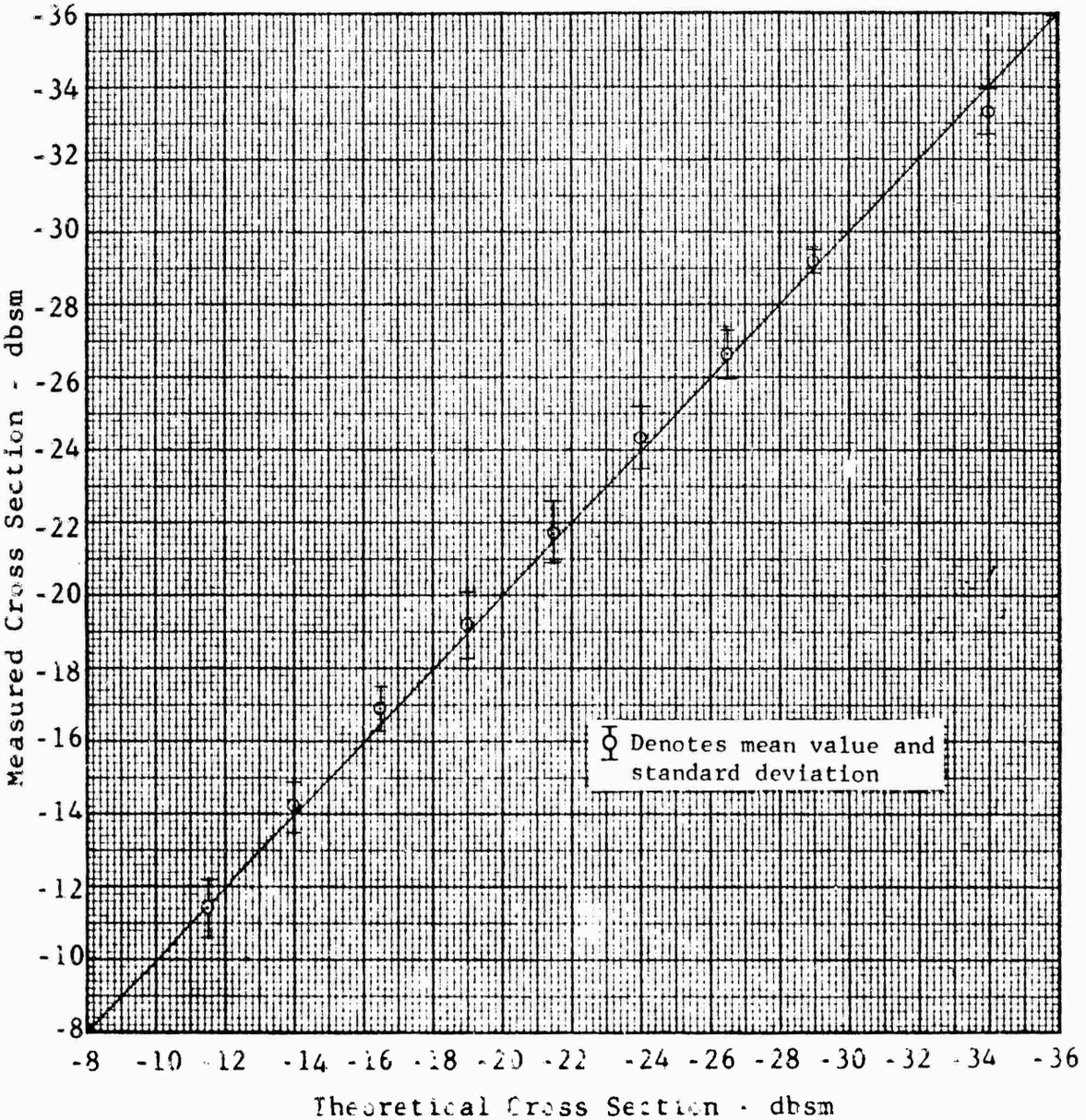

Fig 55 EXPECTED CALIBRATION ERROR BASED UPON QUALIFICATION TEST DATA. VERTICAL POLARIZATION

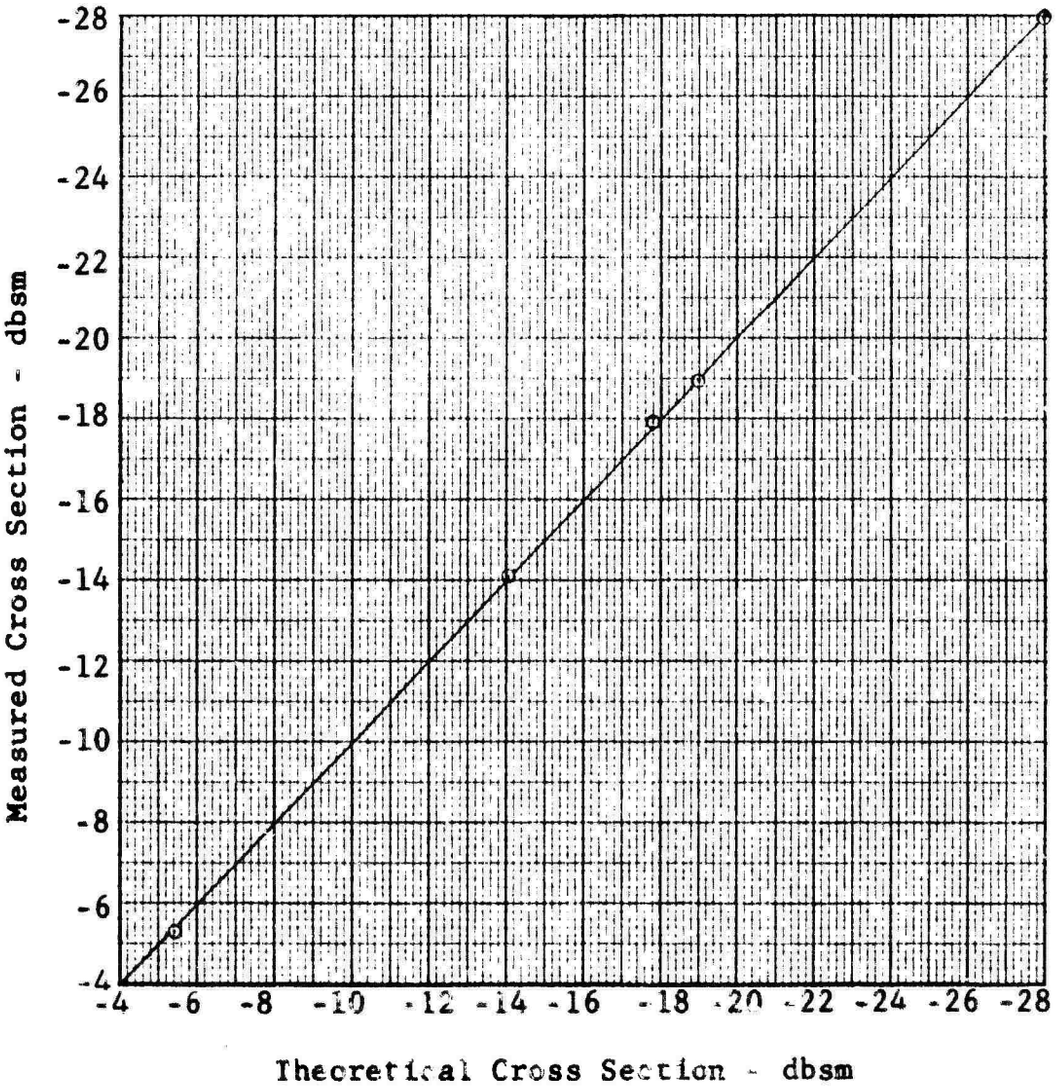

Fig. 56 CALIBRATION ERROR BASED UPON R&D EXPERIMENT RESULTS, HORIZONTAL POLARIZATION

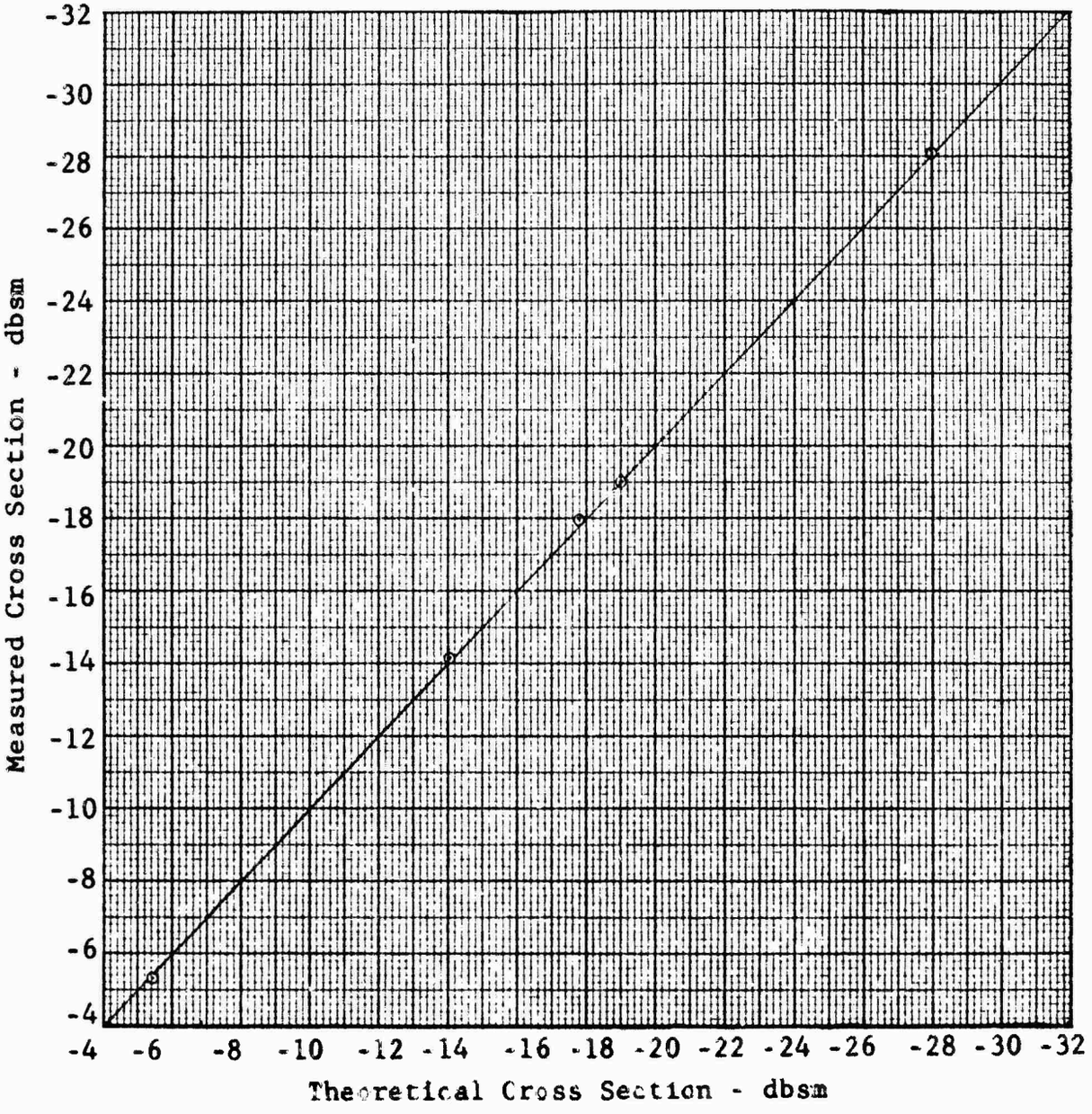

Fig. 57 CALIBRATION ERROR BASED UPON R&D EXPERIMENT RESULTS, VERTICAL POLARIZATION

obtainable using spheres available at the RAT SCAT Site. In addition, the experiment was designed to investigate the calibration error problem at low cross section levels. It consisted of the following procedure for the range of cross section levels shown on the figures. The cross section of a carefully measured sphere mounted atop the center of a tuned Styrofoam support column was recorded as the target was rotated through 360 degrees of azimuth. Also, the frequency of the illumination was carefully measured. The sphere was then rotated 90 degrees about a horizontal axis and the cross section measurement was repeated. Similar measurements were made with the sphere translated vertically a distance of $\lambda/4$ from its initial position, and with the sphere translated horizontally a distance of $\lambda/4$ from the second position.

The above steps were intended to detect the following:

1. Calibration error
2. Effects of asphericity
3. Effects of extraneous illumination
4. Effects of background noise.

Except for the lowest cross section level investigated (-28.0 dbsm) all of the measured data for a particular sphere corresponded with one another to within less than the system resolution (0.1 db). In the case of the lowest cross section the $\lambda/4$ horizontal shift revealed that the support column return had been previously adding in phase with the sphere return to produce a 0.5 db error in the recorded cross section. The data plotted on Figures 56 and 57 are the actual measured values of sphere cross section versus the theoretical values of sphere cross section. It should be noted that on none of the above figures does the reference level used for the measurements appear.

Instrumentation Error

Receiver Noise

The presence of receiver noise or incoherent noise in the measurement system perturbs the measured data and is an error source. As indicated previously, this noise has inherently been considered in the background error analysis of Section 3. If it were possible to isolate the incoherent noise from the coherent noise in an experiment, a measure of the error due to each could be obtained. The total error would consist of a term very similar

to the randomly varying quantity presented in Section 3 and a term due to the incoherent noise. Because the incoherent noise exhibits the property of randomly varying phase it can be considered to add power wise to the cross section return. Hence, its primary effect upon the total error (coherent plus incoherent) will be a shift of the mean.

Test Results

Shown in Table 1 are values of the mean receiver noise level from the RAT SCAT Acceptance Tests. With the aid of this table and the relationship shown in Equation 31 the shift of the mean of the total noise error due to incoherent noise can be computed.

$$\Delta E = 10\log_{10}\left[\, 1 - 10^{-0.1\,(\bar{E}_t - \sigma_n/\sigma_t)}\right], \qquad (31)$$

where

$\Delta E = \bar{E}_b' - \bar{E}_t$

$\bar{E}_b'$ = mean error due to background only in db

$\bar{E}_t$ = mean total error ($\bar{E}_b$ of Section 3) in db

σ_n = receiver noise in dbsm

σ_t = target level in dbsm.

From Table 1 it can be seen that the Band 6 receiver noise represents a larger fraction of the mean of the total noise (-44.8 dbsm for horizontal polarization) than does the receiver noise of any other band; hence, it represents the extreme case. For a reasonably low target level (e.g., 5 db above the -44.8 dbsm mean) the mean of the total error due to noise can be computed as 1.2 db. Consequently, it can be shown that the largest deviation of the total error from the background error, excluding receiver noise, is 0.18 db. This result follows from Equation 31.

System Power Stability

If the receiver gain or transmitter power changes during the time a particular measurement is being made, the measurement may be in error. Likewise, if the gain or power changes during the

Table 1 MEAN NOISE LEVELS FOR THE CASES OF INTEREST

Band No.	Frequency (Gc)	Range (ft)	Mean Background Level (-dbsm)		Receiver Noise (-dbsm)
			VP	HP	
4	1.529	1155	59.8	64.9	79.0
5	2.955	1155	52.1	52.1	83.0
6	5.497	2455	41.7	44.8	52.0
7	9.472	2455	41.0	37.7	54.0

time a sequence of measurements are being made, the individual measurements cannot be directly compared with one another. Test results concerning power stability of the equipment at the RAT SCAT Site are presented in this section.

Shown in Table 2 is an array of samples that were randomly selected from the results of a RAT SCAT Power Stability Qualification Test. The test consisted of sampling the Band 4 receiver output at a uniform rate during a 6-hour period of continuous operation. The system was operating in a closed loop manner in that the transmitter output was coupled to the receiver input through an attenuator. On the basis of a random sample of the data from this test the power level remained at the original value of 48.9 db to within a tolerance of $\pm$0.1 db.

Table 2 RELATIVE POWER LEVELS RANDOMLY CHOSEN FROM POWER STABILITY TEST

48.9	48.9	49.0	48.9	49.0	48.9	49.0	48.9	48.9	48.9
48.9	48.9	48.9	48.9	48.9	48.8	48.9	48.9	48.9	49.0
48.9	48.9	49.0	48.9	48.9	48.9	48.9	48.9	49.0	49.0
48.9	48.9	48.9	48.9	48.8	48.9	48.9	49.0	48.9	48.9
49.0	48.9	48.9	48.9	49.0	48.9	48.9	48.9	48.9	48.9

System Frequency Stability

Because the radar cross section of a target is normally a function of frequency any change in frequency during a measurement will perturb the return and thus introduce error. The nature of the equipments involved in the generation and processing of the illumination energy are such that a certain amount of frequency instability is to be expected.

Frequency stability measurements from the RAT SCAT Qualification Tests are shown in Figures 58 through 61. These tests provide an indication of the deviation of the transmitter frequency from its original frequency as operation time increases. In the worst case (Band 6) the maximum variation was 0.067 percent of the original frequency.

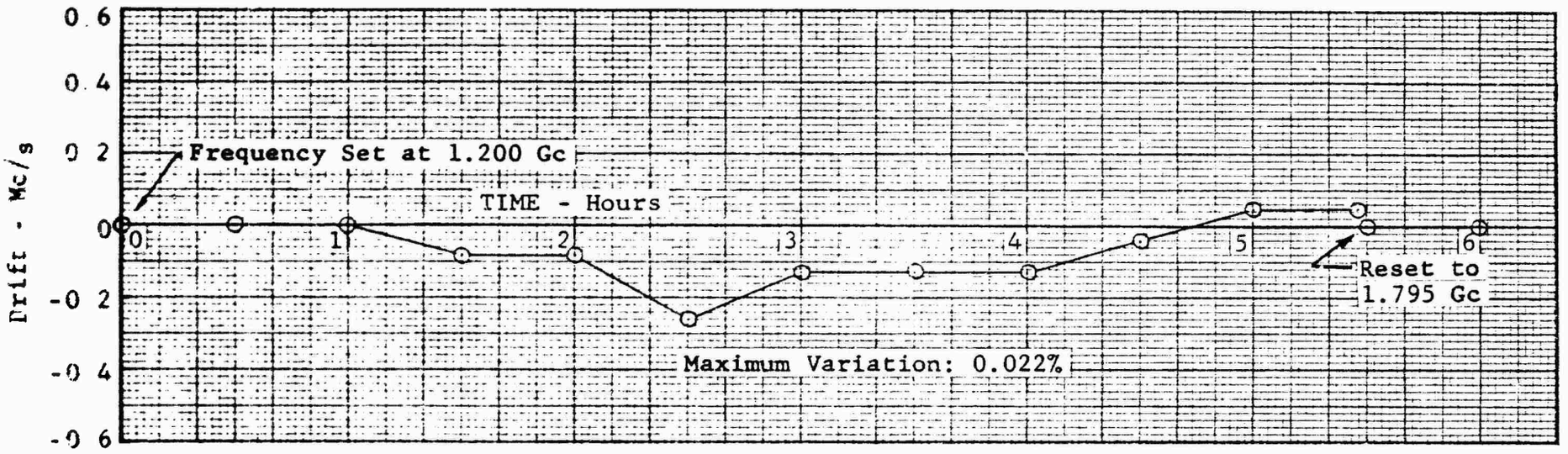

Fig 58 BAND 4 FREQUENCY STABILITY TEST

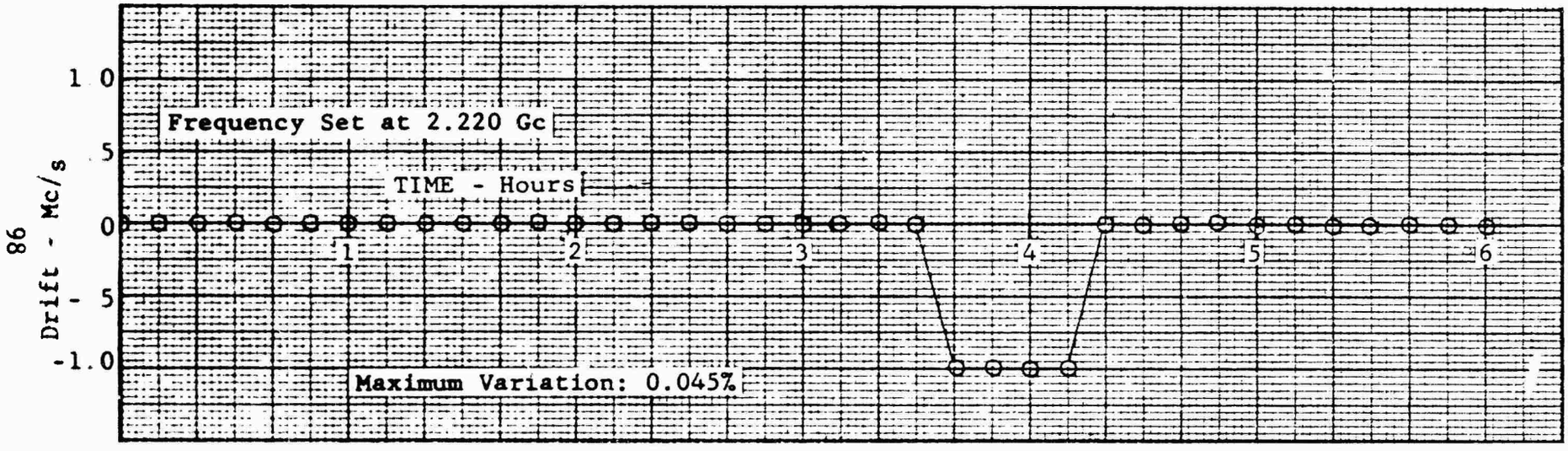

Fig. 59 BAND 5 FREQUENCY STABILITY TEST

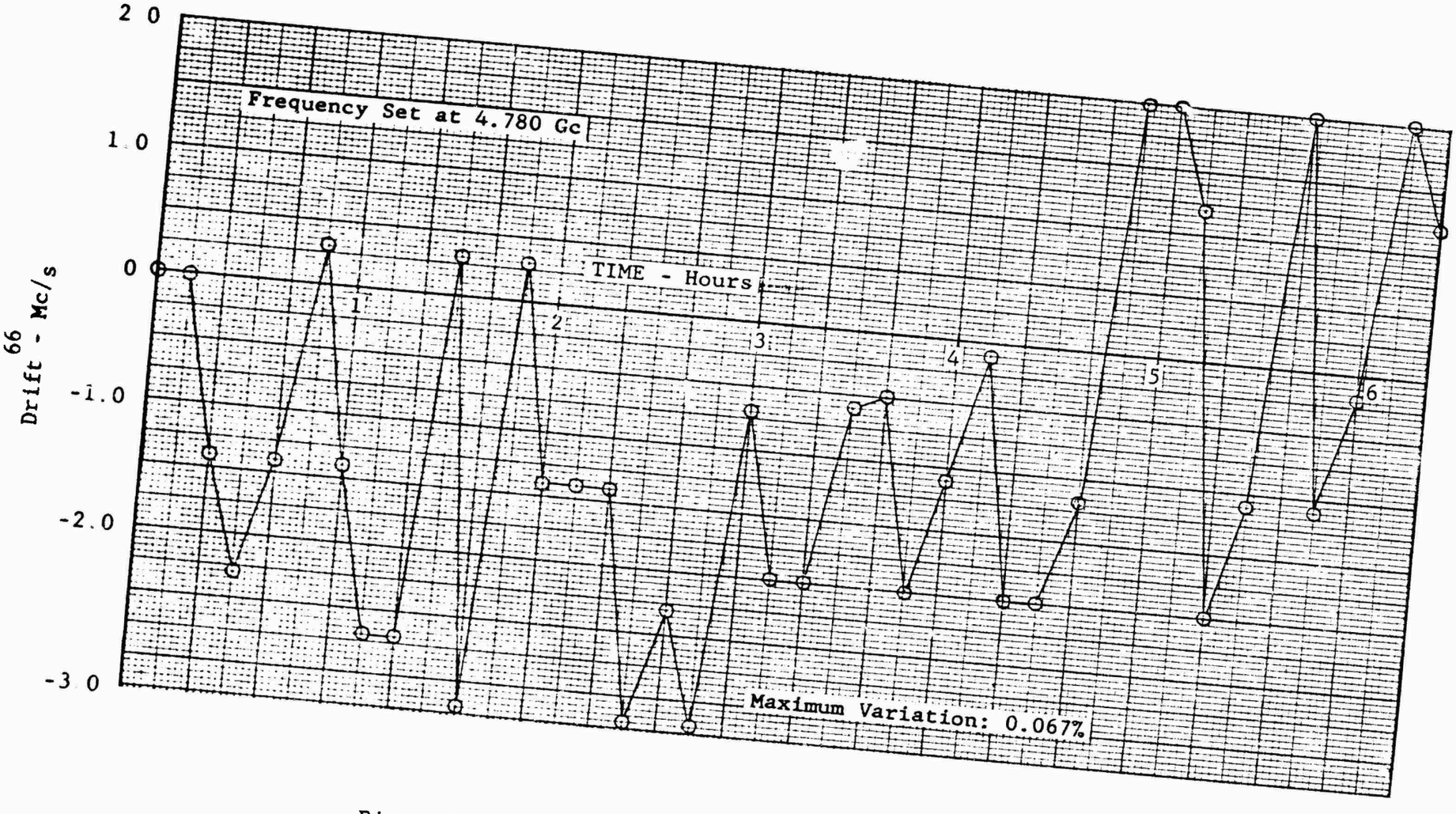

Fig 60 BAND 6 FREQUENCY STABILITY TEST

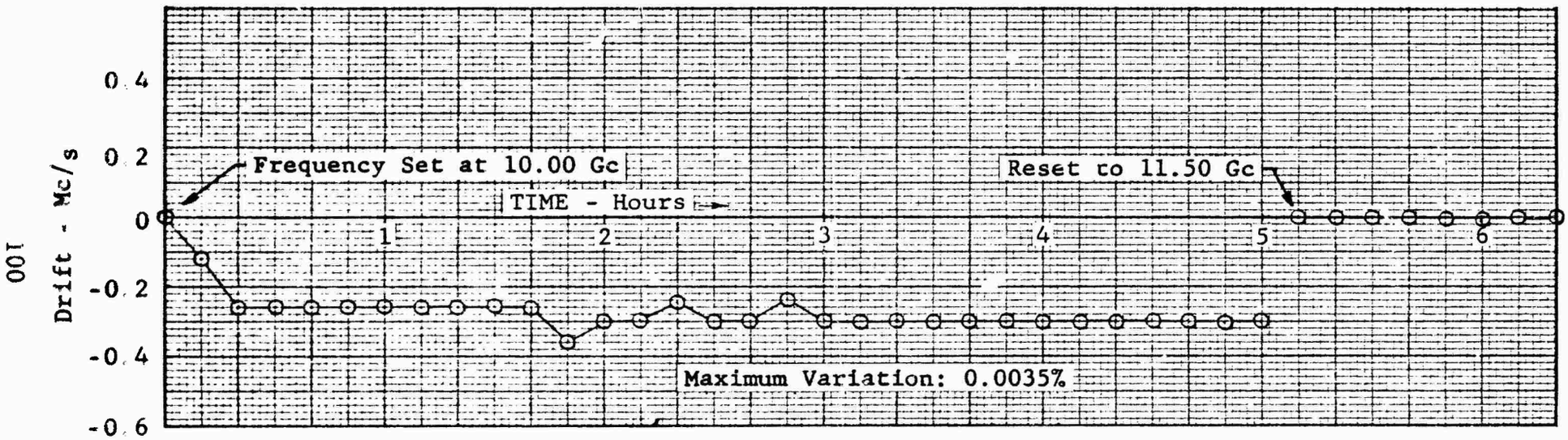

Fig. 61 BAND 7 FREQUENCY STABILITY TEST

System Linearity Check

If the receiver tends to process any level of radar return differently than any other level within the dynamic range of the equipment, a source of error is present. Specifically, a given change in the input signal level to the receiver must result in the same relative change in the output signal level of the receiver.

Shown in Figures 62 through 65 are the results of receiver linearity checks from the RAT SCAT Acceptance Tests. The tests were carried out by inserting a known amount of attenuation into the line in front of the receiver and observing the resultant change in the receiver output. From the figures it is apparent that in the worst case the output increment differs from the input increment by less than 0.5 db.

Summary

On the basis of the above test results the following conclusions can be drawn with regard to the calibration and instrumentation errors of the equipment used to make radar cross section measurements at the RAT SCAT facility:

1. Calibration error at cross section levels above -25 dbsm can be reduced to the point of being inconsequential if tuned support columns are employed and precision is used in the calibration process.

2. Calibration error at cross section levels below -25 dbsm can be greatly reduced by the method discussed.

3. The error due to receiver noise was included in the background error analysis, but, in general, the error is very small in comparison to the error due to coherent noise.

4. Errors due to system power drift, frequency drift, and receiver nonlinearity are inconsequential in comparison to other error sources that have been considered.

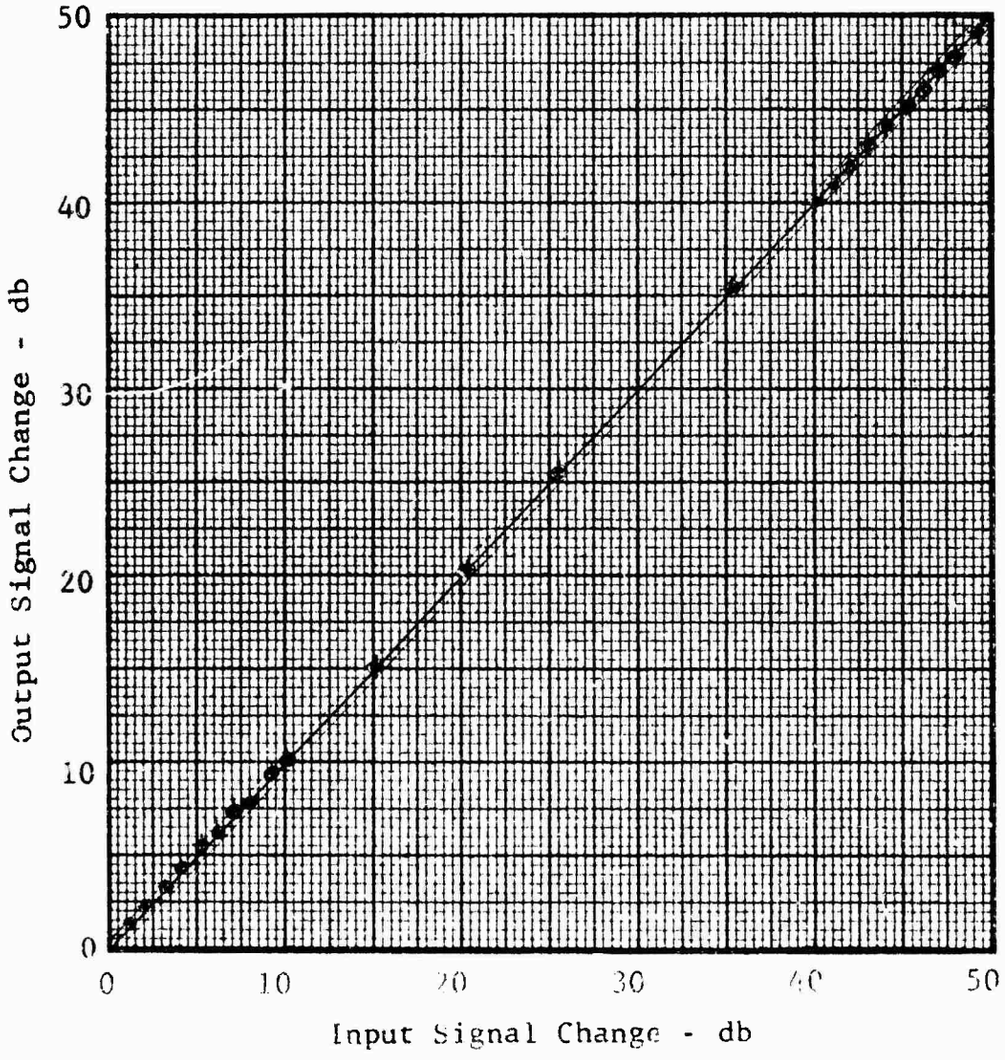

Fig 62 BAND 4 LINEARITY CHECK

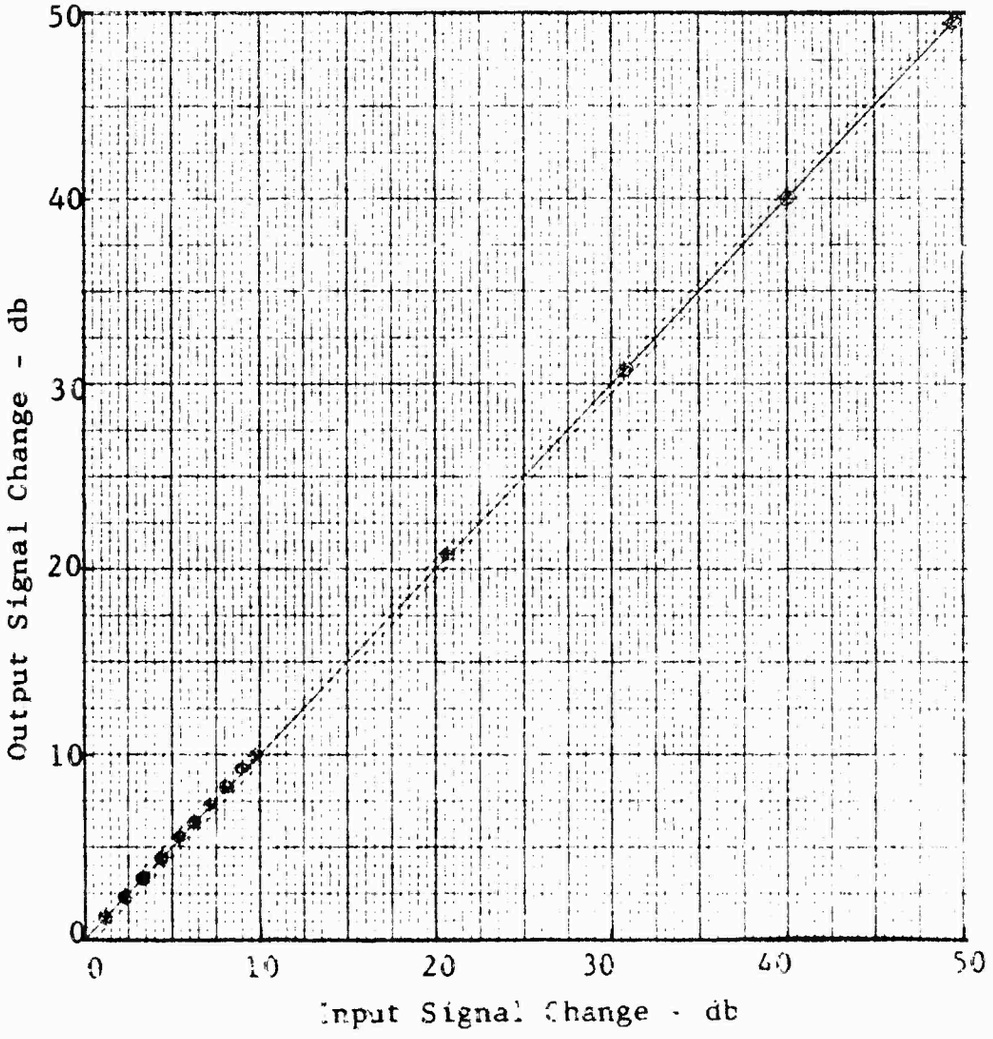

Fig. 63 BAND 5 LINEARITY CHECK

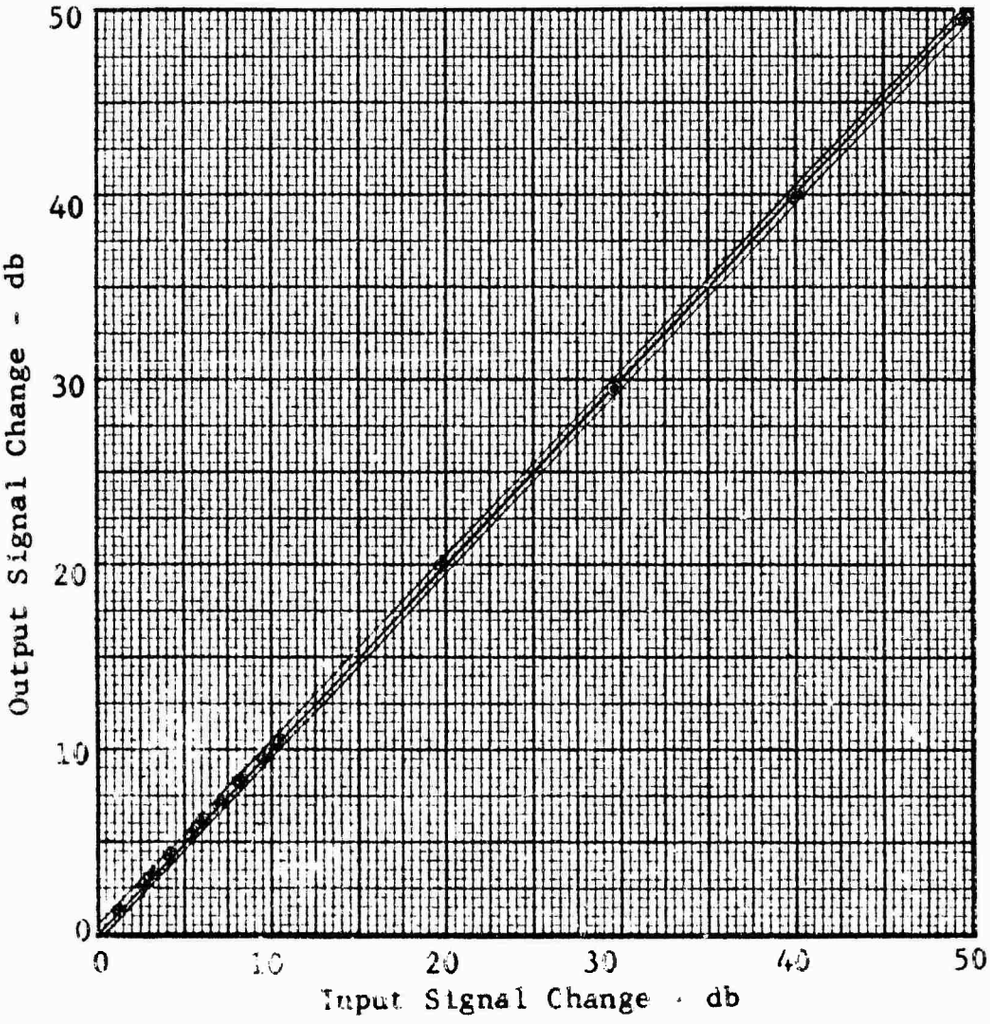

Fig. 64 BAND 6 LINEARITY CHECK

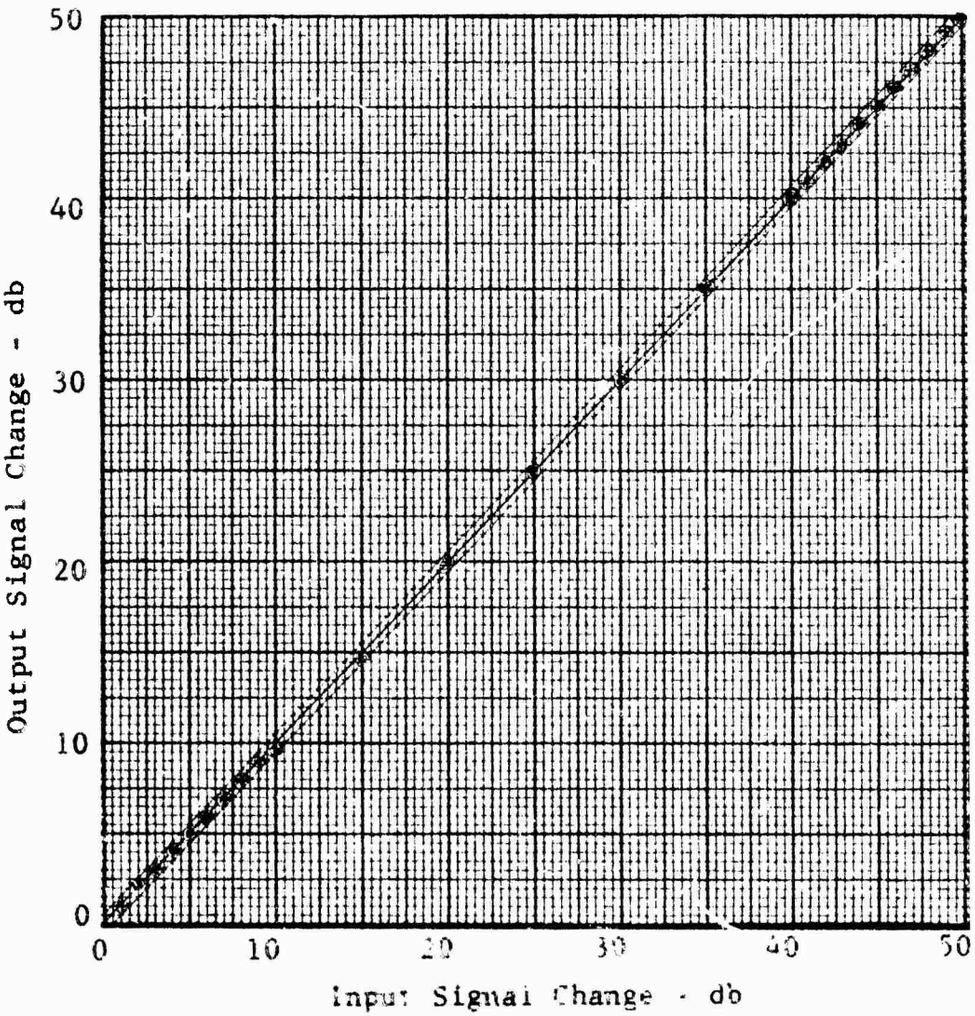

Fig 65 BAND 7 LINEARITY CHECK

SECTION 6

SUMMARY AND EXTENSION OF ERROR INVESTIGATIONS

When the measurement conditions are controlled as discussed in Section 5, errors due to calibration and instrumentation may be reduced to negligible amounts.

The results of the investigation concerning extraneous illumination, discussed in Section 4, indicate that except for those cases where the side lobes of a target are of interest, errors due to extraneous illumination are of little concern if RAM is used to cover the rotator and edge of the pit.

To summarize the results of the near field and background error investigations it is expedient to group targets into three nominally separate classes. The first of these is the class composed of geometrically large targets, i.e., the targets for which the primary contributor to cross section measurement error is field curvature. Targets which exhibit a low radar cross section characterize members of the second class of targets; i.e., those targets for which the primary contributor to cross section measurement error is background noise. The third class of targets are those that exhibit characteristics between the two extremes defined above. This group of targets would be characterized by radar cross section measurement errors due to both near field effects and to background noise.

For large targets the results shown in Section 2 are appropriate. Specifically, the results of the investigation indicate that the following models provide reasonable approximations of the measuring fields and near field error to be expected at the RAT SCAT Site:

1. The expressions for amplitude and phase in the horizontal and vertical planes given in Section 2

2. The one-dimensional error models given in Equations 6 and 9

3. The two-dimensional error model described in Figure 30.

For low cross section targets the results presented in Section 3 provide a means for determining the expected error due to background for the case of tuned columns. Figure 46 provides this estimate for a given target level and D/λ parameter where D

is the diameter of the Styrofoam target support. The reader is cautioned, however, that the analysis of Section 3 depends upon the assumption of a uniform distribution for the relative phase between the target and the background return. For example, the phase between a particular target and the background could be a constant. The worst case error shown on the figures does not depend upon this assumption.

To consider the remaining class of targets a combination of previous results provide a means whereby the cross section measurement errors due to both near field effects and background noise can be considered. The parameter linking these two types of errors is vertical target size. With the aid of Equation 5 a more general expression can be written for the vertical plane near field error model. This expression is given in Equation 32. Equation 5 has been generalized in the sense that account has been taken of the fact that target center does not have to coincide with the center of the first lobe of the antenna pattern.

$$\sigma_{nf_v} = 20 \log_{10} \left| \frac{1 - \frac{K_b}{D_V} \left(\text{Sin} \left(\frac{h_c + D_V}{K_b} \right) - \text{Sin} \left(\frac{h_c}{K_b} \right) \right)}{2 \, \text{Sin}^2 \left(\frac{(h_c + D_V/2)}{2 K_b} \right)} \right| \qquad (32)$$

where

$K_b = \frac{R\lambda}{4\pi h_a}$

h_c = column height

D_V = characteristic vertical target dimension.

Because the target center (calibration point) may now take on positions other than the peak of the lobe, the illuminating field cannot be considered symmetric about the center of the target.

The manner in which the mean cross section of a tuned Styrofoam support column varies as the parameter D/λ varies is illustrated in Figure 45. The data presented in Figure 45 indicated that the cross section of a tuned column (for the case of the uniform illumination) is proportional to $(D/\lambda)^3$ as predicted in Reference 4. If account is taken of the fact that the illumination is not uniform, then the return per unit length of support column should be weighted appropriately. Formally this can be written as in Equation 33, where the mean noise $\bar{\sigma}_b$ is expressed in dbsm.

$$\bar{\sigma}_b = 20 \log_{10} \left\{ C_f (D/\lambda)^{3/2} \left| \frac{1 - \frac{\sin h_c/k_b}{h_c/k_b}}{2 \sin^2 \left[\frac{(h_c + D_V/2)}{2 k_o} \right]} \right| \right\}, \quad (33)$$

where

C_f = constant of proportionality

D/λ = column diameter/wavelength ratio

Here also the right hand side has been normalized by the illumination level at target center. With this equation and an estimate of the target level, the worst case background error (based upon the mean background noise) can be written in db.

$$E_{w_c} = 20 \log_{10} (1 - \sqrt{\bar{\sigma}_b / \sigma_t}) \quad , \quad (34)$$

where

σ_t = target level in dbsm.

An estimate of error due to both background and near field effects can be obtained by observing error terms of Equations 32 and 33 as a function of target dimension D_V. For illustrative purposes plots of the two error values versus the target dimension D_V are shown in Figure 66 for a particular case. The calculations were based upon the target center being located at the peak of the lobe. The range parameters for the particular case shown are noted on the figure. The constant of proportionality used for the calculation ($C_f = 3.65 \times 10^{-4}$) was based upon measured values of $\bar{\sigma}_b$ from the background error investigation of Section 3. Inspection of Figure 66 indicates, for the particular case used, the range of target vertical dimension for which both near field errors and background errors are negligible. The target used to compute cross section used in Equation 34 as a function of vertical dimension D_V was a 5-inch diameter cylinder.

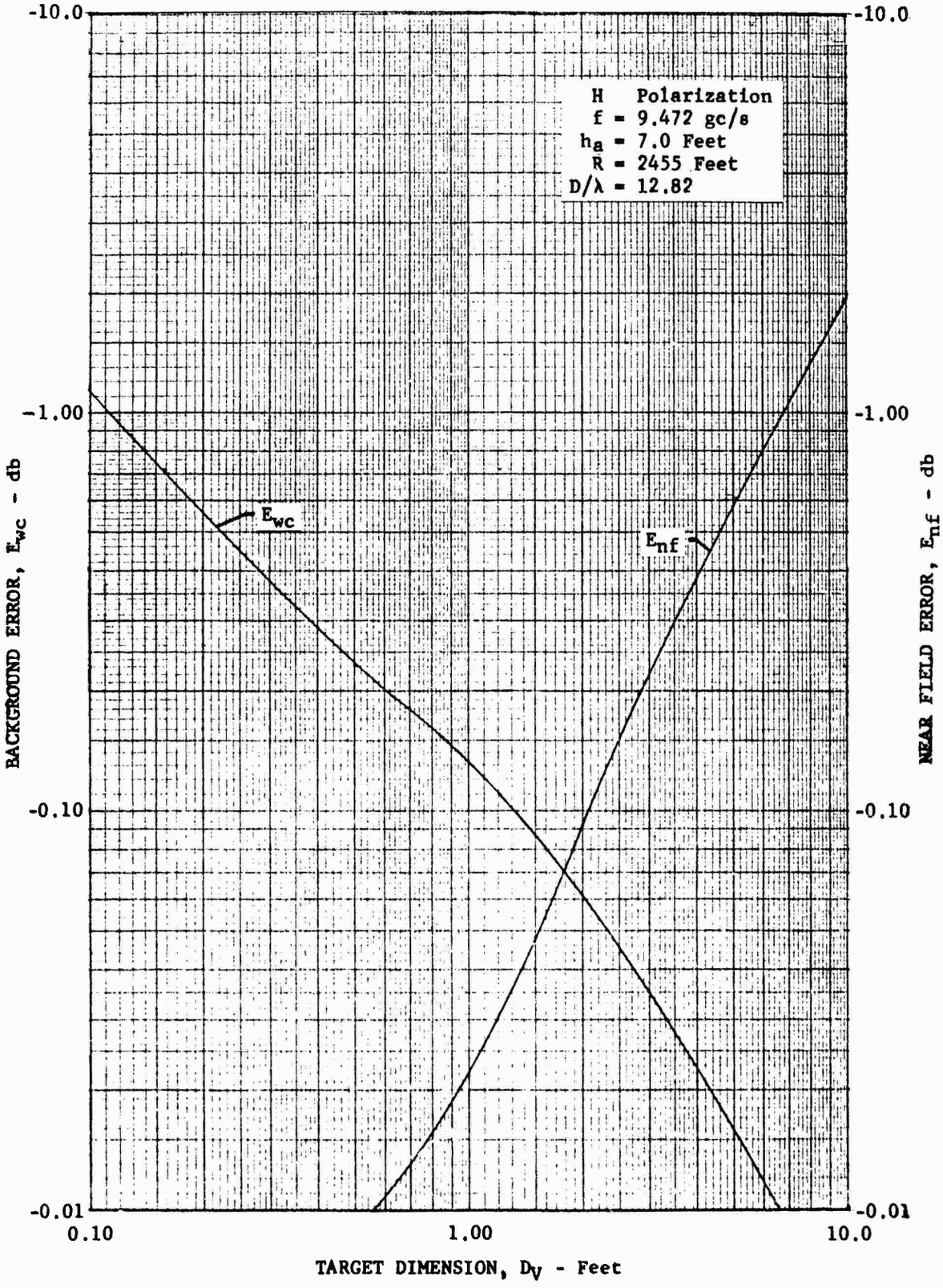

Fig. 66 NEAR FIELD ERROR AND BACKGROUND ERROR AS A FUNCTION OF TARGET DIMENSION

REFERENCES

1. Kerr, Donald E., Editor, Propagation of Short Radio Waves, McGraw-Hill Book Co., Inc., New York, 1951

2. Silver, Samuel, Editor, Microwave Antenna Theory and Design, McGraw-Hill Book Co., Inc., New York, 1949

3. Mentzer, J. R., Scattering and Diffraction of Radio Waves, The Macmillan Company, New York, 1959

4. Mood, Alexander Mr., Introduction To The Theory of Statistics, McGraw-Hill Book Co., Inc., New York, 1950

5. Radar Cross Section Target Supports - Plastic Materials, Report No. RADC-TDR-64-381, June, 1964